NASA CR-134852

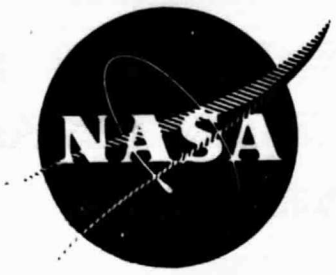

QUIET CLEAN SHORT-HAUL EXPERIMENTAL ENGINE (QCSEE)

Hamilton Standard Cam/Harmonic Drive Variable Pitch Fan Actuation System Detail Design Report

by

Aircraft Systems Department, Propulsion Design Group

Hamilton Standard
Division of United Technologies Corporation

Under Subcontract to General Electric Company
(P.O. 200-4XX-14G38570)

Prepared For

National Aeronautics and Space Administration

NASA Lewis Research Center
Contract NAS3-18021

NASA CR-134852

QUIET CLEAN SHORT-HAUL EXPERIMENTAL ENGINE (QCSEE)

Hamilton Standard Cam/Harmonic Drive Variable Pitch Fan Actuation System Detail Design Report

by

Aircraft Systems Department, Propulsion Design Group

Hamilton Standard
Division of United Technologies Corporation

Under Subcontract to General Electric Company
(P.O. 200-4XX-14G38570)

Prepared For

National Aeronautics and Space Administration

NASA Lewis Research Center
Contract NAS3-18021

1. Report No.	2. Government Accession No.	3. Recipient's Catalog No.
NASA CR-134852		

4. Title and Subtitle	5. Report Date
QUIET CLEAN SHORT HAUL EXPERIMENTAL ENGINE (QCSEE) HAMILTON STANDARD CAM/HARMONIC DRIVE VARIABLE PITCH FAN ACTUATION SYSTEM, DETAIL DESIGN REPORT.	March 1976
	6. Performing Organization Code
7. Author(s)	8. Performing Organization Report No.
Aircraft Systems Department Propulsion Design Group	HSER 7001
	10. Work Unit No.
9. Performing Organization Name and Address	11. Contract or Grant No.
Hamilton Standard Division of United Technologies Corporation Windsor Locks, Connecticut 06096 Under sub-contract to General Electric Company, Cincinnati, Ohio 45215	NAS 3-18021
	13. Type of Report and Period Covered
12. Sponsoring Agency Name and Address	Contractor Report
National Aeronautics & Space Administration Washington, D.C. 20546	14. Sponsoring Agency Code

15. Supplementary Notes

Design Report. Project Manager, C.C. Ciepluch, QCSEE Project Office
Technical Advisers, D.A. Sagerser and D.C. Reemsnyder
NASA Lewis Research Center, Cleveland, Ohio 44135

16. Abstract

A variable pitch fan actuation system was designed which incorporates a remote nacelle-mounted blade angle regulator. The regulator drives a rotating fan-mounted mechanical actuator through a flexible shaft and differential gear train. The actuator incorporates a high-ratio harmonic drive attached to a multi-track spherical cam which changes blade pitch through individual cam follower arms attached to each blade trunnion. Detail design parameters of the actuation system are presented. These include the following: design philosophies, operating limits, mechanical, hydraulic and thermal characteristics, mechanical effeciencies, materials, weights, lubrication, stress analyses, reliability and failure analyses.

17. Key Words (Suggested by Author(s))

Spherical cam
Harmonic drive
No-back
Flexible shaft
Pitch change mechanism
Beta regulator

19. Security Classif. (of this report)	20. Security Classif. (of this page)	21. No. of Pages	22. Price*
Unclassified	Unclassified		

TABLE OF CONTENTS

SECTION 1.0

SUMMARY

A variable pitch fan actuation system was designed for NASA's QCSEE engine under subcontract to the General Electric Company in accordance with the requirements defined in General Electric Specification M50TF1635-S1. These requirements include provisions for changing fan blade pitch from forward to reverse thrust positions through flat pitch and through stall in less than one second. The fan operating conditions and loads specified for the actuator design were determined by the General Electric Company and represented both normal and extreme loads, such as bird strikes.

Hydraulic motors in a remote nacelle-mounted blade angle (Beta) regulator module receive high pressure hydraulic power from an engine-driven pump through an electro-hydraulic servo valve (EHV) which is controlled by electrical command inputs from the engine control. The high speed, low torque motor output drives a fan disk-mounted mechanical actuator through a flexible shaft passing through the engine reduction gearing. Actuator input torque from the Beta regulator passes through a planetary differential gear train, a spring-type no-back friction brake, a high ratio harmonic drive, a spherical multi-track cam and individual cam follower arms to the blade trunnions.

The differential gear train increases torque with a 5:1 ratio and permits the rotary drive to cross the boundary between the stationary regulator module and the rotating actuator. The no-back locks the blades from rotation in either direction when the regulator is not controlling. A 201:1 increase in torque is provided by the single-stage harmonic drive which drives the spherical cam. Cam follower arms splined to each blade trunnion mate with respective slots in the spherical cam surface through steel rollers to provide blade pitch change in accordance with a small varying torque ratio. The total gear ratio between the Beta regulator and the blades is approximately 1000:1.

Lubrication flow for the actuator is provided from the engine through the flexible shaft casing via the Beta regulator. The actuator components are force-lubricated centrifugally by the lubrication flow which then returns to the engine in the reduction gear scavenge section. All components of the actuator system are flight weight design except for the Beta regulator and the servo valve. These two components utilize readily available commercial parts for reasons of cost and time effectiveness. The total weight of the actuator system including an estimate of the flight weight of the Beta regulator and servo valve is 40.4 kg (89.2 lbs). The actuator system design satisfies the requirements of GE Specification M50TF1635-S1.

SECTION 2.0

INTRODUCTION

The variable pitch fan represents a key part of the technology being developed for the NASA Quiet Clean Short-haul Experimental Engine (QCSEE) Program. Hamilton Standard conducted preliminary design study of a variable pitch fan actuation system for the QCSEE under General Electric Company purchase order 200-4XX-14G31376, a subcontract to NASA's QCSEE Program. Trade-off studies of several actuation concepts were made with reference to weight, reliability and production cost. Relative evaluations of maintainability, development risk, development cost and background were also made. As a result of these studies, the cam/harmonic drive actuation system was selected because of its lowest weight, superior reliability and maintainability and reasonable production costs. Results of this preliminary design study are presented in detail in Hamilton Standard Report SP 08A74. Summarizing excerpts from the report are provided in APPENDIX D.

A second actuator was also developed by the General Electric Company. Details of the design of the General Electric actuator are presented in "QCSEE Ball Spline Pitch Change Mechanism Design Report", NASA CR 134873.

The objective of this report is to present the detail design parameter of the cam/harmonic drive actuation system for the QCSEE. The design principles and concepts presented in this report are relevant to incorporation of the variable pitch principle in any fan engine. During the course of the design, a static load test was conducted on the blade trunnion arm to verify that stress levels were within acceptable limits as calculated. The complete actuation system will be tested under simulated torque moments and centrifugal forces at Hamilton Standard before delivery to General Electric Company for engine test to demonstrate the required performance characteristics. Details of the QCSEE engine design are presented in QCSEE Under-the-Wing Engine Final Design Report (CR 134847).

SECTION 3.0

DESIGN REQUIREMENTS AND CRITERIA

The variable-pitch fan actuation system is designed in accordance with requirements defined in GE Specification M50TF1635-S1. A life requirement of 36,000 hours (48,000 mission cycles) was specified for all component parts, with the exception of bearings and standard nonreusable parts, when the actuation system was operated in accordance with the conditions specified in the Mission Duty Cycle presented in Figure 1. The mechanism is designed for no replacement of parts (including bearings and nonreusable parts) at intervals of less than 9,000 hours.

The variable pitch system must also meet the duty cycle requirements of the experimental engine, defined as follows:

Experimental Engine Duty Cycle

Item No.	Fan Speed (rpm)	Time (hours)
1	3447	.3
2	3347	1
3	3157	181
4	2841	500
5	2368	1000
6	947	1000

The above operation is assumed to occur on a 90° day.

In addition, the actuation system for the experimental engine ground test must be capable of providing the following:

- Item 1. No actuation required.
- Item 2. 10 actuations at 5 minute intervals in the range of operation from 5 degrees to 5 degrees closed.
- Item 3. 500 total reversals through flat pitch and stall. 1000 actuations at 5 minute intervals in the range of operation from 5 degrees open to 10 degrees closed.

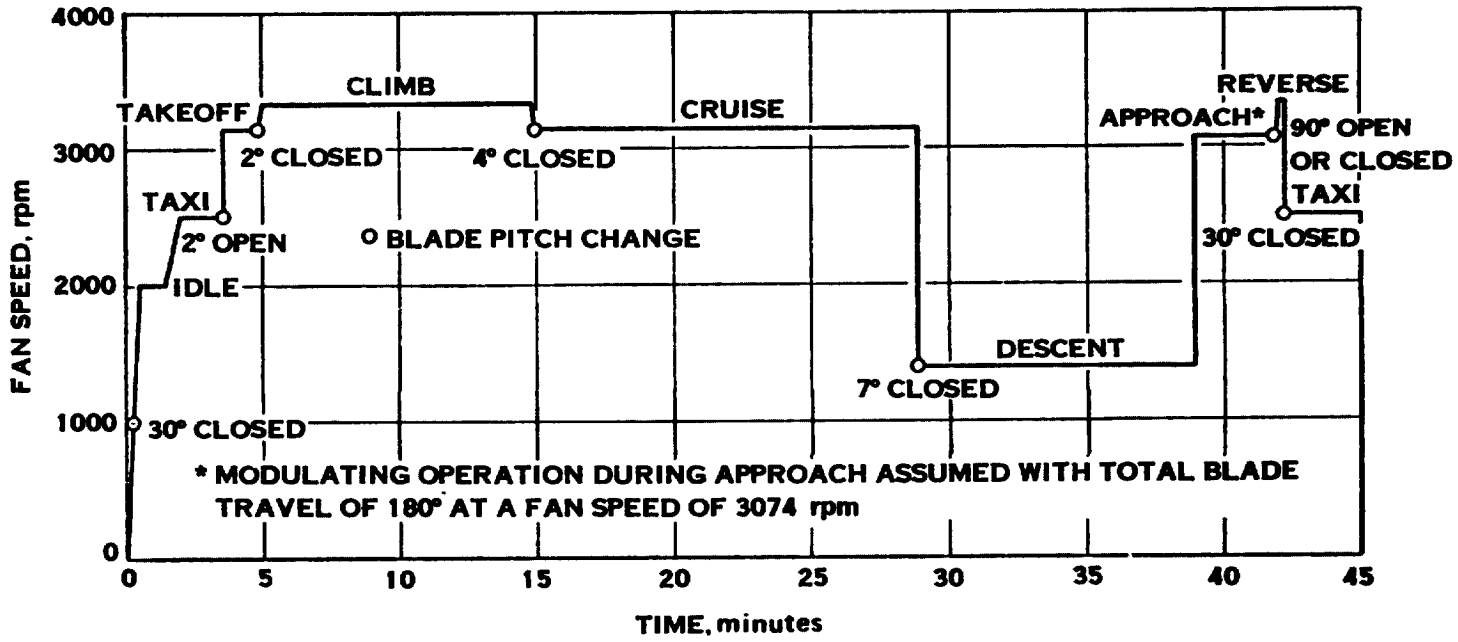

Figure 1. Mission duty cycle

- Items 4 through 6

  10,000 actuations in 5 degree increments from 5 degrees open to 30 degrees closed.

The actuation rates should cover the range from 0 degrees/second to an average rate of 135 degrees/second.

Additional system design requirements imposed at the start of the program are shown in Table I and Figure 2. Note that the maximum blade twisting moment is determined by the bird strike tolerance requirement which greatly exceeds the expected normal operating moments shown in Figure 2.

The design is also based on consideration of the following aircraft flight requirements:

- Following foreign object ingestion the dynamic pitch change mechanism must be capable of 10 additional cycles at maximum torque and actuation rate.

- The system must be capable of withstanding 20 g vibratory and should not impose over 5 g vibratory on the engine.

- The system must be capable of operation after exposure to fluids conventionally used by Airlines such as "Skydrol Type" hydraulic fluids, methylene chloride, and butyl cellasolve.

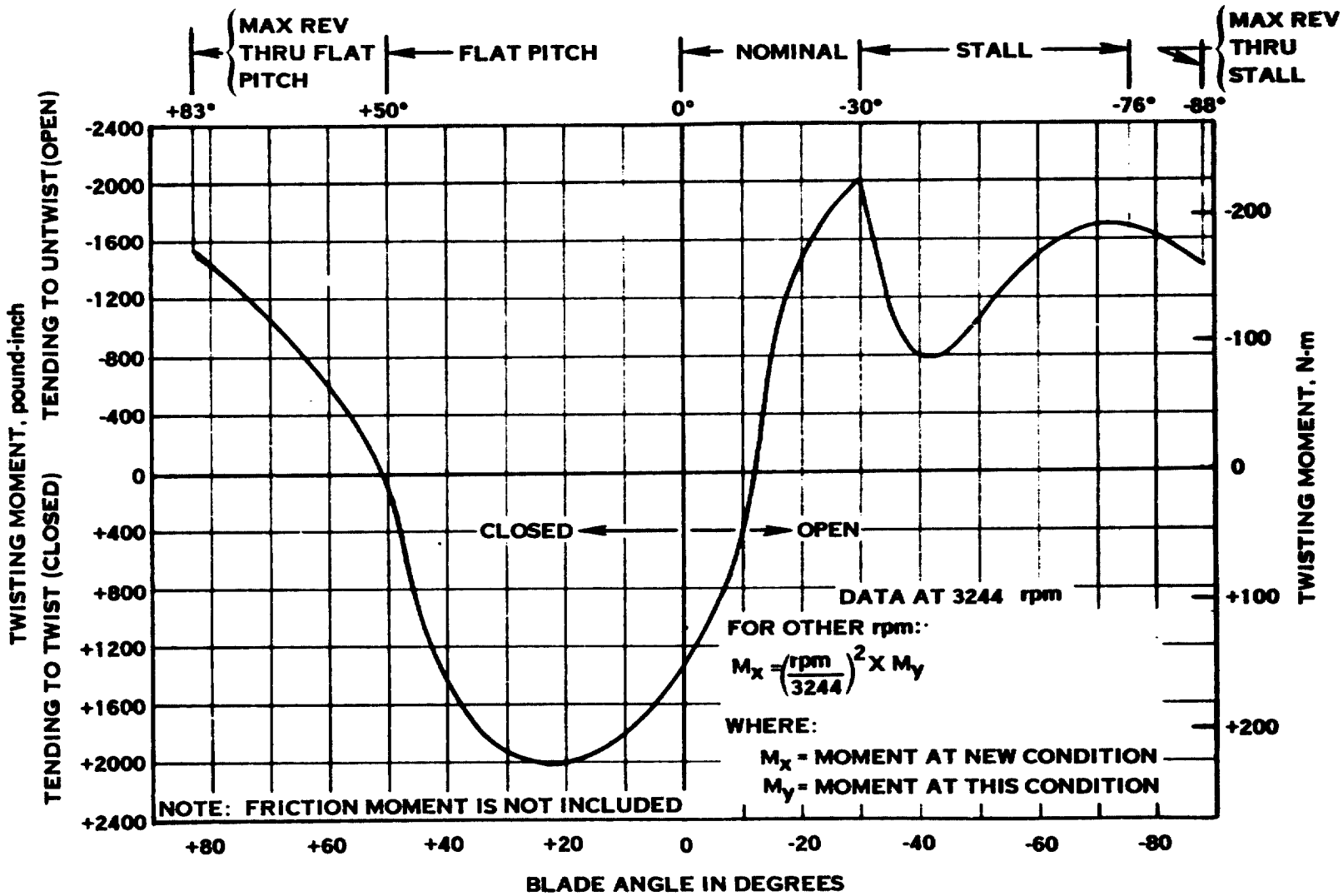

Figure 2. Blade maximum net twisting moment - 3244 rpm. SLS std day

Table I. Variable Pitch System Design Requirements

	Normal Range	Extreme Range
Fan rpm	0 - 3326	3450 without actuation
Blade Twisting Torque(1)	See Figure 2	1695 N-m (15,000 lb-in)(2)
Blade Overturning Moments		22,600 N-m (200,000 lb-in)(2)
Centrifugal Load for Blade and Dovetail only	15,196 kg (33,500 lb) (at 3200 rpm)	Must not burst at 4432 rpm (141% of T/O rpm)
Actuation Rate	135°/sec max	
Actuation Jogging at Blades	0.5° Steps min	
Feedback Signal Accuracy	±0.25° Blade Position	
Flight Maneuver Forces(3)	Per MIL-E-5007C (12/30/65) Par 3.14 except Precession Rate shall be one Radian per sec max	

(1) Add 800 in-lbs friction moment @ 3244 rpm to this data during actuation and zero friction for locked pitch.

(2) FAA Advisory Circular AC 33-1B, 4/22/70. These moments are calculated from the maximum impact force of a large 1.8 kg (4 lb) bird striking the blade at take-off engine output and at initial climb speeds.

(3) Polar moment of inertia of blades = 305 MN/m^2 (44,376 psi)

SECTION 4.0

SYSTEM DESCRIPTION

The Hamilton Standard variable pitch actuator system is shown schematically in Figure 3 and in detail in Figure 4. An electrical input command signal from the digital control to the electro-hydraulic servo valve (EHV) directs high pressure oil to a hydraulic motor in the beta regulator. This provides rotary mechanical input to the actuator differential gear train through a flexible drive shaft. Rotary motion is then transmitted through a no-back, harmonic drive, rotating cam and cam follower arms to the blade trunnions. There is a fixed mechanical relationship between hydraulic motor rotation and blade angle (beta). Two Linear Variable Differential Transformers (LVDT's) driven by the hydraulic motor output shaft provide a blade angle feedback signal to the digital control to close the control loop and null the input signal when the blades reach the commanded position.

The overall gear ratio from the blades to the drive shaft is nearly 1000:1 with most of the ratio (201:1) taken near the blades in the harmonic drive. This permits the low-torque power transmission elements between the beta regulator and the harmonic drive to be designed for low weight and improved blade angle accuracy.

The mechanical pitch change command and blade angle feedback functions are provided by the beta regulator module which is remotely mounted in a readily accessible area of the engine core cowling. A simplified schematic of the beta regulator is shown in Figure 5. A blade angle change command from the engine control to the EHV mounted in the accessory section, causes movement of the servo valve to direct supply oil to either the open (toward feather) or closed (toward flat) pitch ports of the hydraulic motor. The hydraulic motor output drives the flexible shaft to change blade angle and drives two LVDT's through a worm gear and screw to provide an electrically redundant blade position feedback. Electrical limit switches are provided to cut off the command signal to the EHV if a blade angle is commanded beyond the maximum operating range. Pressure relief valves across the hydraulic motor ports limit input pressure to 3000 psi during rapid accelerations of the actuator system.

The rotary output of the beta regulator is transmitted to the actuator differential gear train through a flexible drive shaft passing through the engine reduction gearing. The shaft core is encased in a flexible teflon lined casing supported in a rigid conduit mounted on the engine reduction gear support. Continuous engine lubrication oil flow is directed through the casing from the beta regulator end to lubricate the shaft core and the actuator components.

A planetary differential gear train is utilized to cross the rotating boundary of the fan. The differential gearing is a conventional 5:1 ratio phase difference type with a grounded sun gear, an input sun gear driven by the flexible shaft, three pairs

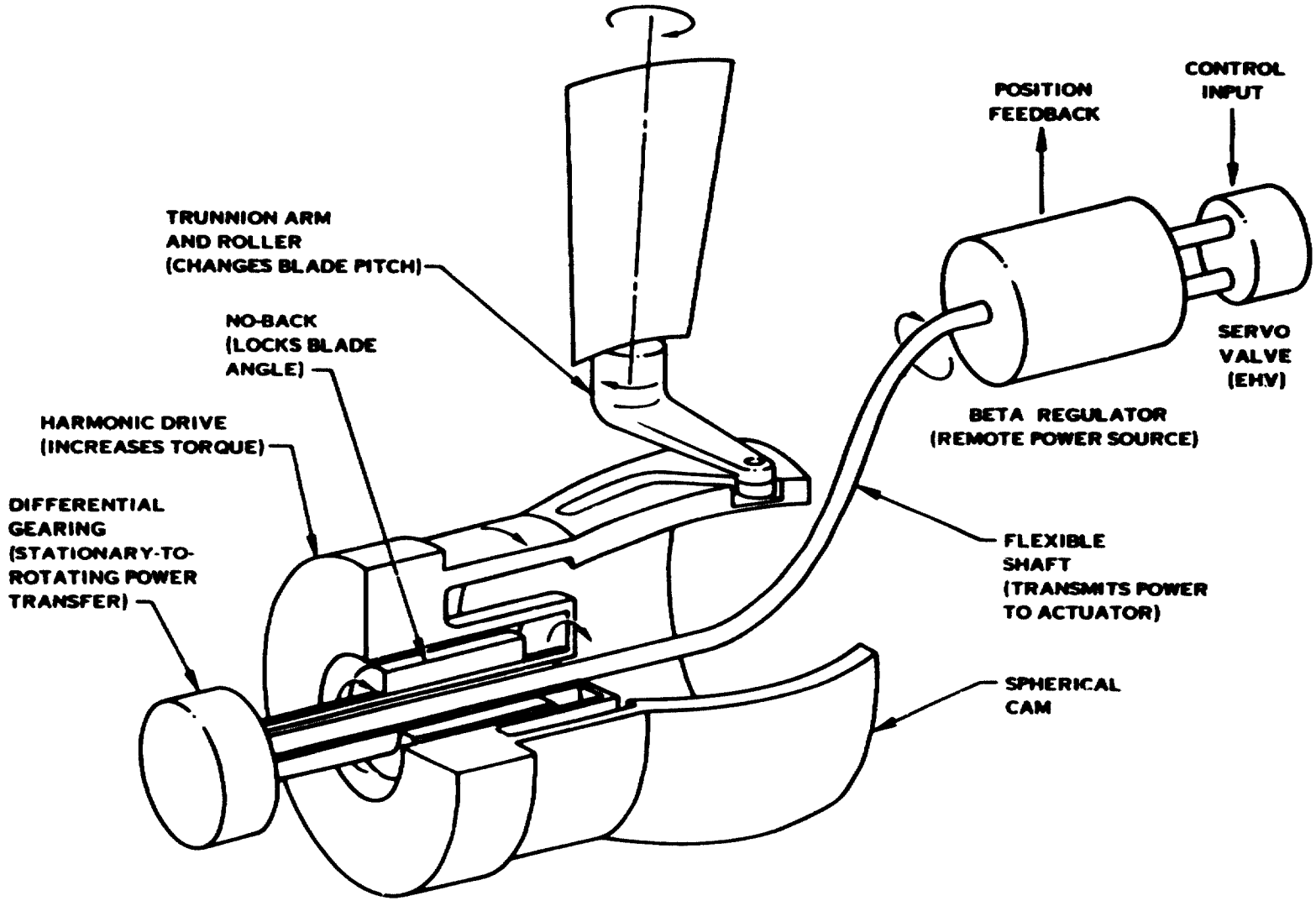

Figure 3. Actuator system functional schematic

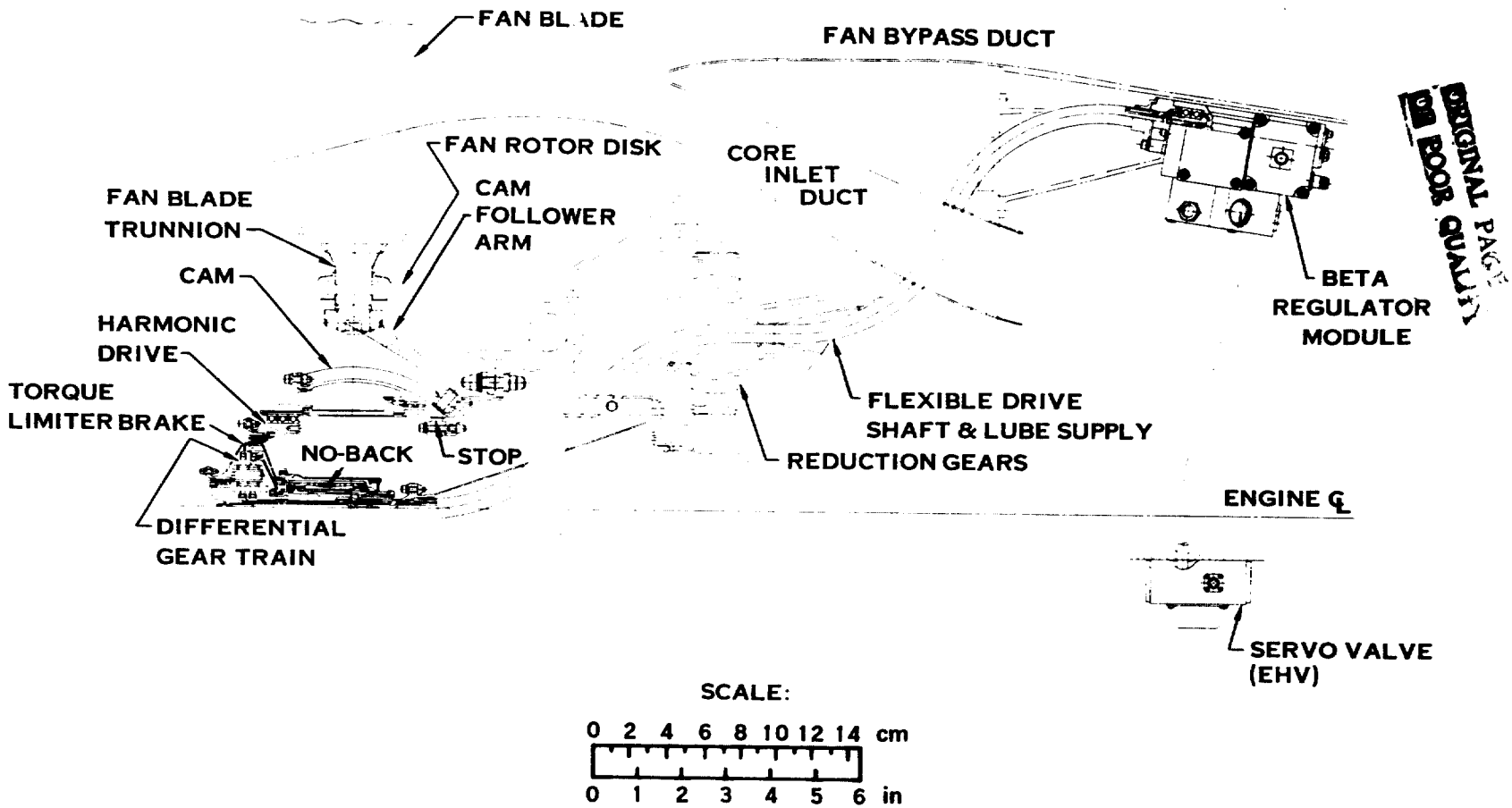

Figure 4. QCSEE cam/harmonic drive variable pitch actuator system

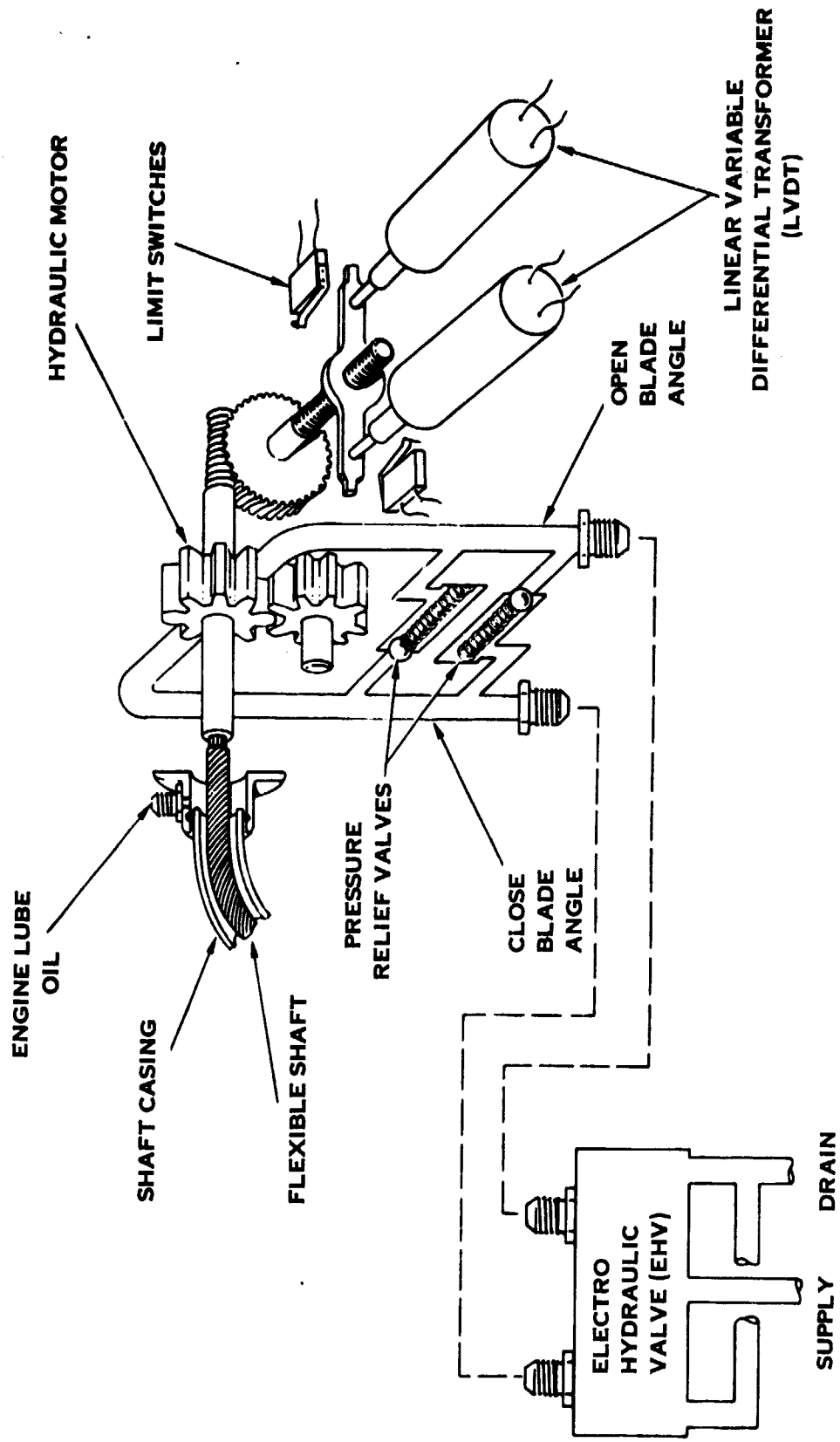

Figure 5. Beta regulator schematic

of planet gears on a bearing supported cage, a reference speed ring gear fixed to the fan disk and an output ring gear driving the no-back input. With no pitch change input the output ring gear rotates at fan speed. Rotation of the input sun gear during pitch change causes the output ring gear to either advance or recede with respect to the fan speed. This change in output is the input to the no-back. The differential gears and bearings are lubricated by oil directed outward centrifugally from the sun gear shafts.

A bi-directional spring clutch or "no-back" is provided between the differential gearing and the harmonic drive to maintain the set blade angle position in the absence of a pitch change command. This device consists of a self-energizing steel spring which is in contact with the inner surface of a fixed housing, the input and output shafts and the necessary couplings and bearings. When holding a fixed blade angle, the blade loads are transmitted to ground (housing) through the spring. When the input acts against opposing blade loads (raising the load), the spring slides in the housing and reacts no blade loading. When the input acts against aiding blade loads (lowering the load), the input releases the spring at the commanded pitch rate and the blade load energy is dissipated in frictional heat between the spring and housing. Due to the short duty cycle, the total heat rise is low and is contained within the no-back. Lubrication oil flows continually through the no-back and is supplied centrifugally from the sun gear shafts.

No-back housing torque is reacted by a disk-type torque limiter brake. The no-back is a high-gain locking device capable of locking more than a million in-lbs of torque at high friction coefficients, and the torque limiter limits no-back torque to acceptable structural limits during rapid pitch change decelerations. The brake disks are lubricated by oil supplied centrifugally from the differential gearing.

The harmonic drive provides the primary gear reduction for the mechanical actuator and increases the input torque to the level required to change blade pitch. Four basic elements are incorporated in this high-ratio (201:1) mechanical transmission of 50,000 lb-in output. They are: a three-lobed harmonic-shaped wave generator input plug for symmetrical loading, a triplex split inner race ball bearing set for high radial stiffness, a flexible spline (flex spline) to convert from the harmonic lobe shape to a grounded circular shape with minimum frictional losses, and a stiff circular output spline which drives the blade pitch cam.

The thin-race ball bearings are pressed on the three-lobed wave generator plug and assume the three-lobe harmonic shape. Spline teeth on the outside diameter of the flex spline mesh with spline teeth on the inside diameter of the circular spline at the three lobe locations. Circular splines on the other end of the flex spline ground it to the fan disk. Due to a three-tooth difference in number of teeth between the circular spline and flex spline (603-600=3), one revolution of the wave generator input rotates the circular spline output 3/603 or 1/201 of a revolution.

Lubrication oil for the harmonic bearings and splines is supplied centrifugally from the differential gearing and no-back.

The cam and follower arms convert output rotation of the harmonic drive to fan blade angle change. Titanium follower (or trunnion) arms, splined and clamped to the blade trunnions, engage individual cam slots in the spherical cam surface through cam rollers to synchronize the blades and sum the blade torques. The radial axis defined by the roller and cam track centerlines always intersects the fan axis of rotation at the same point similar to the apex point of a bevel gear mesh. Figure 6 shows the relationship between the blades and trunnion arms for both the reverse through stall and reverse through flat pitch configurations. Blade angle convention, allowable blade angle travel and both forward and reverse thrust positions are also shown in Figure 6.

Cam support is provided by a preloaded duplex bearing set mounted on a support ring attached to the fan disk mounting flange for accurate balance control. Lubrication oil from the harmonic drive lubes the bearing set and is returned centrifugally to the engine scavenge area. A single dynamic oil seal with centrifugal venting precludes a dynamic pressure head.

Fixed mechanical stop lugs between the cam and cam support ring restrict the blades to 7° overtravel at each end of the maximum operating range.

The component speed/torque relationships are summarized in Table II. The actuator load condition presented in the table represents the peak blade twisting moment at β_F=22° from Figure 2 of GE Specification M50TF1635-S1 applied as an opposing torque on the actuator at the specified fan rpm and at maximum pitch change rate.

Table II. Component Operating Characteristics

	rpm	Gear Ratio	Efficiency (%)	Operating Torque N-m	(lb-in)
Blade	22.5	-	-	288.15	(2550)(1)
Harmonic Output	17.3	0.97	94	5683.90	(50,300)
Harmonic Input	3477	201:1	75	37.74	(334)
Differential Input	17,385	5:1	98	7.68	(68)
Flex Shaft Input	17,385	-	90	8.59	(76)
Hydraulic Motors (2)	14,490	0.833	99	10.40	(92)

(1) Blade torque includes 30.51 N-m (270 lb-in) counterweight balancing effect of trunnion arm.

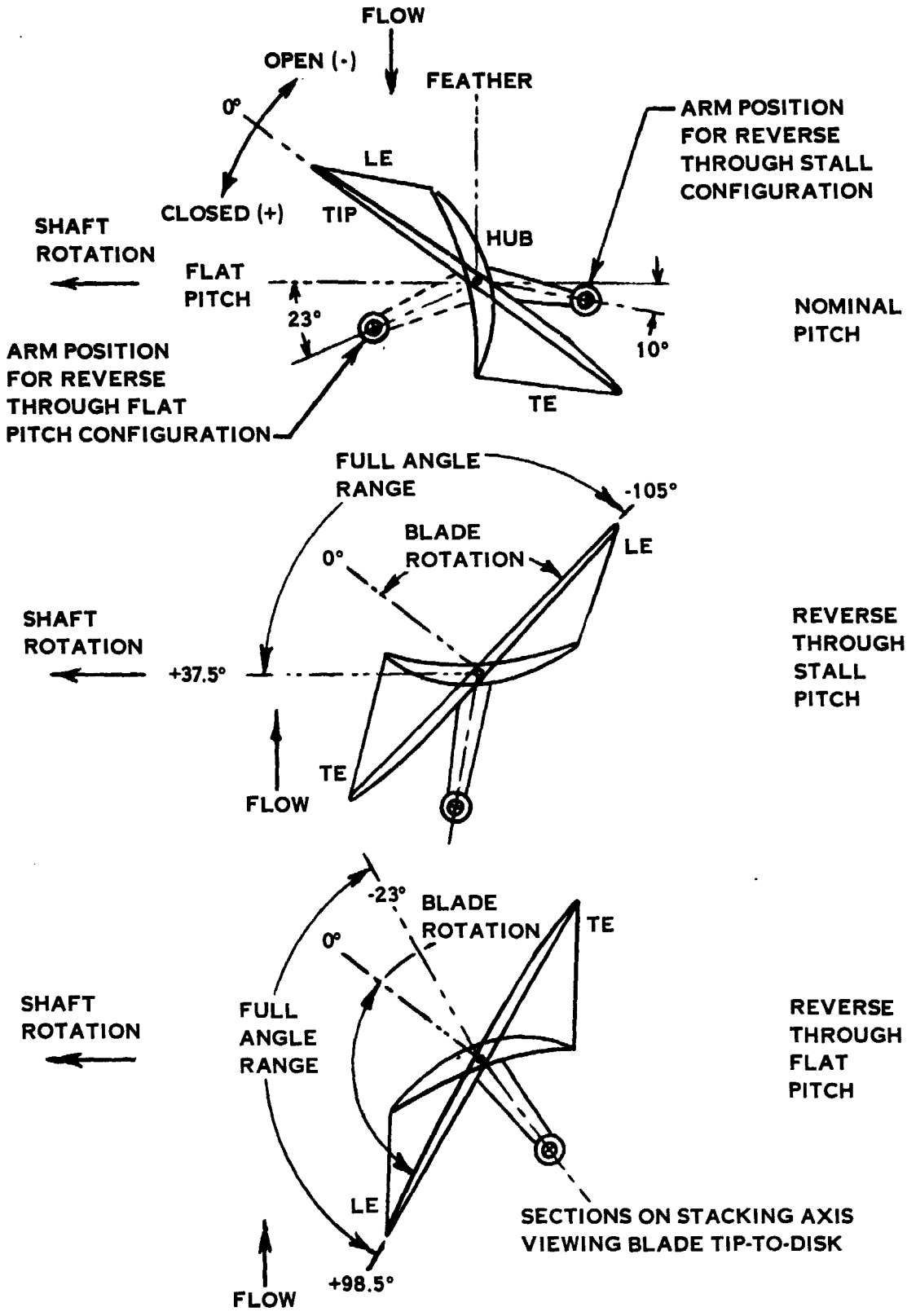

Figure 6. Blade/arm geometry at different pitch angle settings

The data in Table II are for 318.66 N-m (2820 lb-in) twisting moment per blade at a blade pitch angle of + 22° (closed) at 3244 fan rpm and 135 deg/sec pitch change rate toward open blade angle. This condition requires 1739 cm^3/s (27.6 GPM) at 1517 N/cm^2 (2200 psi) pressure differential across the motors.

SECTION 5.0

COMPONENT DESIGN

5.1 TRUNNION ARM AND ROLLER

The trunnion arms and rollers shown in Figure 7 produce a counterweight effect which balances a portion of the blade twisting moment to reduce system power requirements. A steel cam roller is attached to each titanium arm by a steel pin pressed and cross-pinned to the arm lug. The arm is shot peened and coated with dry film lubricant to inhibit fretting at the trunnion spline and retention bearing. A thin chrome plating is applied to the roller and pin for corrosion protection and to provide a hard bearing surface for the roller bushing. Fibriloid woven teflon bushing and thrust washers are bonded to the roller to provide a low friction bearing requiring no additional lubrication. The arm and roller design characteristics are summarized in Table III. The contribution of the arm and roller to total blade twisting moment is represented by: $M_{arm} = -790 \sin \left[2(\beta_F - 10)\right]$.

The arm is designed basically for minimum deflection with the critical stresses occurring in the roller pin lug area. Centrifugal loading, F_C, produces arm bending and the roller/cam normal load, F_R, produces transverse and longitudinal bending, axial force and torsion in the arm. Maximum arm loads occur with the arm axis located near the plane of fan blade rotation ($\beta_F = +7^\circ$ closed) at 3347 rpm. At this condition the maximum operating roller load, F_R = 3114N (700 lbs) at 25,199 cmN (2330 lb-in) blade torque, acts at $\theta = 32^\circ$. F_R is equal to 19349N (4350 lbs) at the blade bird strike torque of 169,500 cmN (15,000 lb-in). Moment distribution due to F_C is shown in Figure 8.

The data in Table II are for 318.66 N-m (2820 lb-in) twisting moment per blade at a blade pitch angle of + 22° (closed) at 3244 fan rpm and 135 deg/sec pitch change rate toward open blade angle. This condition requires 1739 cm^3/s (27.6 GPM) at 1517 N/cm^2 (2200 psi) pressure differential across the motors.

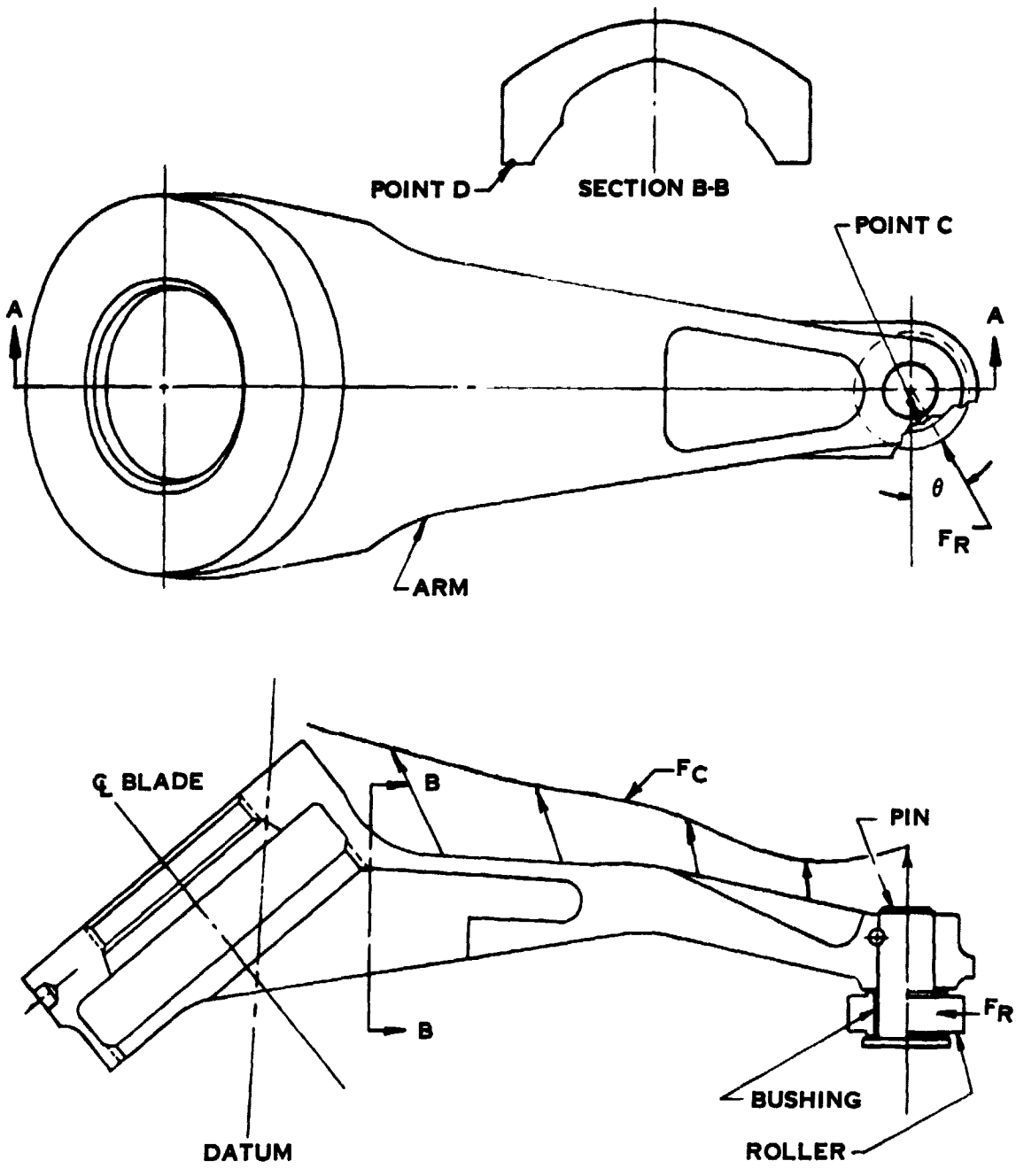

Figure 7. Blade trunnion arm and roller

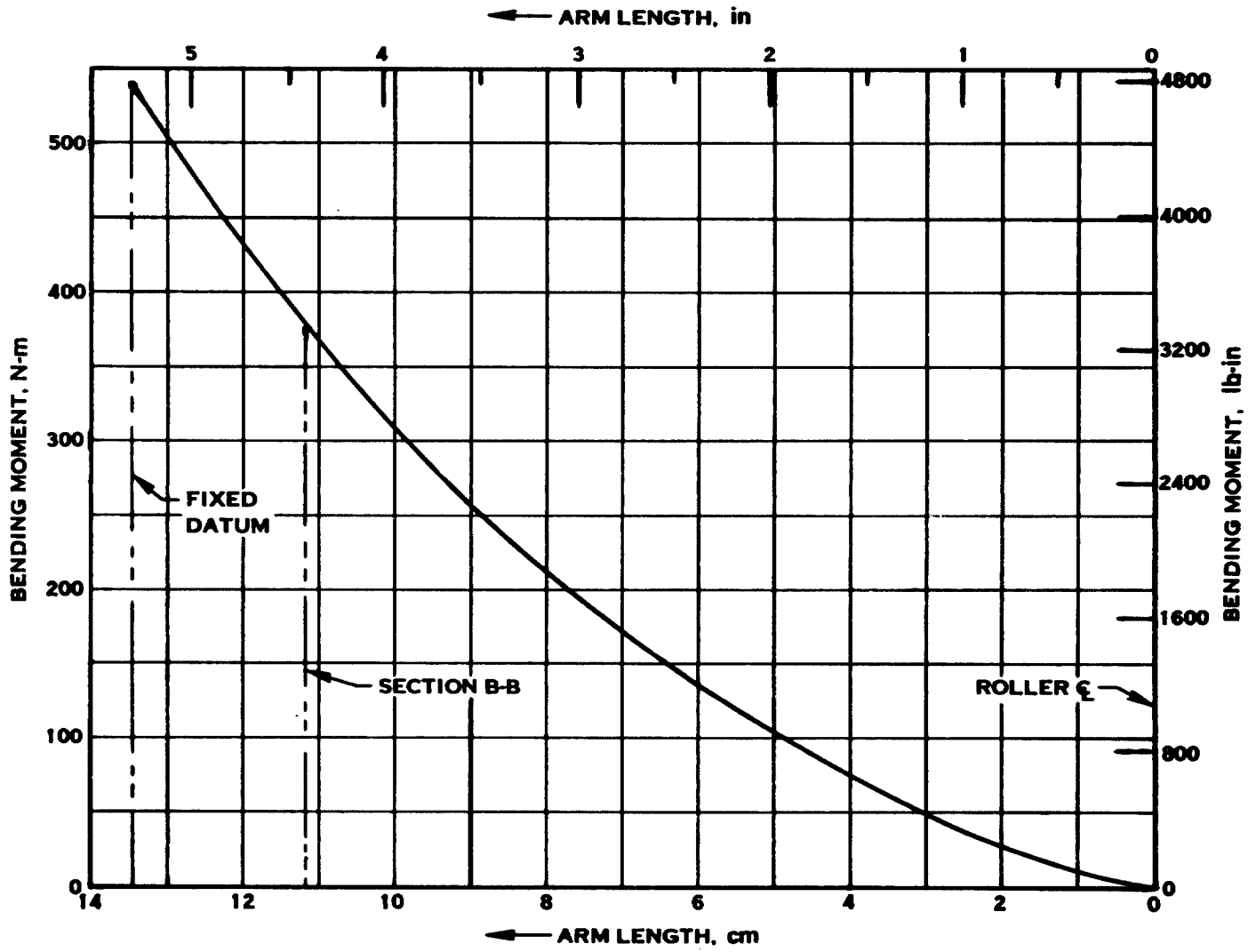

Figure 8. Trunnion arm bending moment distribution from centrifugal force at 3347 rpm

Table III. Arm and Roller Design Characteristics

Normal Torque Range:	0 to 263.3 N-m[1] (0 to 2330 lb-in)
Bird-Strike Torque:	1695 N-m (15,000 lb-in)
Trunnion rpm:	0 to 27
Roller rpm:	0 to 500
Roller Mechanical Efficiency:	94%

Selected Materials:

Item	Material	Heat Treat	Surface Treatment
Arm	AMS 4928	30-39 Rc	Flange peened and dry film coated
Roller	AMS 5630	53-58 Rc	Chrome plated 0.0001 - 0.00025 thk.
Roller Bushing	Fibriloid	-	-
Pin	AMS 6415	36-40 Rc	Peened, chrome plated 0.0004 - 0.0006 thk $\sqrt{8}$ finish

Arm and Roller Assembly Weight:

0.43 kg (0.94 lbs.) each
7.67 kg (16.9 lbs.) total for 18

(1) Blade torque includes 30.51 N-m (270 lb-in) counterweight balancing effect of trunnion arm.

Maximum bending stress occurs in Section B-B (Figure 7) at point D ($K_t = 1.0$). The resulting stress levels are shown in Table IV. Maximum arm deflections are specified at the roller, and were obtained by graphical integration of M/EI over the arm length. Results are presented in Table V. F_c at 3347 rpm and F_R equal to 3144N (700 lb) are the maximum arm loads. The cam slot height has been designed to preserve adequate roller engagement for these radial deflections in addition to fan disk deflections and tolerances. Transverse arm deflections are accommodated within the $\pm 0.25^\circ\beta$ accuracy required.

The roller, roller bushing, roller pin and arm lug stresses were evaluated under cyclic loading conditions in addition to bird strike load. Two load cases (Figure 9) were considered. Load Case No. 1 represents roller loading during approach modulation over a 5 degree blade pitch angle range. A total of 864,000 cycles are required to meet the specification requirements. Load Case No. 2 represents roller loading for the full blade pitch angle range during reverse through stall. A total of 48,000 reverse cycles plus the 864,000 cycles for approach modulation are required to meet the full system life. Stress analysis results based on these requirements are summarized in Tables VI, VII and VIII.

Trunnion arm spline data and stresses are given under items 19 and 20 of Table XXIV, Section 5.10.

Table IV. Trunnion Arm Stresses

Load	Stress(1)	Required Cycles	Allowable Cycles
F_c	17169 N/cm^2 (24,900 psi)		
F_R = 3114N (700 lb)	6000 N/cm^2 8,700 psi		
F_c+ [F_R = 3114N (700 lb)]	0 to 23,200 N/cm^2 (33,600 psi)	10^5	10^8
	11,600 ± 11,600 (16,800 ± 16,800)		
F_c + [F_R = 19349N (4350 lb)]	54,471 N/cm^2 (79,000 psi)	1	MinUTS = 81,361 N/cm^2 (118,000 psi)

(1) Maximum bending stress at point D, Section B-B (Figure 7).

Table V. Trunnion Arm Deflections

Load	Deflection at Roller	Direction
F_C	0.123 cm (0.0485 in.)	Radially outward from fan axis of rotation.
F_R	0.005 cm (0.002 in.)	Radially inward from fan axis of rotation.
F_R	0.023 cm (0.0092 in.)	Transverse to arm axis.

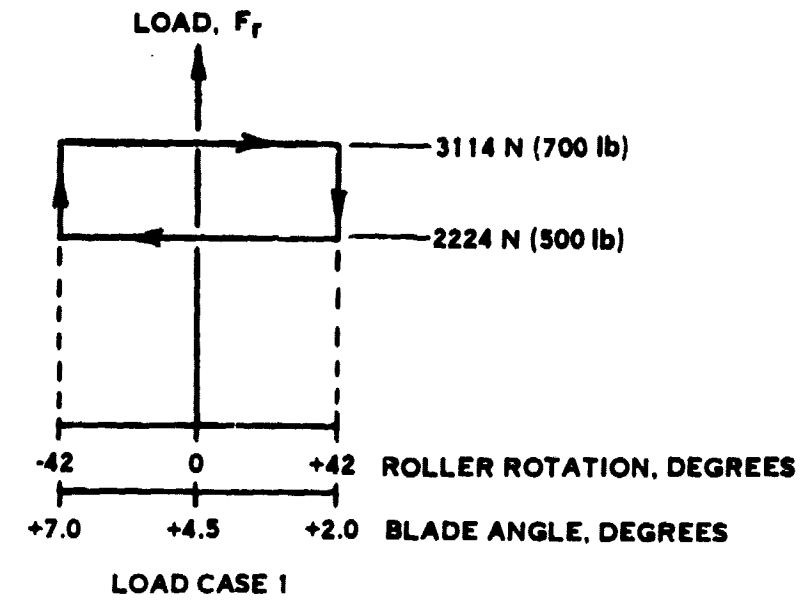

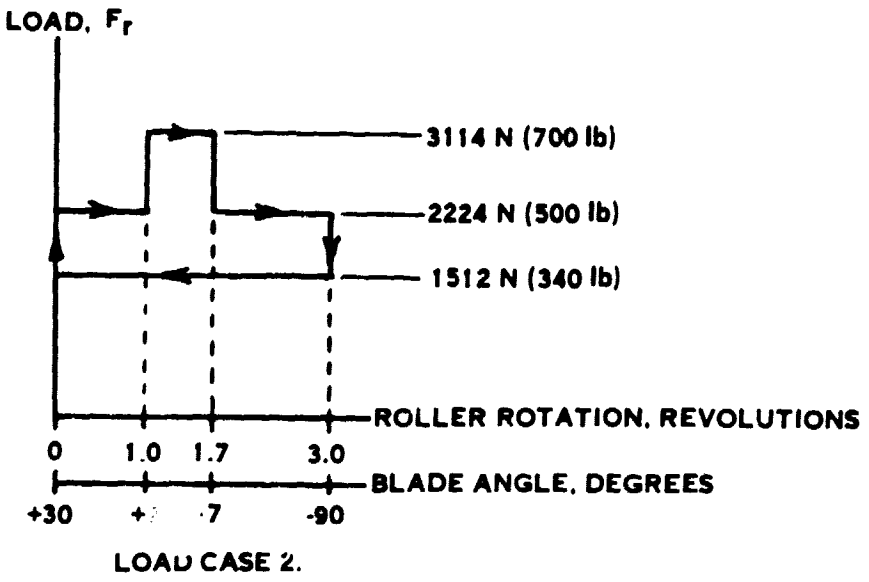

Figure 9. Roller cyclic load conditions

Table VI. Roller and Pin Stresses

Roller Load, F_R	Required Cycles	Roller Contact Stress	Allowable Contact Stress	Bushing Compressive Stress	Allowable Compressive Stress
0–3114N (0–700 lbs)	2×10^6	146,170 N/cm^2 (212,000 psi)	151,690 N/cm^2 (220,000 psi)	3447 N/cm^2 (5000 psi)	27,580 N/cm^2 (1) (40,000 psi)
19,349 (4350)	1	266,830 (387,000)		21,374 (31,000)	68,948 (1) (100,000)

Pin Bending Stresses ($K_t = 1.0$):

Roller Load, F_R	Bending Stress	Required Cycles	Allowable Cycles
1557 ± 1557N (350 ± 350 lbs)	7722 ± 7722 N/cm^2 (11,200 ± 11,200 psi)	0.48×10^5	10^8
2669 ± 445 (600 ± 100)	13238 ± 2206 psi) (19,200 ± 3200)	1.0×10^6	10^8
2313 ± 801 (520 ± 180)	11,473 ± 3971 (16,640 ± 5760)	0.96×10^5	10^8
1112 ± 1112 (250 ± 250)	5516 ± 5516 (8000 ± 8000)	0.96×10^5	10^8
19,349 (4350)	95,148 (138,000)	1	Min UTS = 110,317 N/cm^2 (160,000 psi)

(1) Typical vendor-quoted allowable stresses for "Fibriloid"

Table VII. Arm Lug Stresses

Bearing Stress at Pin Socket:

Roller Load, F_R	Bearing Stress	Required Cycles	Allowable Cycles
1557 ± 1557 N (350 ± 350 lbs)	6895 ± 6895 N/cm^2 (10,000 ± 10,000 psi)	0.48×10^5	10^8
2669 ± 445 (600 ± 100)	11,818 ± 1972 (17,140 ± 2860)	1.00×10^6	10^8
2313 ± 801 (520 ± 180)	10273 ± 3544 (14,900 ± 5140)	0.96×10^6	10^8
1112 ± 1112 (250 ± 250)	4928 ± 4928 (7140 ± 7140)	0.96×10^6	10^8
19,349 (4350)	85,700 (124,300)	1	Bearing Ultimate = 122,000 N/cm^2 (177,000 psi)

Table VIII. Arm Lug Stresses

Combined Axial and Bending Stress at Point "C" (Figure 5):

Roller Load, F_R	Stress	Required Cycles	Allowable Cycles	n/N
1557 ± 1557 N (350 ± 350 lbs)	18,478 ± 18,478 N/cm^2 (26,800 ± 26,800 psi)	0.48×10^5	10^5	0.48
2669 ± 445 (600 ± 100)	31,647 ± 5275 (45,900 ± 7650)	1.00×10^6	10^8	-
2313 ± 801 (520 ± 180)	27,441 ± 9515 (39,800 ± 13,800)	0.96×10^5	10^8	-
1112 ± 1112 250 ± 250)	13,170 ± 13,170 (19,100 ± 19,100)	0.96×10^5	10^6	0.10
				Σ n/N = 0.58
19,349 (4350)	71,775 (104,100)	1	Min UTS =	81,360 N/cm^2 (118,000 psi)

5.2 CAM ASSEMBLY

The cam assembly shown in Figure 10 includes a spherical cam, duplex ball bearing set and cam support housing. The spherical cam slots engage the trunnion arm rollers and are contoured to obtain a variable torque ratio. This permits the blade/cam ratio to be tailored to the blade torque curve to reduce system power requirements. The relationships of blade/cam torque ratio to blade angle for the reverse through feather and reverse through flat pitch configurations are shown in Figures 11 and 12, respectively. Also shown are diagrams of trunnion arm positions about the blade stacking axis at various blade angles. These diagrams represent the positions when viewed from blade tip to disk. The cam is made of M250 maraging steel heat treated after machining to 48-52 Rc hardness. Wall thickness between cam slots varies with stroke and material is removed where possible to reduce weight. A Dow Corning 3400A molybdenum disulfide coating is applied all over the cam for track lubrication and corrosion protection.

The roller load normal to the cam track has a component tangent to the cam about the axis of rotation which develops the cam torque reacted by the harmonic drive output, which is bolted and splined to the forward end of the cam. The axial component of the roller load is reacted by the preloaded duplex cam support bearing set. Support for the cam and bearings is provided by a forward steel cone attached through a bolted face spline to a titanium adapter cone mounted on the disk mounting bolts. A face spline joint is used to provide accurate centering of the parts for balance control coupled with ease of disassembly for maintenance. Eighteen 1/4 inch steel bolts preload the joint against separation under maximum operating loads and temperature.

The primary stresses in the cam are contact stress and localized slot wall bending stress due to roller load. Stress and deflection were determined in the support rings by a computer shell program. Stresses were maximum at the cone-to-flange junctures and ring stiffness was designed to maintain roll deflections under the duplex bearings within acceptable limits. The cam assembly design characteristics are summarized in Table IX.

Table IX. Cam Assembly Design Characteristics

Normal Input Torque Range:	0 to 5650 N-m (0 to 50,000 lb-in)
Blade/Cam Torque Ratio:	Reference Figures 9 and 10
Normal Cam rpm Range:	0 to 23

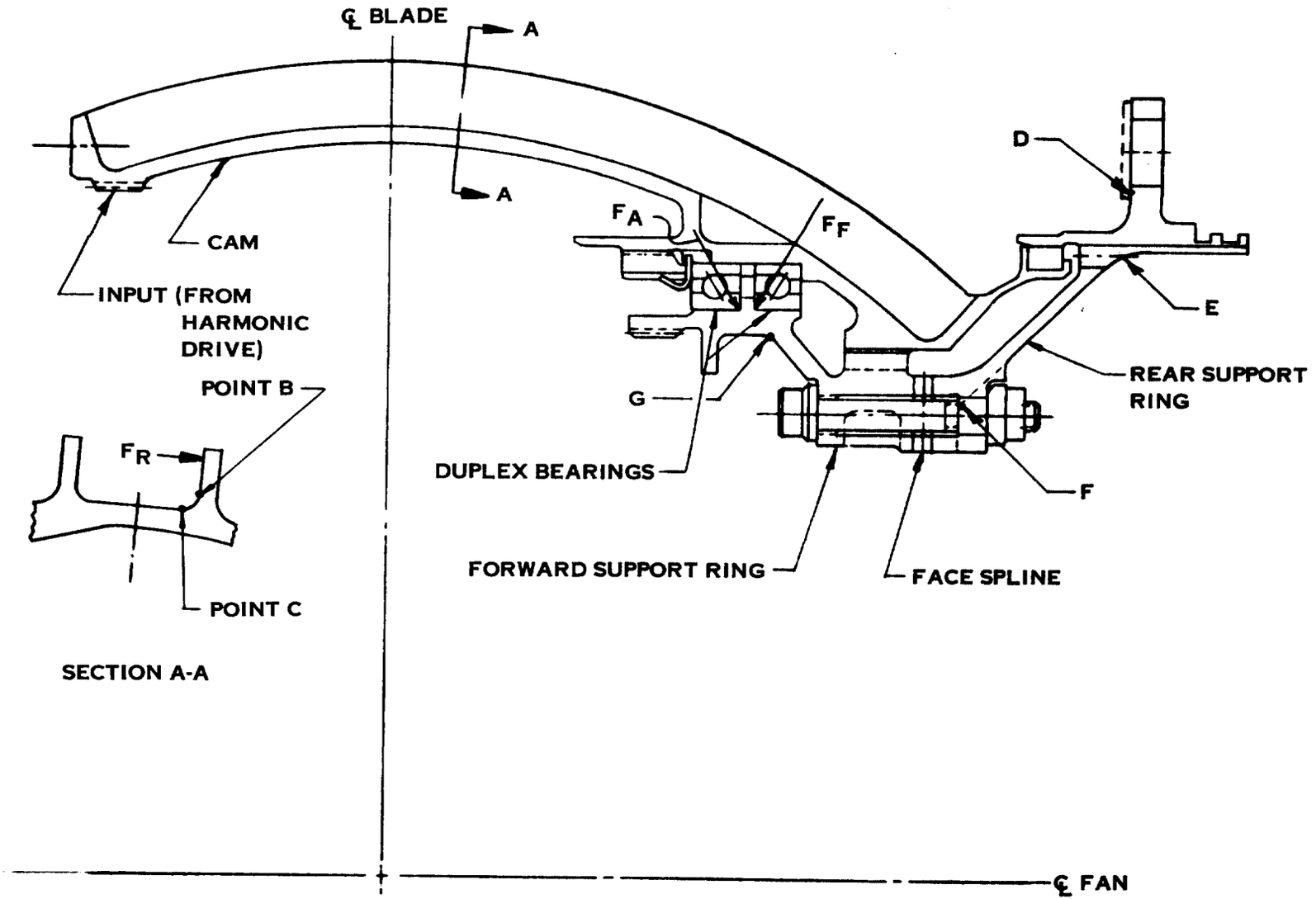

Figure 10. Cam assembly

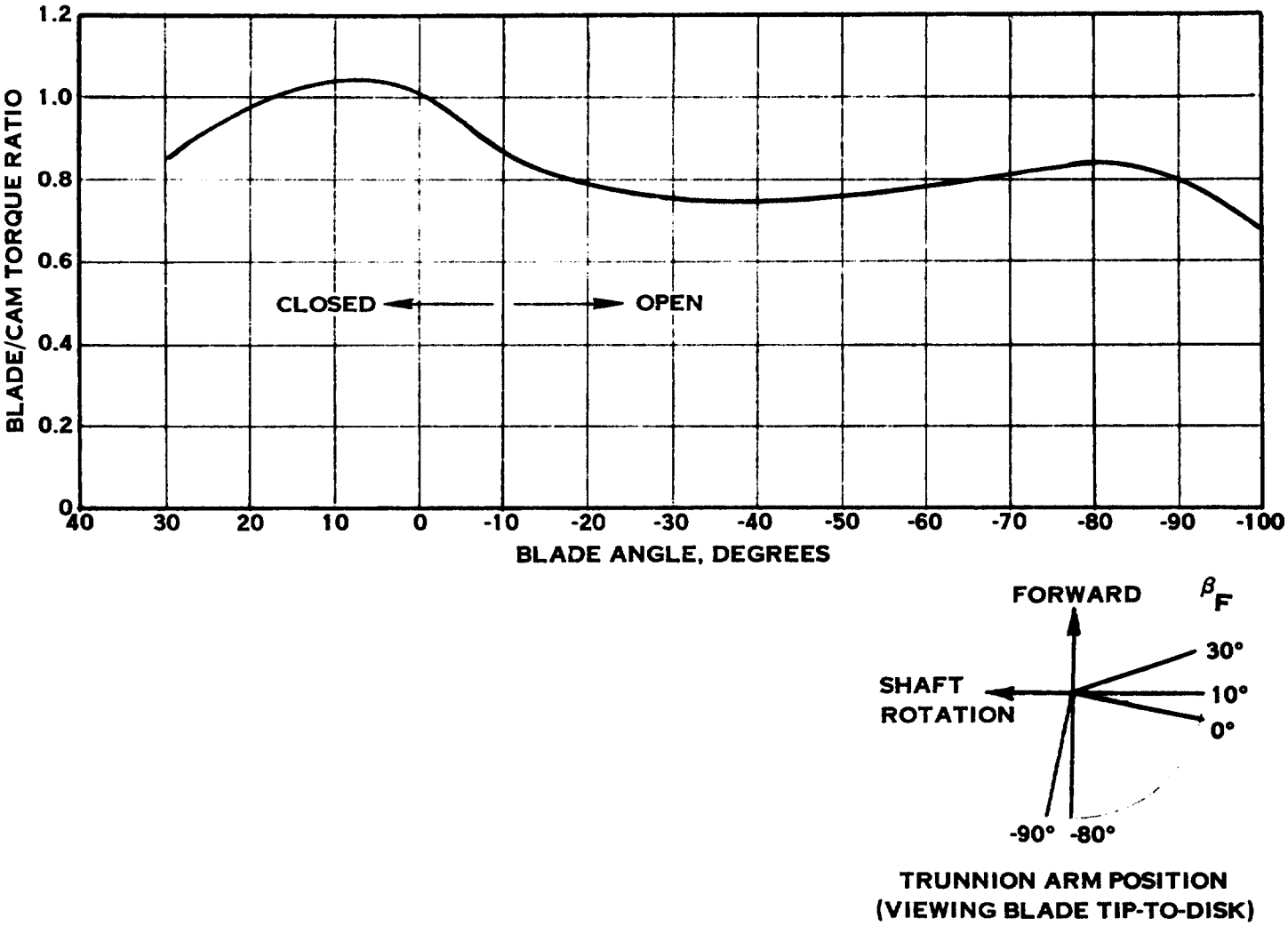

Figure 11. Cam ratio for reverse through stall

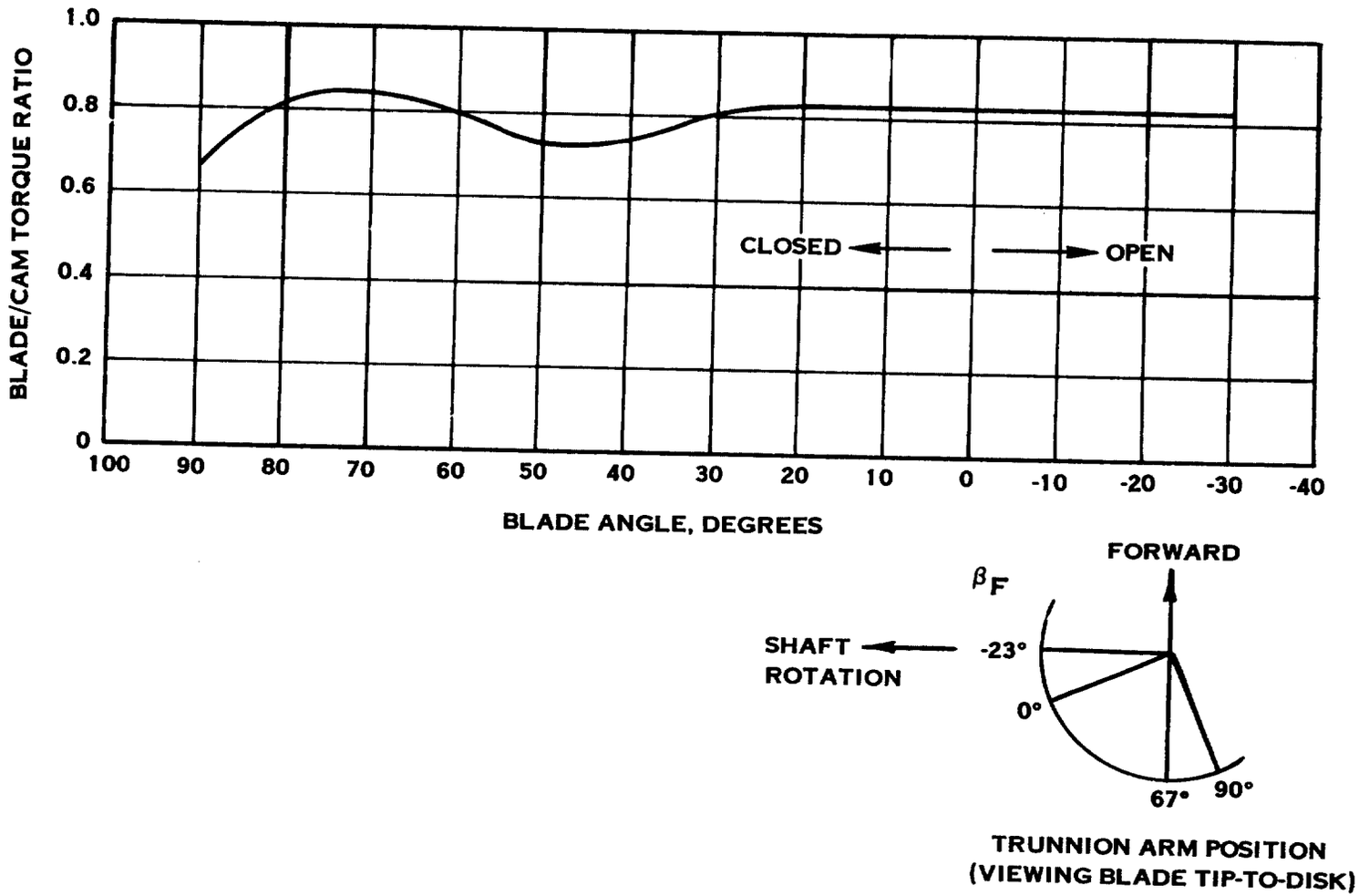

Figure 12. Cam ratio for reverse through flat pitch

Table IX. Cam Assembly Design Characteristics (Cont)

Selected Materials:

Item	Material	Heat Treat	Surface Treatment
Cam	AMS 6512	48-52 Rc	Dow Corning 3400A
Support, Rear	AMS 4928	30-39 Rc	Peened and Dow Corning 3400A
Support, Forward	AMS 6415	40-44 Rc	-
Bearing, Duplex	AISI 52100 (CEVM)	-	-

Cam Assembly Weight: 14.88 kg (32.8 lbs)

The maximum cam stress occurs in the cam slot wall, subjected to the roller load. The highest load occurs at Section A-A (Figure 10) resulting in a roller contact stress at the load, and a maximum wall bending stress in the wall fillet radius at Point B.

Evaluation of contact stresses under cyclic load conditions indicated that at the resulting stress conditions the total number of required cycles was 24% of the allowable cycles. Under bird strike conditions the contact stress in the cam wall reaches a level of 364,400 N/cm^2 (528,500 psi) versus an allowable minimum bearing ultimate strength of 258,563 N/cm^2 (375,000 psi). This indicates that local brinelling will occur which is considered acceptable for bird-strike. Cam wall contact stresses are summarized in Table X.

Analysis of the bending stress at Point B (Figure 10) indicates that at the resulting stress conditions the summation of required cycles is 13.7% of the total number of allowable cycles. Bird strike results in a stress at Point B of 159,275 N/cm^2 (231,000 psi) versus a minimum ultimate strength of 162,033 N/cm^2 (235,000 psi). The bird strike stress includes a factor of 1.4 representing material plastic flow. Bending stresses at Point B are provided in Table XI. Stresses at Point C are less than stresses at Point B.

Table X. Cam Wall Contact Stresses

Roller Load, F_R	Contact Stress	Required Cycles	Allowable Cycles	n/N
0-3114N (0-700 lbs)	146,170 N/cm^2 (212,000 psi)	0.48×10^5	2×10^6	0.024
0-1334 (0-300)	95,700 (138,800)	0.48×10^5	10^8	-
0-2224 (0-500)	116,660 (169,200)	0.48×10^5	10^8	-
534-2891 (120-650)	60,536-140,860 (87,800-204,300)	8.64×10^5	4×10^6	0.216
			Σ n/N =	0.240
19,349 (4350)	364,390 (528,500)	1	Bearing Ultimate =	258,550 N/cm^2 (375,000 psi)

Table XI. Cam Wall Bending Stresses

Roller Load, F_R	Bending Stress[1]	Required Cycles	Allowable Cycles	n/N
1557 ± 1557N (350 ± 350 lbs)	17,926 ± 24,132 N/cm^2 (26,000 ± 35,000 psi)	0.48 x 10^5	3.5 x 10^5	0.137
667 ± 667 (150 ± 150)	7695 ± 10,340 (11,160 ± 15,000)	0.48 x 10^5	10^8	-
1112 ± 1112 (250 ± 250)	12,825 ± 17,235 (18,600 ± 25,000)	0.48 x 10^5	10^8	-
1712 ± 1179 (385 ± 265)	19,720 ± 18,270 (28,600 ± 26,500)	8.64 x 10^5	10^8	-
				Σ n/N = 0.137
19,349 (4350)	159,270 (231,000)	1		Min UTS = 162,000 N/cm^2 (235,000 psi)

(1) Stress location is at Point B, Figure 10.
Stress concentration factor for cyclic stresses: $K_t = 1.34$

The cam support housing is shown as part of the cam assembly (Figure 10). The maximum loads on the housing are cam thrust loads of 31,136 N (7000 lb) aft and 48,038 N (10,800 lb) forward acting through the 30° contact angle duplex bearings. The resultant loads, F_A = 62,272 N (14,000 lb) and F_F = 96,077 N (21,600 lb), act around the housing periphery at the bearing mounting sections. Combined axial bending and torsional stresses at key housing points, D, E, F and G are presented in Table XII. Stress at Point D is based on forward load, F_F, only since the flange receives backing from the mating engine flange for aft loads. Stresses at the remaining points are based on reversed loading.

The critical housing deflection is the radial deflection at the support bearings. The maximum radial deflection, δ = 0.0033 cm (0.0013 in.) is a result of load, F_F = 96,077 N (21,600 lbs). The allowable δ required to maintain an acceptable contact angle under load is 0.0038 cm (0.0015 in.).

The bolted joint at the face spline between support housings has been designed to prevent flange separation at maximum loads, F_A and F_F, with minimum bolt preload at 394°K (250°F). Table XIII gives the bolted joint characteristics and bolt stresses. Face spline data is given in Table XXIV, Item 18, Section 5.10.

Design data for the duplex cam support bearing is provided in Table XXV, Section 6.0.

5.3 HARMONIC DRIVE

A cross-section of the harmonic drive component is shown in Figure 13. The harmonic drive is flange-mounted to the forward end of the spherical cam and drives the cam through this bolted and splined joint. A three-lobe harmonic drive was selected for this design instead of a two-lobe configuration because the three-lobe unit is inherently stiffer radially, and lighter due to more uniform load distribution. More effective radial support and centering of parts is possible with three lobes and should result in improved balancing capability. Except for the flex spline and bearing races, the harmonic drive components are designed for high radial stiffness. This minimizes radial deflection under load at the harmonic tooth mesh to maintain safe tooth stresses under operating loads and to increase the ratcheting capacity of the unit. Ratcheting can occur if radial and tangential deflections at the tooth mesh are sufficiently high to permit tooth tip-to-tip interference between the flex and circular spline teeth. For maximum assurance, a ratcheting capacity of three times the maximum operating torque or 16,950 N-m (150,000 lb-in.), has been designed into this harmonic drive by the addition of five pounds of additional weight. The ratcheting capacity of the flight-weight design is 12,653 N-m (112,000 lb-in.). All clearances, tolerances, deflections and thermal effects that affect tooth meshing under load were considered in the design.

Table XII. Cam Support Housing Stresses

Stress Location[1]	Stress N/cm^2	Stress (psi)	SCF[3] K_t	Required Cycles	Allowable Cycles
D	11,997 ± 11,997	17,400 ± 17,400	1.0	0.48×10^5	10^6 [2]
E	690 ± 12,825	1,000 ± 18,600	3.0	0.48×10^5	10^8
F	1,379 ± 13,997	2,000 ± 20,300	1.45	0.48×10^5	10^8
G	3,965 ± 27,028	5,750 ± 39,200	1.34	0.48×10^5	10^8

(1) Reference Figure 10.

(2) Allowable cycles at point D are based on acceptable stresses including possible fretting under the washer face.

(3) Stress Concentration Factor, K_t, is included in the stress values.

Table XIII. Bolted Joint Characteristics

Bolt Part Number: MS 9209-26
Number of Bolts: 18, equally spaced
Material: AMS 6304, 42-46 Rc
Size: 0.250-28 UNJ-3
Wrench Torque: 10.17-11.30 N-m (90-100 lb-in.)
Preload (@ μ_f = 0.15 to 0.10): 7673-12,900N(1725-2900 lbs.)
Maximum assembly stress
@ maximum preload and torque: 69362 N/cm^2 (100,600 psi)
Bolt bending stress due to
flange deflections: -896 to +1380 N/cm^2
(-1300 to +2000 psi)

Bolt axial stress from
loads F_A and F_F: -1815 to +2800 N/cm^2
(-2630 to +4060 psi)

Total maximum bolt stress: 73,500 N/cm^2
(106,600 psi)

Reduction in bolt load at 394°K (250°F): 890N (171 lbs)

Table XIII. Bolted Joint Characteristics (Cont)

Total maximum bolt stress @ 394°K (250°F), 0 applied load:	65247 N/cm^2 (94,630 psi)
Bolt stress = 69,360 ± 3540 N/cm^2 (100,600 ± 5930 psi)	
Required cycles:	0.48×10^5
Allowable cycles:	10^8

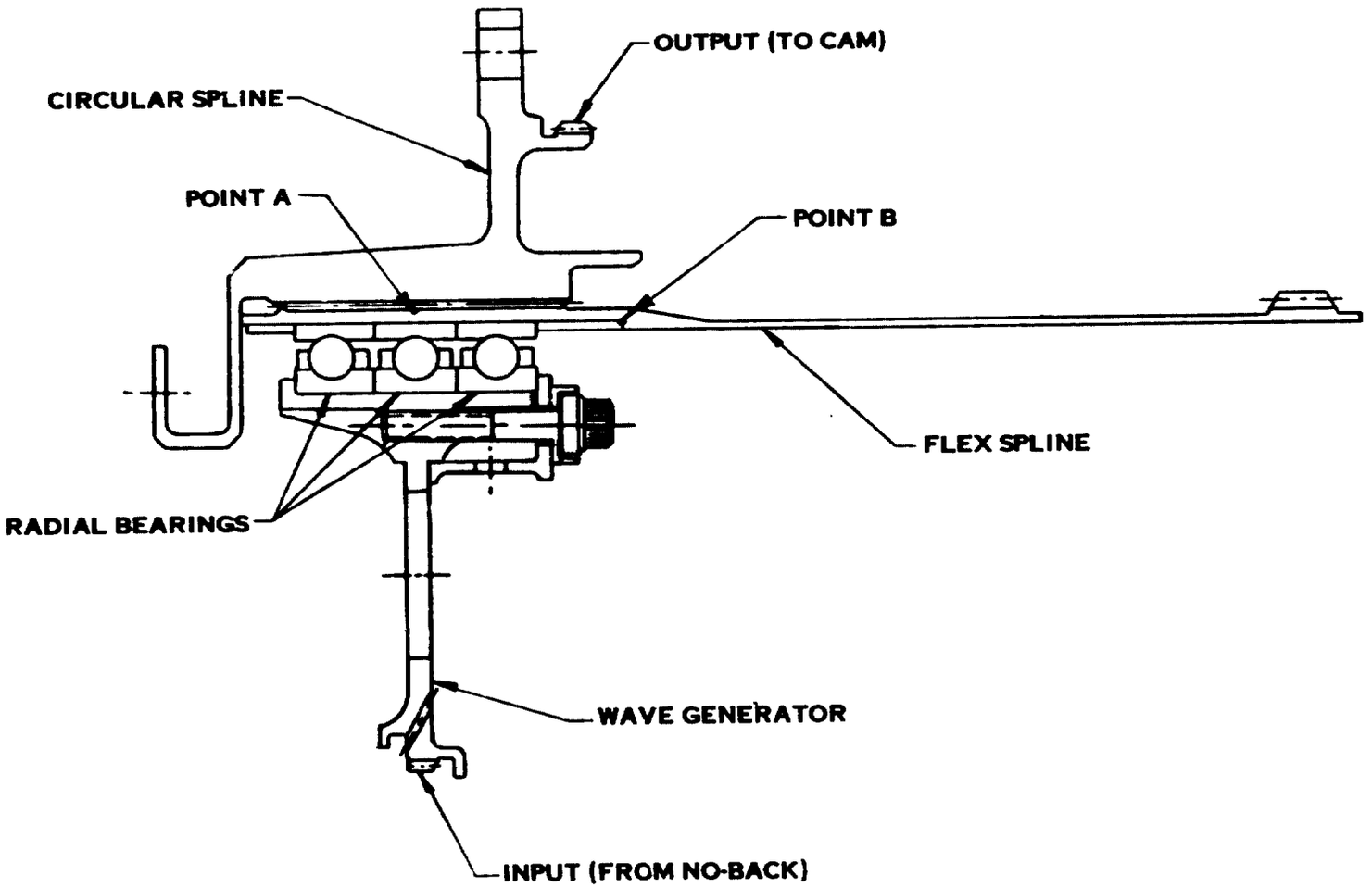

Figure 13. Harmonic drive

A computer shell program was utilized to arrive at a balanced stiffness design for the circular spline and wave generator. A computer program was developed to solve for the tooth load distribution at the three lobe meshes taking into account bearing radial stiffness along with the other members. Figure 14 shows the model used in this analysis. The four structural components shown schematically are the circular spline ring, the flex spline ring, the ball bearings represented as springs and the wave generator plug ring. The outer and inner bearing races were combined with the flex spline and wave generator plug, respectively, in the ring stiffness calculations and the small clearance between the outer race and the flex spline was assumed to have a negligible effect on the analysis. The actual number of balls was used in the analysis, but for practical reasons, the model was simplified to represent the spline teeth between balls by a single tooth acting at each ball. This program has become a valuable tool for determining deflections and tooth meshing paths in addition to load distribution. Loads and deflections from this program were used in the computer shell program to determine deflections and stresses over the entire flex spline length. The maximum stress is at the root of the flex spline teeth.

A triplex ball bearing set is used in the harmonic drive for maximum radial stiffness. Three bearings with smaller cross-section and more balls than a comparable duplex bearing support the flex spline over the full tooth length and provide more uniform radial support with the larger number of balls. The inner race is split to permit a solid one-piece cage to be used. The solid steel cage is silver plated and rides on the inner race at the three lobe points. Ball pockets are designed to accept the full ball excursion and speed variations in traversing the harmonic path. The bearing outer race thickness was designed based on flexing stress and overhang bending stress transverse to the ball path.

No practical analysis has been found for bearing skidding but reasonable safeguards have been used in the bearing design to reduce the tendency for ball skidding and to improve life if skidding occurs. The bearing material is M50 steel, vacuum induction melted with vacuum arc remelting. Ball race finish is held to 15.24×10^{-6} cm (6×10^{-6} in) AA with 127×10^{-6} cm (50×10^{-6} in) waviness control. Control on internal clearance, O.D. and bore tolerances is held closer than specified for ABEC-7 bearings. All thermal and centrifugal effects on clearances and fits have been considered. Contact angle on the inner races and conformity are such that the contact pattern is always on the race for loads based on harmonic output torque in excess of maximum operating torque. Bearing life was calculated for the bearing set using A.B. Jones' "Rolling Element" program with a load distribution factor between bearings of 1.45. A curve of B_{10} life vs. harmonic output torque was plotted and used with the mission torque requirements to determine bearing life as a function of cubic mean mission torque. A design data summary for the triplex bearing is presented in Table XXV, Section 6.0. Bearing load and life calculations are located in Appendix A.

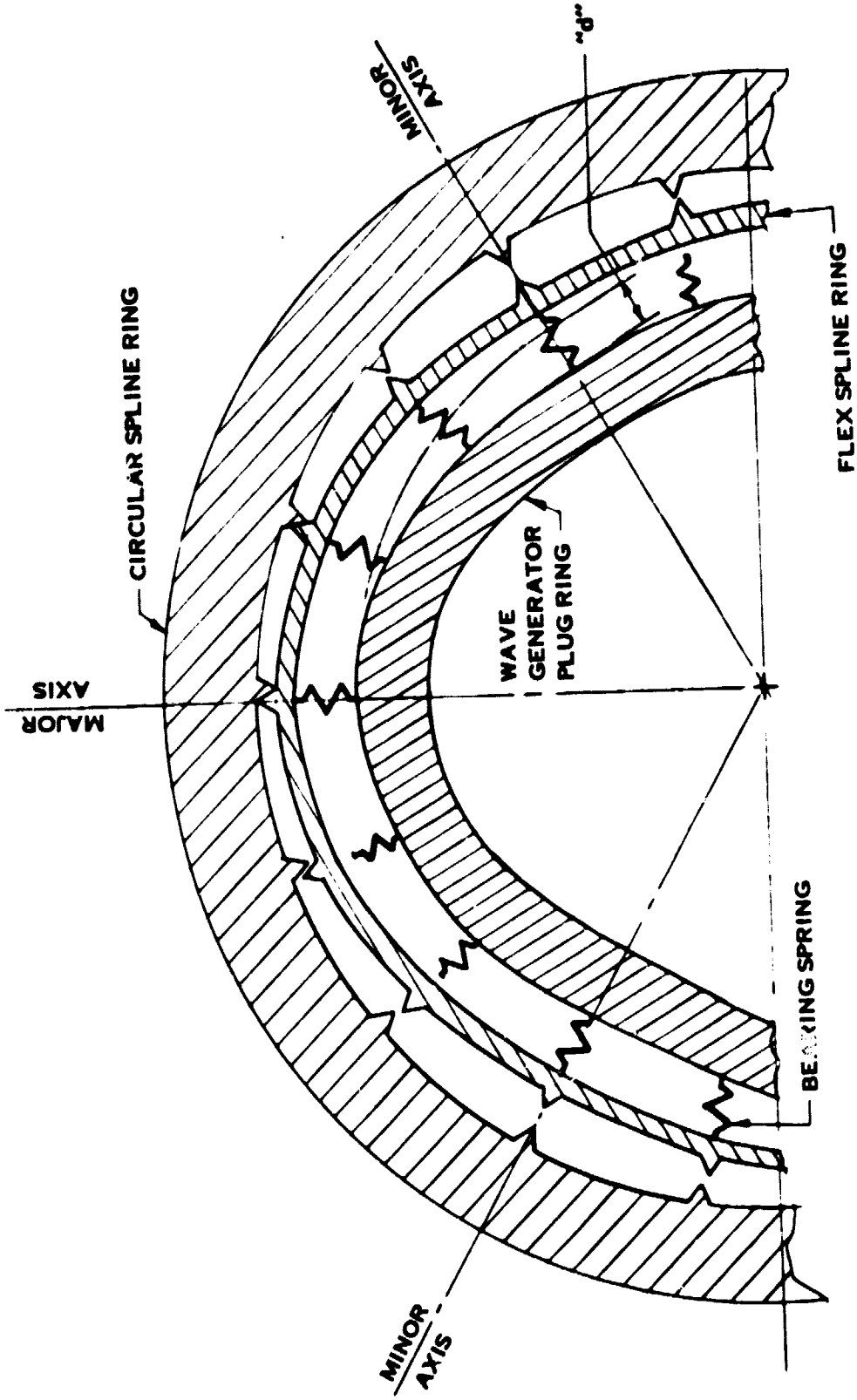

Figure 14. Load distribution model

The harmonic design and operating characteristics are summarized in Table XIV and flex spline tooth dimensions are shown in Figure 15.

Shown in Table XV are the radial deflections at the tooth mesh and loss of "d" for the maximum design operating torque and design non-ratcheting torque, where "d" is defined as the cam rise of the wave generator from minor to major axis (Reference Figure 14). The value of "d" for this unit is 0.109 cm (0.043 in.). Radial deflections reduce tooth engagement directly while loss in "d" is listed only to show that an empirical harmonic design rule based on experience of the USM Corporation, is satisfied. The rule states that loss in "d" under maximum operating torque shall be less than 10 percent.

For the normal operating thermal environment of hot oil inside and cold air outside the harmonic drive, the thermal radial deflection at the tooth mesh is 0.00434 cm (0.00171 in.) into mesh for 383°K (230°F) oil and 244°K (-20°F) air. For a transient thermal inversion condition of 268°K (23°F) oil and 328°K (130°F) air, the radial tooth deflection is 0.00185 cm (0.00073 in.) out of mesh. Figures 16, 17 and 18 show the tooth engagements for various combinations of torque, temperature extremes and manufacturing tolerances. A minimum engagement of 0.0505 cm (0.0199 in.) from Figure 17 is used for tooth bearing stress calculations for life requirements. The tooth bearing stress at the flex spline/circular spline mesh is 7585 N/cm^2 (11,000 psi) at the maximum operating torque tooth load of 1601 N (360 lbs). Allowable bearing stress for 1×10^6 required cycles is 7929 N/cm^2 (11,500 psi).

Figure 19 shows tooth engagement and disengagement motion at zero torque and at peak design non-ratcheting torque 16,950 N-m (150,000 lb-in). Minimum tooth-to-tooth engagement clearance is reduced from 0.0178 to 0.0091 cm (0.0070 to 0.0036 in) by the peak torque. A clearance at the peak torque is required to prevent ratcheting.

The maximum flex spline stresses occur at the spline root, Point "A", and the shoulder fillet at Point "B" (Reference Figure 13). Stress at "A" is combined tooth bending stress due to 1601 N (360 lbs) maximum tooth load and member hoop and bending stress due to forced harmonic deflection. Stresses at "B" are hoop and axial due to the forced deflection. These stresses are summarized in Table XVI.

The critical torsional buckling shear stress for the flex spline is 29,097 N/cm^2 (42,200 psi). Torsional shear stress at non-ratcheting torque of 16,950 N-m (150,000 lb-in) is 23,926 N/cm^2 (34,700 psi). The torsional shear stress margin is 22%. Torsional natural frequency of the flex spline is 3880 cps or 233,000 cpm.

Stresses in the wave generator and circular spline are not critical since they are designed for radial stiffness. The gyroscopic moment (M_{GYRO}) of the wave generator and bearing inner races at 3350 fan rpm and 4500 input rpm (7850 rpm

Table XIV. Harmonic Drive Design and Operating Characteristics

Max Output Torque: 5650 N-m (50,000 lb-in.) Normal
16,950 N-m (150,000 lb-in.) Non-Ratchet

Min Input rpm: 2800 @ Maximum Normal Output Torque
4500 @ No-Load

Reduction Ratio: 201:1

Min Torque Efficiency: 70% @ 2870 rpm and Maximum Normal Output Torque

No. Wave Generator Lobes: 3

No. Circular Spline Teeth: 603
No. Flex Spline Teeth: 600
Tooth Pressure Angle: 20°

Torsional Stiffness: 40° Max Input Rot. @ Maximum Normal Output Torque

Max Operating "K" Value: 76

Circular Spline Pitch Diameter: 22.098 cm (8.700 in.)

Selected Materials:

Item	Material	Heat Treat	Surface Treatment
Circular Spline	AMS 6415	32 - 38 R_c	Cad Plate (External)
Flex Spline	AMS 6414 (CEVM)	40 - 44 R_c	Peened and Black Oxide
Wave Generator	AMS 6415	36 - 40 R_c	
Bearings	M-50		

Harmonic Drive Weight: 7.57 kg (16.7 lbs)

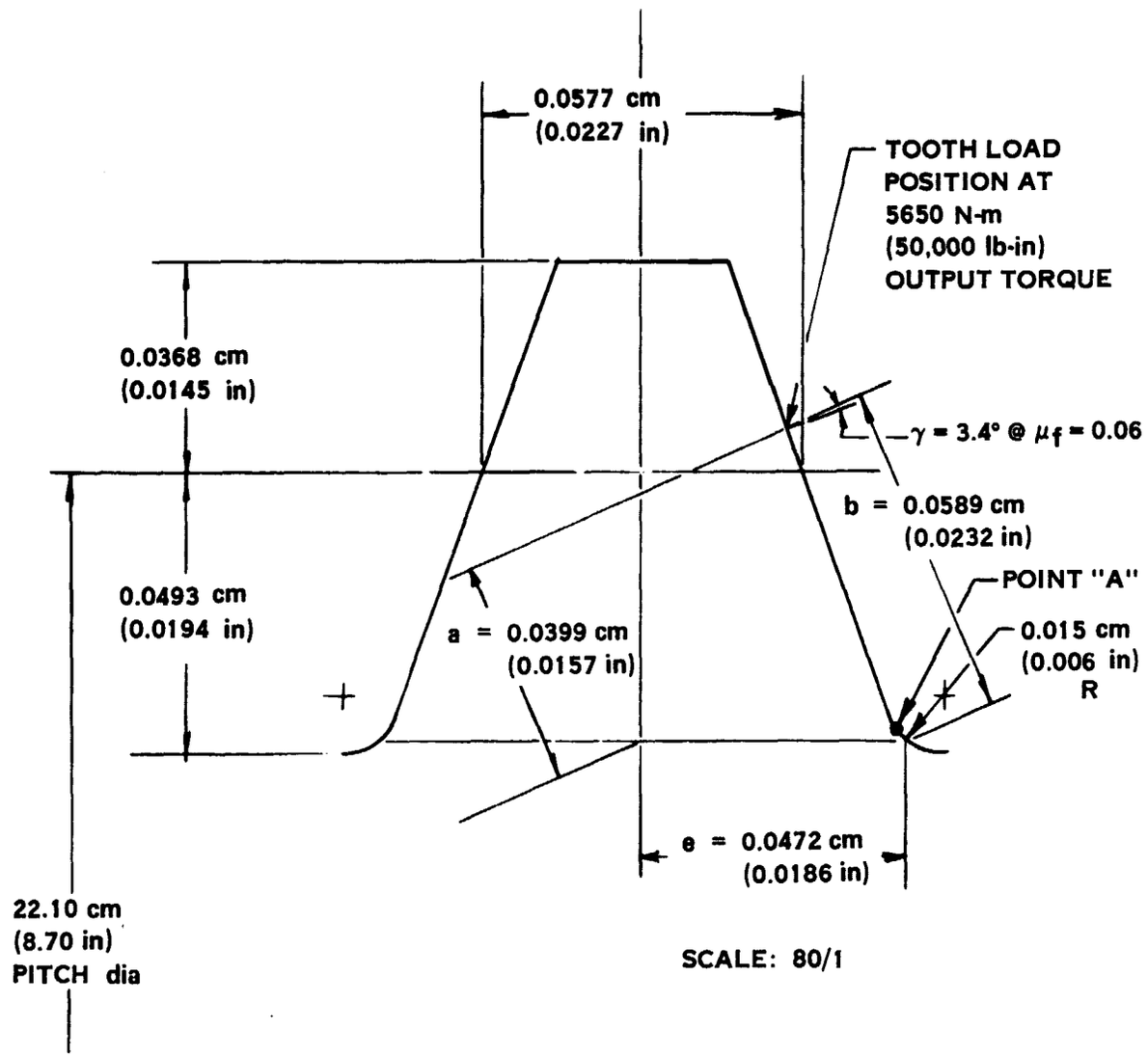

Figure 15. Flex spline tooth dimensions

Table XV. Harmonic Drive Radial Deflection at Tooth Mesh and Loss of "d"

	5650 N-m (50,000 lb-in.)				16,950 N-m (150,000 lb-in.)			
	Loss in "d"		Radial Deflection		Loss in "d"		Radial Deflection	
	cm	(in.)	cm	(in.)	cm	(in.)	cm	(in.)
Circular Spline	0.00338	0.00133	0.00257	0.00101	0.01016	0.00400	0.00767	0.00302
Bearing	0.00376	0.00148	0.00376	0.00148	0.00660	0.00260	0.00660	0.00260
Plug Ring	0.00163	0.00064	0.00137	0.00054	0.00485	0.00191	0.00406	0.00160
Plug Overhang	0.00028	0.00011	0.00025	0.00010	0.00086	0.00034	0.00076	0.00030
	0.00905	0.00356	0.00795	0.00313	0.02247	0.00885	0.01909	0.00754
% Loss In "d"	8.18	8.18			20.3	20.3		

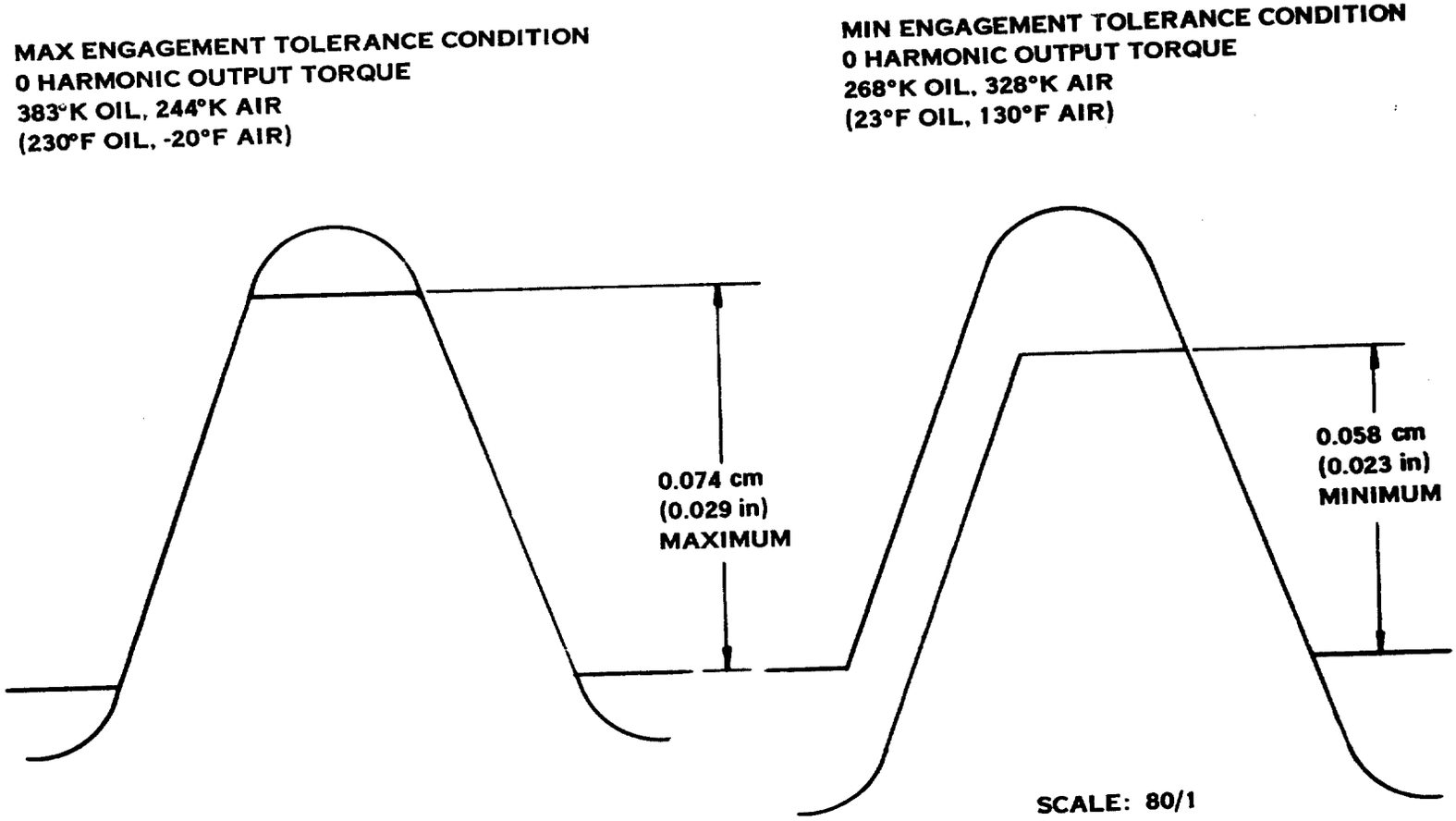

Figure 16. Tolerance effect on engagement

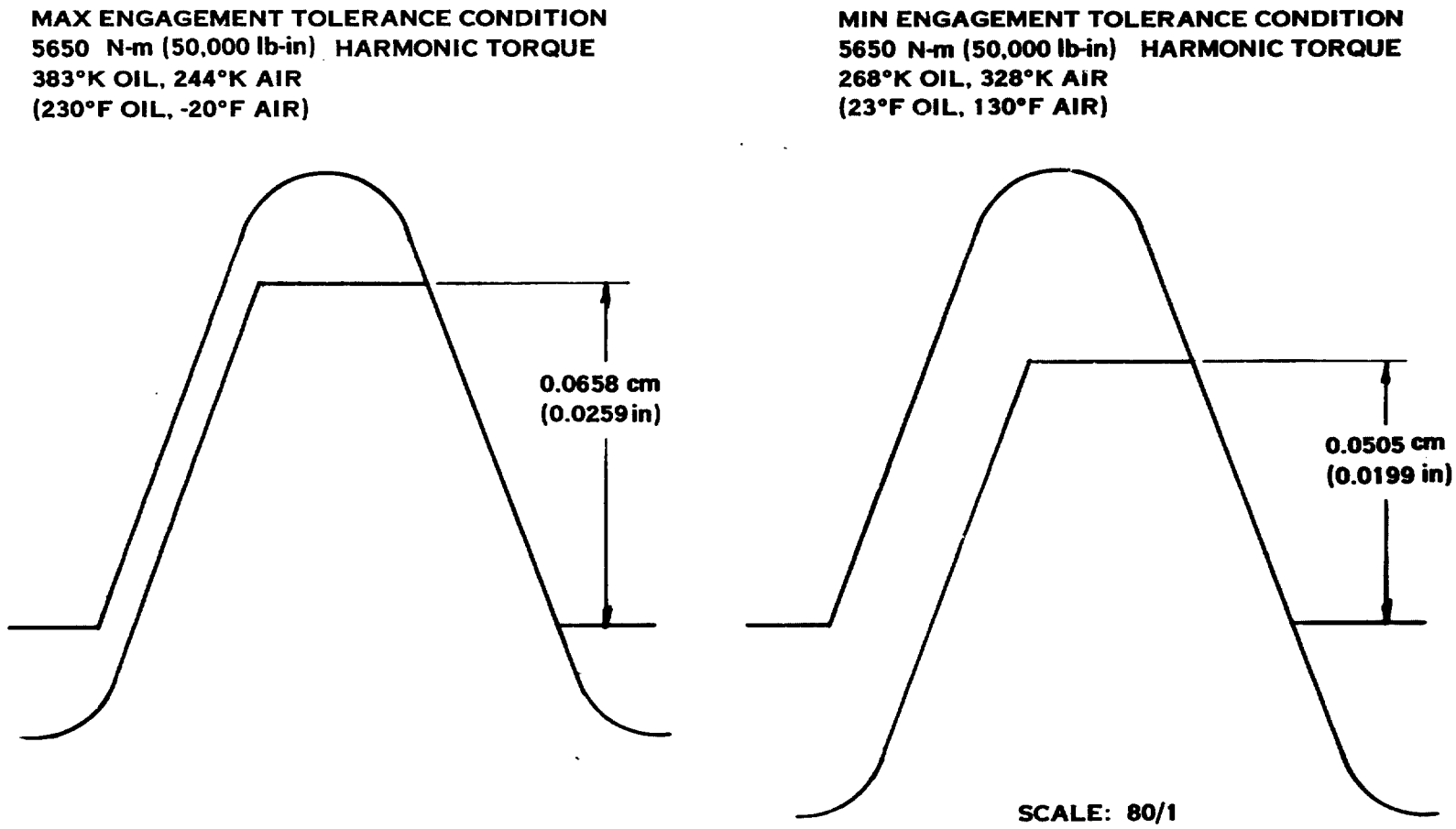

Figure 17. Tolerance effect on engagement

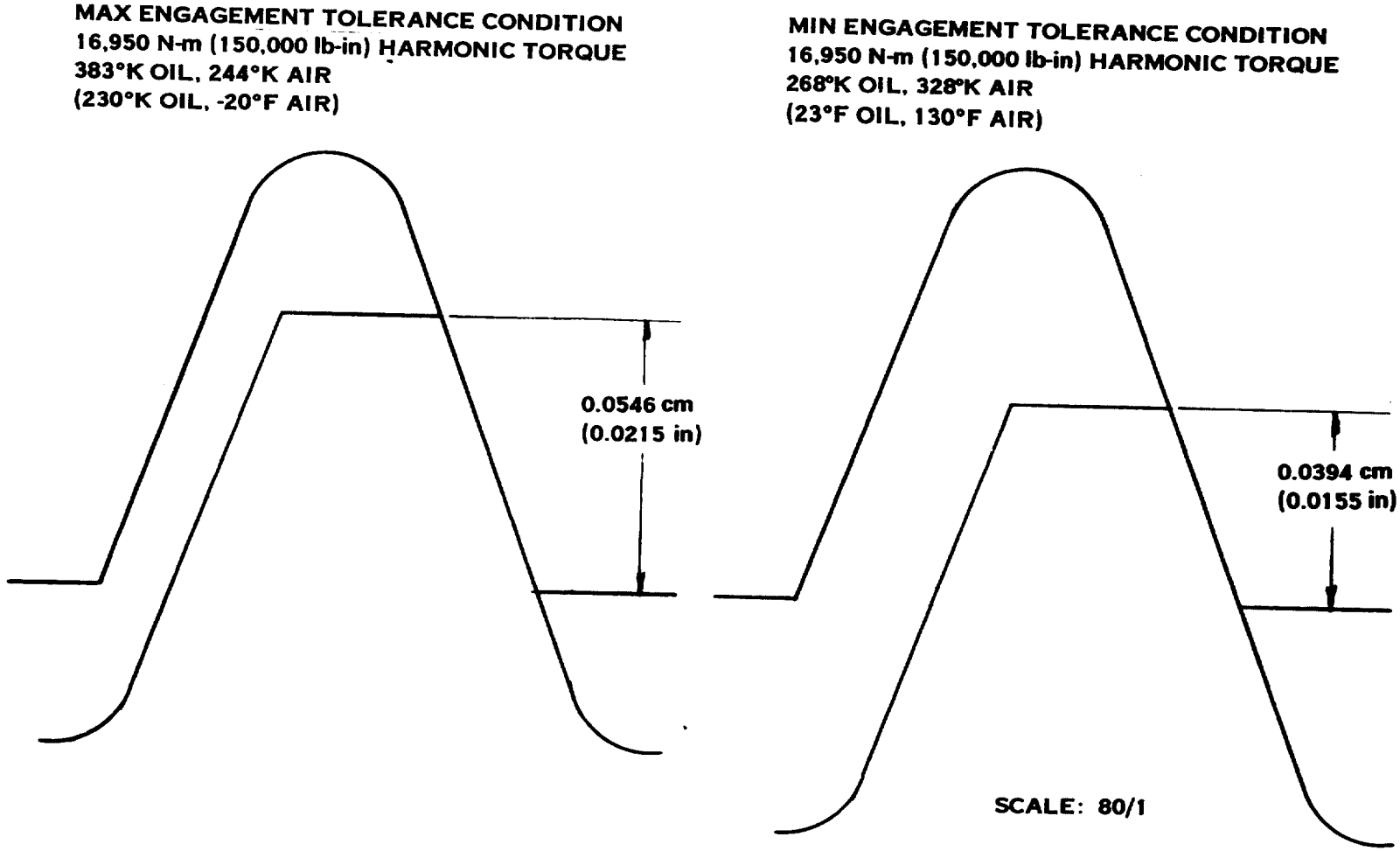

Figure 18. Tolerance effect on engagement

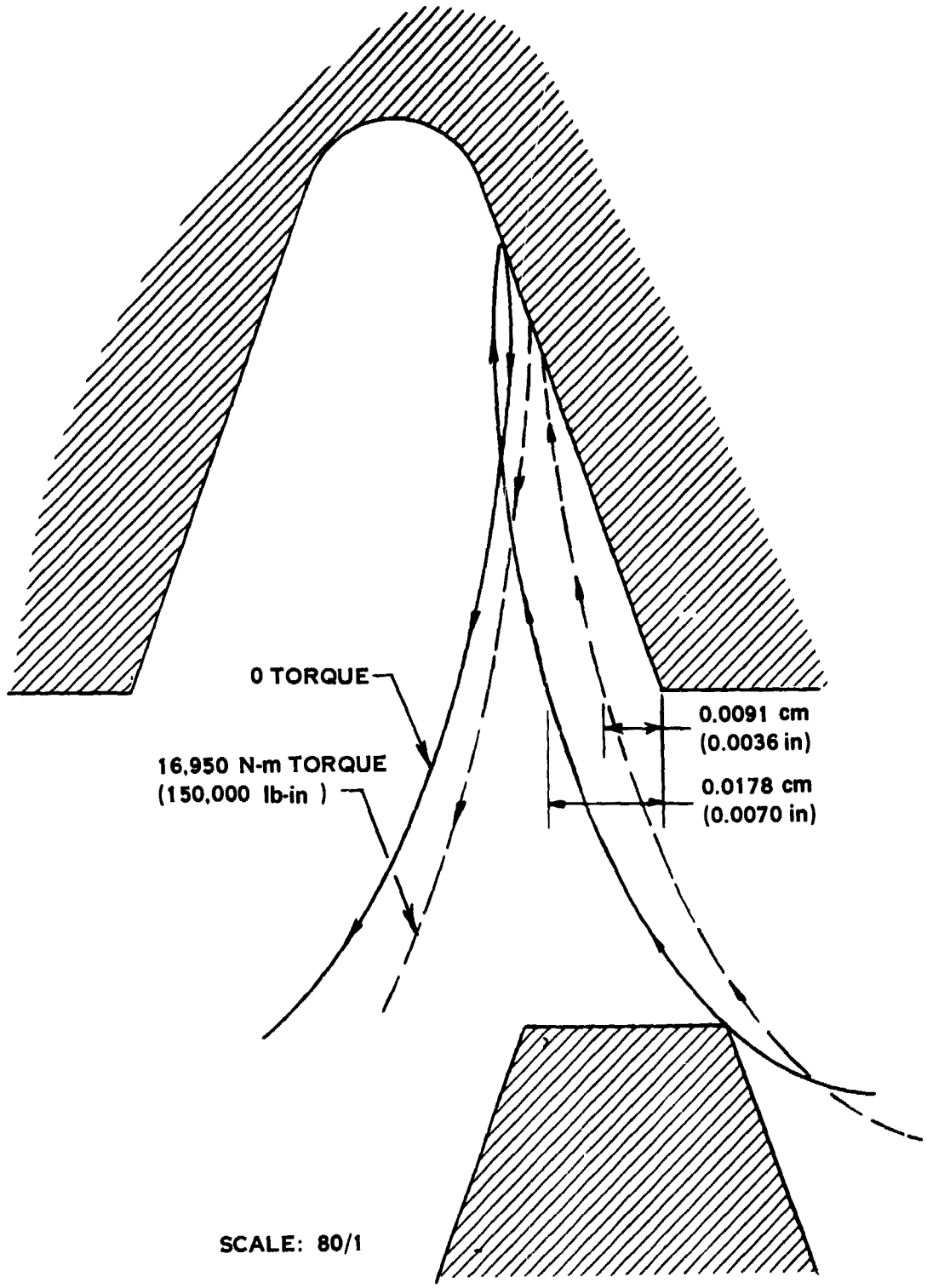

Figure 19. Tooth engagement/disengagement clearance

Table XVI. Flex Spline Stresses

Location[1]	Stress Type	SCF[2] K_t	Stress N/cm^2	Stress (psi)	Required Cycles	Allowable Stress @ 10^8 Cycles N/cm^2	Allowable Stress @ 10^8 Cycles (psi)
A	Combined	1.75	9584±29,855	(13,900±43,300)	10^8	9584±32,407	(13,900±47,000)
B	Hoop	1.0	-1076±17,582	(-1560±25,500)	10^8	-1076±35,165	(-1560±51,000)
B	Axial	1.93	-4723±14,066	(-6850±20,400)	10^8	-4723±35,165	(-6850±51,000)

(1) Reference Figure 13

(2) Stress Concentration Factor, K_t, is included in the stress values.

total) at a precession rate of 1 rad/sec is 16.95 N-m (150 lb-in.). This moment is reacted by the bearings with a negligible effect on life.

The harmonic drive input flex spline ground and circular spline output spline data is presented in Table XXIV, Section 5.10, Items 6, 16, and 17.

5.4 NO-BACK

A cross-section of the bi-directional spring clutch (no-back) is shown in Figure 20. The self-energizing no-back spring locks blade torque in either direction by locking the harmonic drive input to ground. Holding torque capacity is at least 19,210 cmN (1700 in-lbs) at a minimum torque limiter brake coefficient of friction of 0.06. Maximum dynamic holding torque capacity is 271.2 N-m (2400 lb-in) as limited by the torque limiter brake. Since the load per coil varies exponentially with the number of coils and friction coefficient, the center coils react less load than the end coils and are therefore smaller in cross section to conserve weight. The housing bore is coated with a chrome oxide flame sprayed coating which experience has shown to provide a durable, low-wear friction surface when lowering an aiding load. Holes in the housing at the spring running surface are used to prevent a hydro-dynamic film from forming which could delay dynamic spring engagement.

Since the no-back is bi-directional, both the input from the differential and the output to the harmonic drive must be capable of acting torsionally on both ends of the spring. This is accomplished with input and output quill shafts splined to both ends of the spring and to each other. All splines are designed with sufficient gaps between teeth to permit the relative motion of the splined members required to engage and disengage the no-back spring under all conditions of load, tolerances, deflections and temperature. All parts in the no-back are steel and the quill shafts are supported on silver-plated journal bearings. The primary design criteria for the various no-back parts are: low hoop deflection in the housing, compressive stress in the spring coils, torsional shear stress in the quills, bending stress at the output shaft cut-outs and spline bearing stress. The no-back design characteristics are presented in Table XVII.

The maximum spring stress is at the start of the first coil (Point B, Section A-A, Figure 20). This stress includes bending due to 0.056 cm (0.022 in.) diametral interference fit of the coil in the housing and compressive stress due to load F equal to 10,186 N (2290 lbs) from the 271.2 N-m (2400 lb-in.) maximum dynamic holding torque. The total maximum compressive stress at Point B is $41,300 \pm 31,165$ N/cm^2 ($59,900 \pm 45,200$ psi) for K_t equal to 1.0. The required number of load cycles is 10^5 as compared with the allowable number of cycles of 10^8.

The maximum pressure between the spring and housing is 5655 N/cm^2 (8200 psi) resulting from the maximum dynamic holding torque. Allowable pressure is 5860

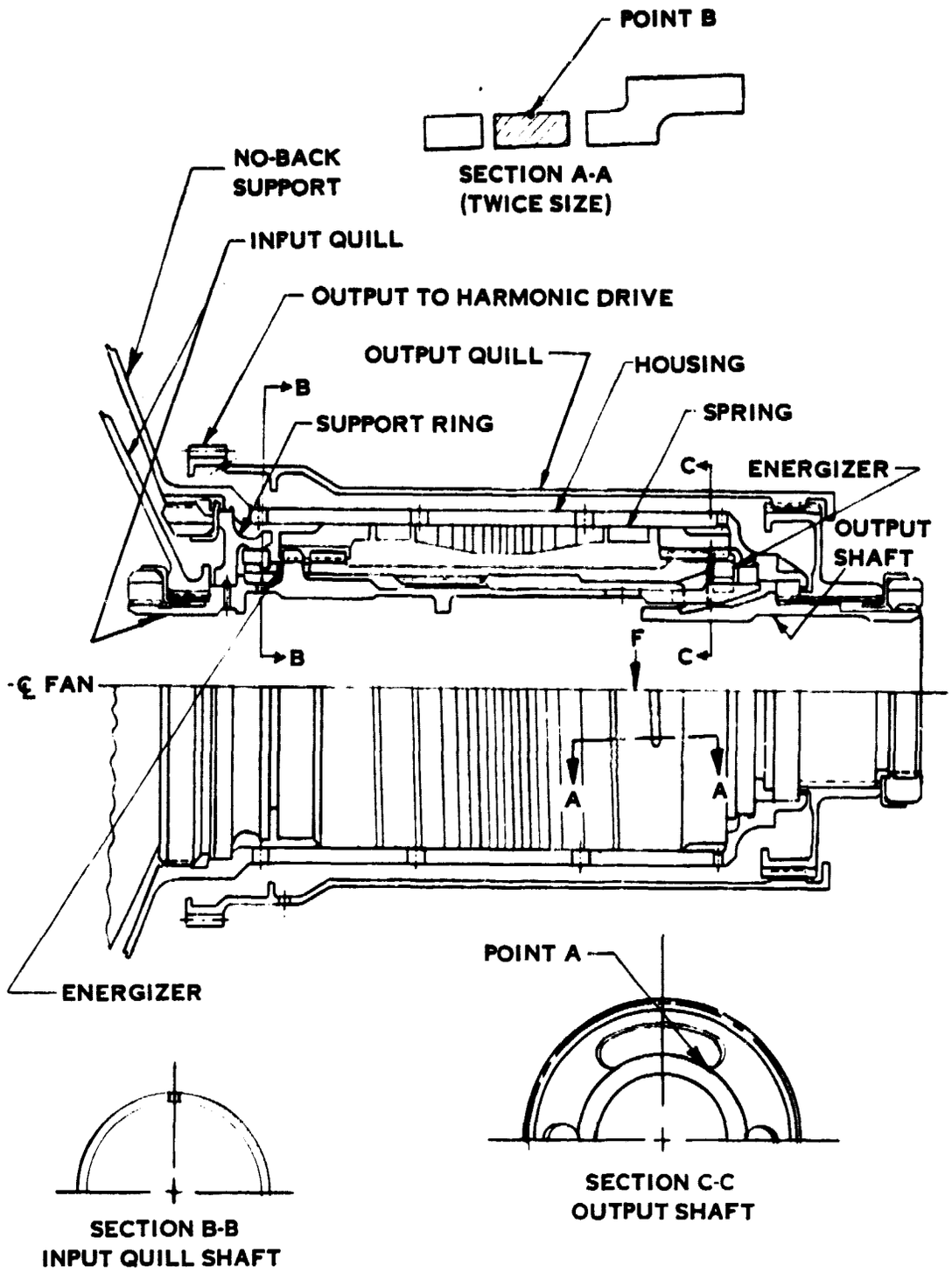

Figure 20. No-back

Table XVII. No-Back Design Characteristics

Max Static Holding Torque Required [1]:	28.25 N-m (250 lb-in)
Max Dynamic Holding Torque Required [2]:	271.2 N-m (2400 lb-in)
Max Input Torque, Aiding Load:	1.81 N-m (16 lb-in)
Max Input Torque, Opposing Load:	40.68 N-m (360 lb-in)
Max Dynamic Input Torque:	96.05 N-m (850 lb-in)
Max rpm, Aiding Load:	4500
Min rpm, Max Opposing Load:	2800
Spring Drag Torque Tare:	1.81 N-m (16 lb-in)

Item	Material	Heat Treat	Surface Treatment
Housing	AMS 6415	40-44 R_C	Chrome Oxide Bore
Spring	AMS 6414	40-44 R_C	Glass Peened OD
Energizers	AMS 6415	40-44 R_C	
Output Shaft	AMS 6414	40-44 R_C	Shot Peened
Quills	AMS 6415	40-44 R_C	
Support Ring	AMS 6415	40-44 R_C	Silver Plated Journals 0.0002 - 0.0004 Thk.

No-Back Assembly Weight: 1.77 kg (3.9 lbs)

(1) Torque required to react the maximum blade twisting moment.

(2) Torque limiter disk brake limits the no-back holding torque to this maximum level.

N/cm^2 (8500 psi). The spring pressure generated while reacting the maximum aiding torque of 28.25 N-m (250 lb-in.) is 586 N/cm^2 (850 psi). Allowable pressure is 3103 N/cm^2 (4500 psi).

Maximum torsional shear stress in the no-back assembly occurs at the lubrication holes in the input quill shaft (Section B-B) at 96.05 N-m (850 lb-in.) dynamic input torque. The shear stress for this condition is 23,440 N/cm^2 (34,000 psi) and includes a stress concentration factor of 4.0. Allowable number of cycles is 10^8 and the required number is 10^6. The critical torsional buckling stress for the input quill shaft is 170,300 N/cm^2 (247,000 psi).

The maximum output shaft stress is located at the slots (Point A, Section C-C) and is due to the 271.2 N-m (2400 lb-in.) maximum dynamic holding torque. The stress at Point A represents combined bending and tangential stress in the inner ring and is ± 56,230 N/cm^2 (± 81,550 psi). A stress concentration factor of 1.37 is included for the effect of the slot corner radius. The allowable number of torque cycles is 1.05×10^5 as compared with 0.96×10^5 required cycles.

All no-back spline data is given in Table XXIV, Items 1 through 7, Section 5.10.

5.5 TORQUE LIMITER BRAKE

The torque limiter brake, shown in Figure 21, is a disk-type brake which grounds the no-back housing to the harmonic output through the differential gear housing. Disks with four rubbing surfaces are loaded axially by an adjustment nut acting against a Belleville-type spring to set the brake slip torque. The brake disk surfaces incorporate radial grooves for continuous lubrication.

The slip torque range is from 192.1 to 271.2 N-m (1700 to 2400 lb-in.). The coefficient of friction range is from 0.08 to 0.113 (total). Disk pressure will be set at 290 N/cm^2 (420 psi) at assembly. Expected maximum temperature is 506°K (450°F). Selected materials are as follows:

Item	Material	Heat Treat	Surface Treatment
Housing	AMS 4928	Annealed 30-39 Rc	Peen Splines, Ni Plate 0.0003-0.0005 thick.
No-Back Support	AMS 6415	40-44 Rc	Silver-plate journal dia., 0.0002-0.0004 thick.
Brake Disks	Gylon EX 38 (1) On AMS 6415	32-38 Rc	

(1) Gylon is a teflon base brake material heavily impregnated with a ceramic material for good thermal stability. It has a close range of static to dynamic friction coefficients in MIL-L-23699 fluid. The material operates in clutches up to 533°K (500°F) and 345 N/cm^2 (500 psi) disc pressure. Disk spline data is provided in Table XXIV, items 13, 14 and 15, Section 5.10.

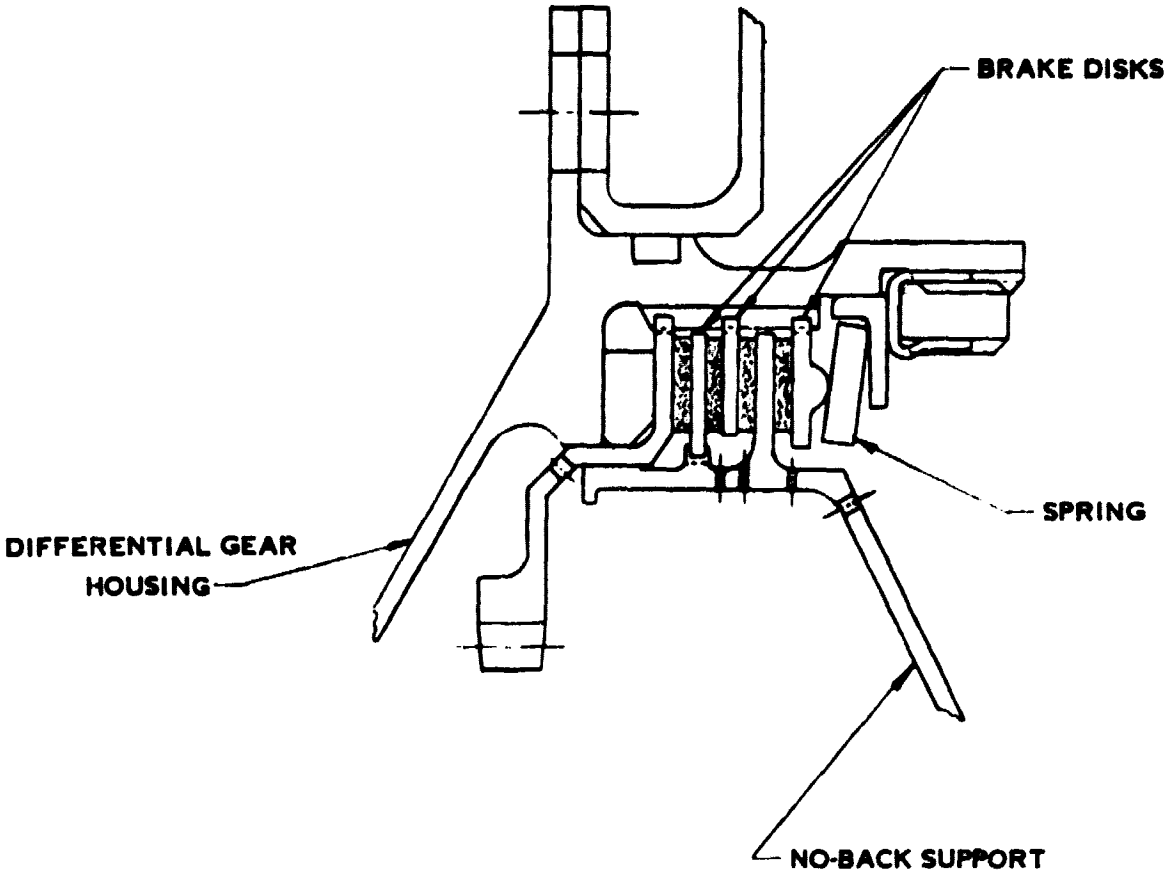

Figure 21. Torque limiter brake

5.6 DIFFERENTIAL GEARING

The differential gear assembly is shown in Figure 22. The gears are made from AMS 6265 (AISI 9310 CEVM) steel and are carburized and ground. They are designed for infinite life at maximum operating torque to the allowable contact and bending stresses specified by the American Gear Manufacturers Association (AGMA). These allowable stresses have been proven by Hamilton Standard gear transmission service experience with propeller controls and F-14 wing sweep actuators and prototype power gearing for the XC-142, X-22, AH56A and VC-400 aircraft.

The sun gears form a floating mesh with three planet gears for equal load sharing. Sun gear shafts are sized for acceptable torsional shear stress. Ring gears are designed with sufficient tooth backing material to maintain low radial ring deflections. Planet gears are mounted on caged needle bearings running on case hardened steel shafts in the planet cage.

A one-piece titanium planet cage is supported on a preloaded duplex ball bearing set mounted in the differential housing. This housing is closely centered on the harmonic output flange and bolted in place. The planet cage incorporates fore and aft rings tied together by integral cross beams located between planets. Pitch change torque on the gearing imposes bending on the cross beams from opposing torques in the end rings. Bending deflection is maintained within acceptable limits of angularity for the planet gear bearings. The lug stresses around the planet shafts were analyzed in much the same manner as the trunnion arm roller pin lugs.

The maximum dynamic input torque to the gears is 19.21 N-m (170 lb-in.) and maximum input rpm is 21,100. The minimum estimated torque efficiency is 98%. A summary of gear geometry and design characteristics is presented in Table XVIII. Selected materials for the differential gear assembly are as follows:

Item	Material	Heat Treat	Surface Treatment
Gears	AMS 6265	685 VH min. case 35-43 Rc core	
Planet Cage	AMS 4928	Annealed 30-39 Rc	Peen, Ni plate bearing surface; 0.0003-0.0005 thick
Planet Shafts	AMS 6265	685 VH min. case 35-43 Rc core	
Planet Bearings	AISI 52100		
Cage Bearings	AISI 52100		

Differential gearing weight is 2.54 kg (5.6 lbs) including the torque limiter brake.

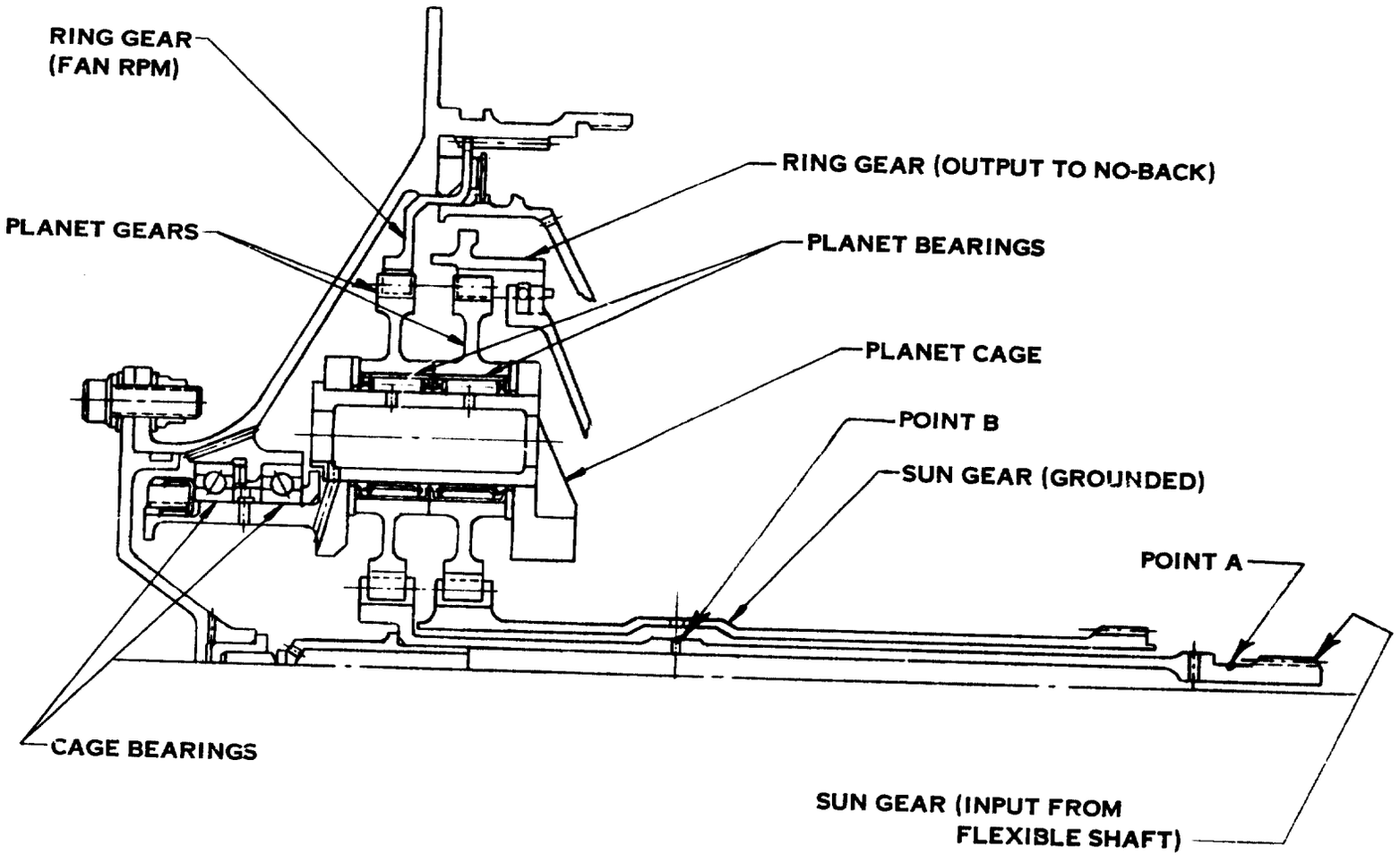

Figure 22. Differential gear assembly

Table XVIII. Differential Gear Data
(Gear Ratio = 5:1)

	Sun	(3) Planets	Ring
Number of teeth	15	30	75
Diametral Pitch	16	16	16
Pressure Angle	22°30'	22°30'	22°30'
Pitch Diameter	2.381 cm (0.9375 in.)	4.763 cm (1.8750 in.)	11.906 cm (4.6875 in.)
Min. Axial Engagement	0.559 cm (0.220 in.)	0.559 cm & 0.457 cm (0.220 in. & 0.180 in.)	0.457 cm (0.180 in.)
Min. Face Width	0.635 cm (0.250 in.)	0.635 cm (0.250 in.)	0.457 cm (0.180 in.)
Torque Condition	19.21 N-m (170 lb-in.)	38.42 N-m (340 lb-in.)	96.05 N-m (850 lb-in.)
Tangent Tooth Load	538 N (121 lbs)	538 N (121 lbs)	538 N (121 lbs)
Dynamic Load	854 N (192 lbs)	854 N (192 lbs)	854 N (192 lbs)
Dynamic Hertz	140,406 N/cm^2 (203,635 psi)	140,406 N/cm^2 (203,635 psi)	69,422 N/cm^2 (100,685 psi)
Dynamic Bending	30,890 N/cm^2 (44,800 psi)	38,875 N/cm^2 (49,130 psi)	30,683 N/cm^2 (44,500 psi)
Static Hertz	111,461 N/cm^2 (161,655 psi)	111,461 N/cm^2 (161,655 psi)	111,461 N/cm^2 (119,930 psi)
Static Bending	19,465 N/cm^2 (28,230 psi)	28,347 N/cm^2 (30,960 psi)	19,337 N/cm^2 (28,045 psi)
Required Dynamic Cycles	3×10^6	5×10^5	1.8×10^6
Allowable Dynamic Hertz	155,138 N/cm^2 (225,000 psi)	155,138 N/cm^2 (225,000 psi)	155,138 N/cm^2 (225,000 psi)
Allowable Dynamic Bending	31,028 N/cm^2 (45,000 psi)	34,475 N/cm^2 (50,000 psi)	31,028 N/cm^2 (45,000 psi)
Gear Separating Loads	222 N (50 lbs)	222 N (50 lbs)	222 N (50 lbs)

The maximum torsional shear stresses in the differential gearing occur in the input sun gear shaft at Points A and B. These stresses are shown in Table XIX and are based upon the ±19.21N-m (±170 lb-in.) maximum dynamic input torque. Torsional spring rate of the input sun gear is 553.7 N-m/radian (4900 lb-in./radian). Torsional spring rate of the ground sun gear is 1118.7 N-m/radian (9900 lb-in./radian).

Figure 23 defines the planet cage configuration. Maximum stresses in the cage occur at the connecting beams at Point A and in the lug material around the planet shafts at Point B. The stresses are based upon the gear tooth loads from maximum dynamic input torque and centrifugal planet gear loads generated at 3347 fan rpm. Angular deflection of the beams between the cage rings due to these loads is 0.0033 cm/cm (0.0013 in./in.). Allowable angular deflection based on permissible planet bearing angularity is 0.0038 cm/cm (0.0015 in./in.).

Ring gear and sun gear spline data is presented in Table XXIV, Section 5.10, Items 9, 10, 11 and 12. Cage and planet bearing summaries are presented in Table XXV, Section 6.0.

5.7 FLEXIBLE DRIVE SHAFT

The flexible drive shaft assembly, shown in Figure 24, consists of a 0.375 inch diameter bi-directional flexible core running in a flexible teflon-lined steel braided casing in a rigid steel conduit. A continuous 9.45 cm^3/s (0.6 qts/min) lubrication flow passes between the core and casing to reduce wear. Bend radii are limited to 17.78 cm (7 in.) minimum. Fittings for "O" ring sealing are swaged to each end of the casing to seal in the lube flow. Identical splined drive fittings are swaged to each end of the flexible core.

The maximum dynamic (start-up) torque is 19.21 N-m (170 lb-in.), versus a yield torque capacity of 28.25 N-m (250 lb-in.). Maximum shaft rpm is 21,100 and the estimated minimum torque efficiency is 85%. Minimum torsional stiffness is 7.23 N-m/rad (64 lb-in./rad).

Fatigue capacity of flex shafts is dependent upon wire strand wear which in turn depends upon the number of revolutions, bend radius, number of bends and lubrication. Fatigue capacity will be determined by tests which monitor wear as a function of torsional stiffness.

Table XIX. Sun Gear and Planet Cage Stresses

Torsional shear stress in the input sun gear:

Location (1)	Stress	SCF (3) K_t	Required Cycles	Allowable Cycles
A	±21,100 N/cm^2 (±30,600 psi)	1.26	2×10^6	2×10^6
B	±10,610 N/cm^2 (±15,400 psi)	1.85	2×10^6	10^8

Combined stress in the planet cage:

Location (2)	Stress	K_t	Required Cycles	Allowable Cycles
A	±8090 N/cm^2 (±11,730 psi)	1.82	2×10^6	10^8
B	±8520 N/cm^2 (±12,350 psi)	1.0	2×10^6	10^8

(1) Reference Figure 22.

(2) Reference Figure 23.

(3) Stress concentration factor, K_t, is included in the stress values.

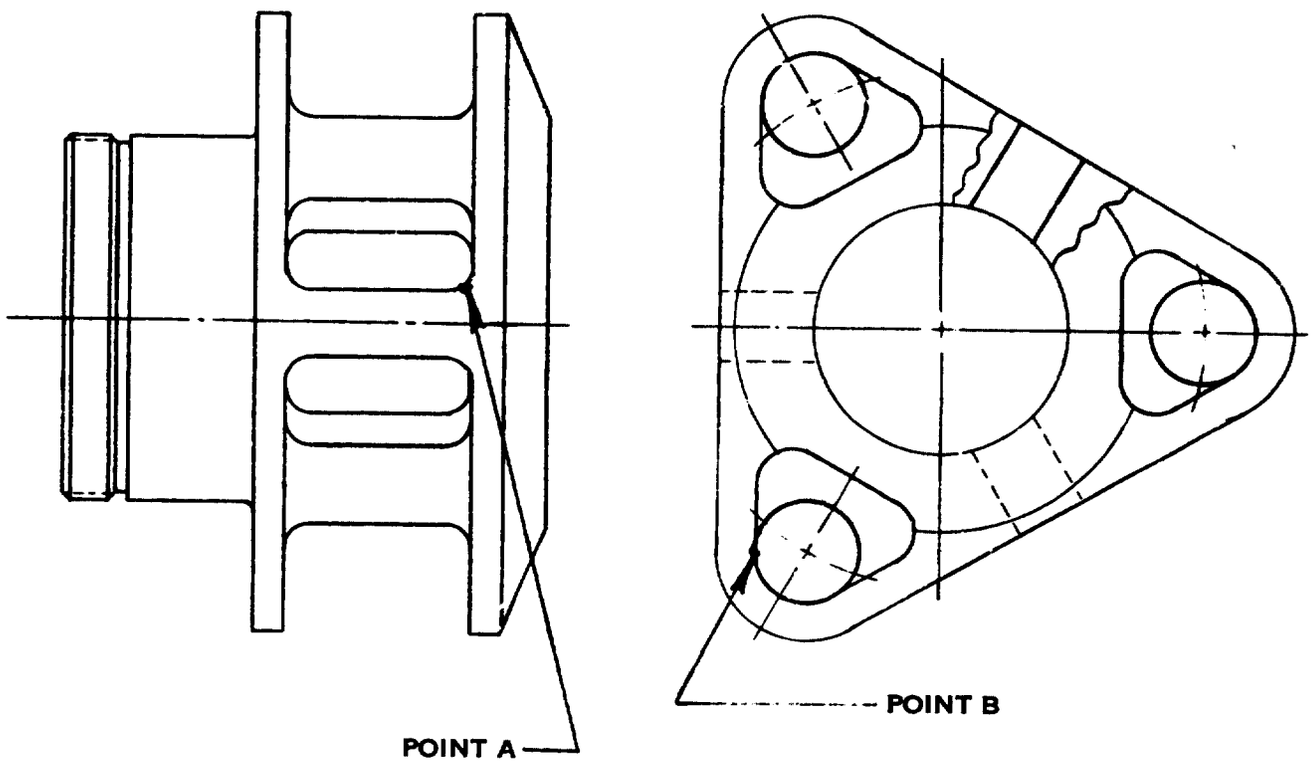

Figure 23. Planet cage

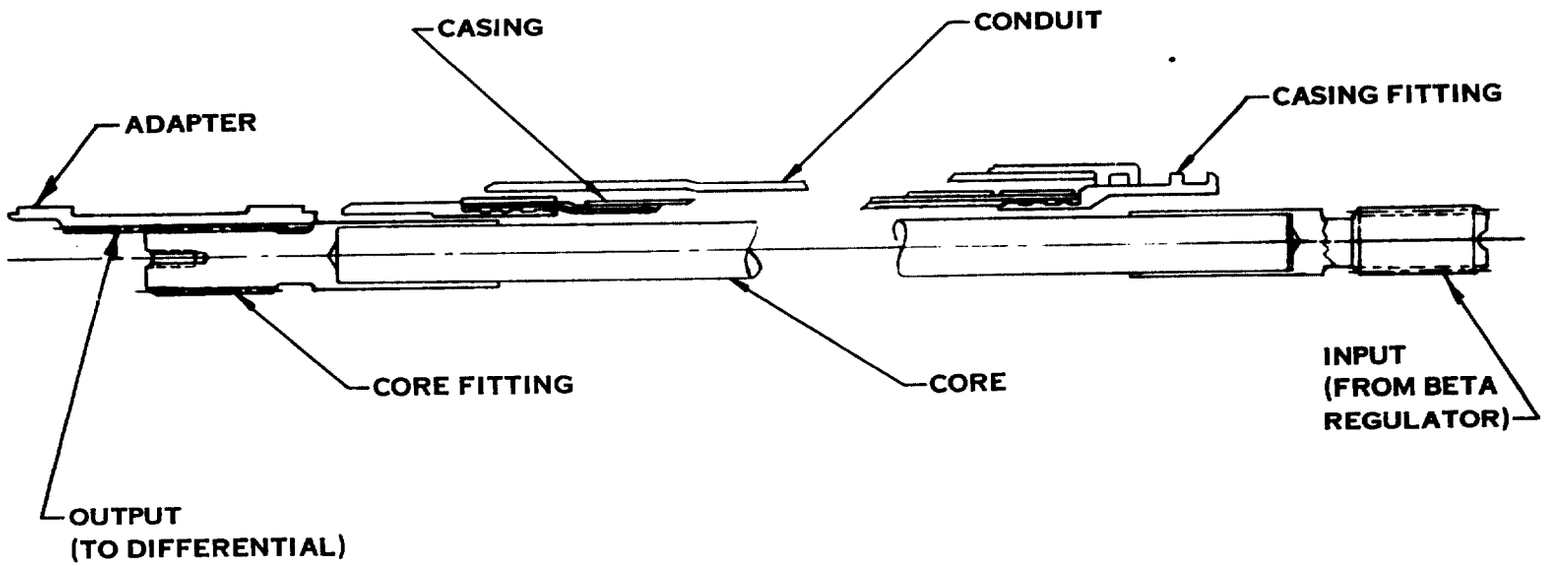

Figure 24. Flexible shaft

The materials selected for the flexible drive shaft assembly are as follows:

Item	Material	Heat Treat	Surface Treatment
Shaft Core	Hi-Carbon Steel Wire		
Core Fittings	AMS 6265	89 R_{15N} Case 40-45 Rc Core	Peened
Casing	CRES Steel Braid Teflon Lining		
Casing Fittings	AMS 5639 (304 CRES)		
Conduit	AMS 5639 (0.875 O.D. x .035 wall)		

Flexible shaft assembly and mounting weight is 1.72 kg (3.8 lbs).

The core fitting spline data is presented in Table XXIV, Section 5.10, Item 8.

5.8 BETA REGULATOR

The test beta regulator illustrated schematically in Figure 5, and shown in cross-section in Figures 25 and 26 is designed with two standard gear-type hydraulic motors driving a common output gear through a Zerol bevel mesh. The bevel gear ratio is 1.2, providing an increase in speed from the hydraulic motor to the flexible shaft. A flight-regulator would use a single positive displacement gear motor driving the output shaft directly. The standard motors have 3.081 cm^3/rev (0.188 $in.^3$/rev.) displacement each and have been modified for side porting. A feedback worm shaft is driven directly by the output shaft and drives a translating screw (0.375-16 UNJC-3A thread) through a 19:1 helical gear mesh. The screw is lapped for low axial play (0.025 blade angle deg) and translates parallel-mounted LVDT cores through a common yoke. Provision is made for a preload spring on the feedback screw if greater accuracy is required. Average LVDT feedback sensitivity is 0.0200 cm/deg (0.00788 in./deg).

The feedback worm shaft has a hexagonal end which can be used to rotate the regulator output shaft manually to change pitch for rigging or troubleshooting. A limit switch mounted adjacent to the feedback screw extension is actuated by adjustable cam nuts on the extension at preset blade angles The switch cuts off the elec-

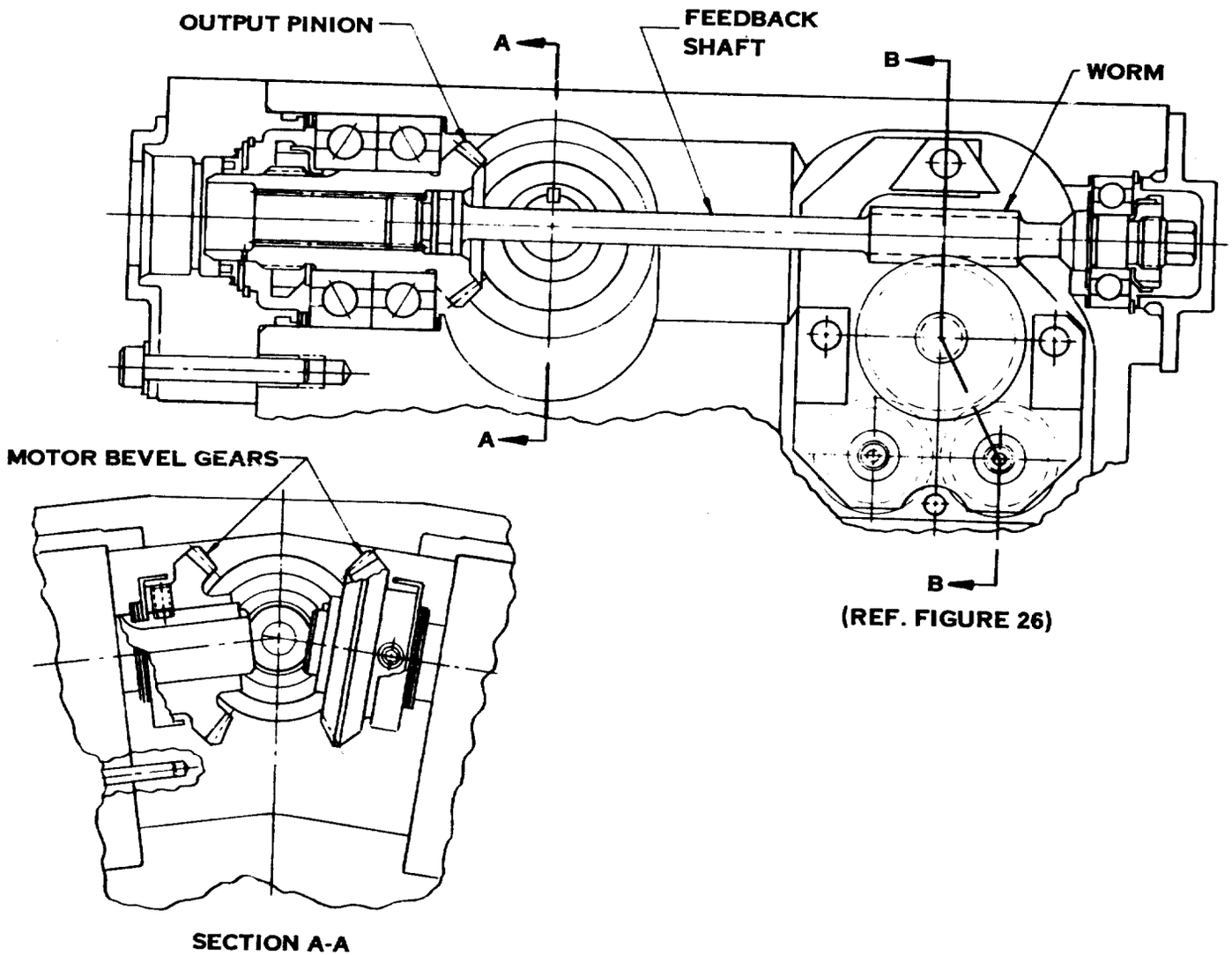

Figure 25. Beta regulator

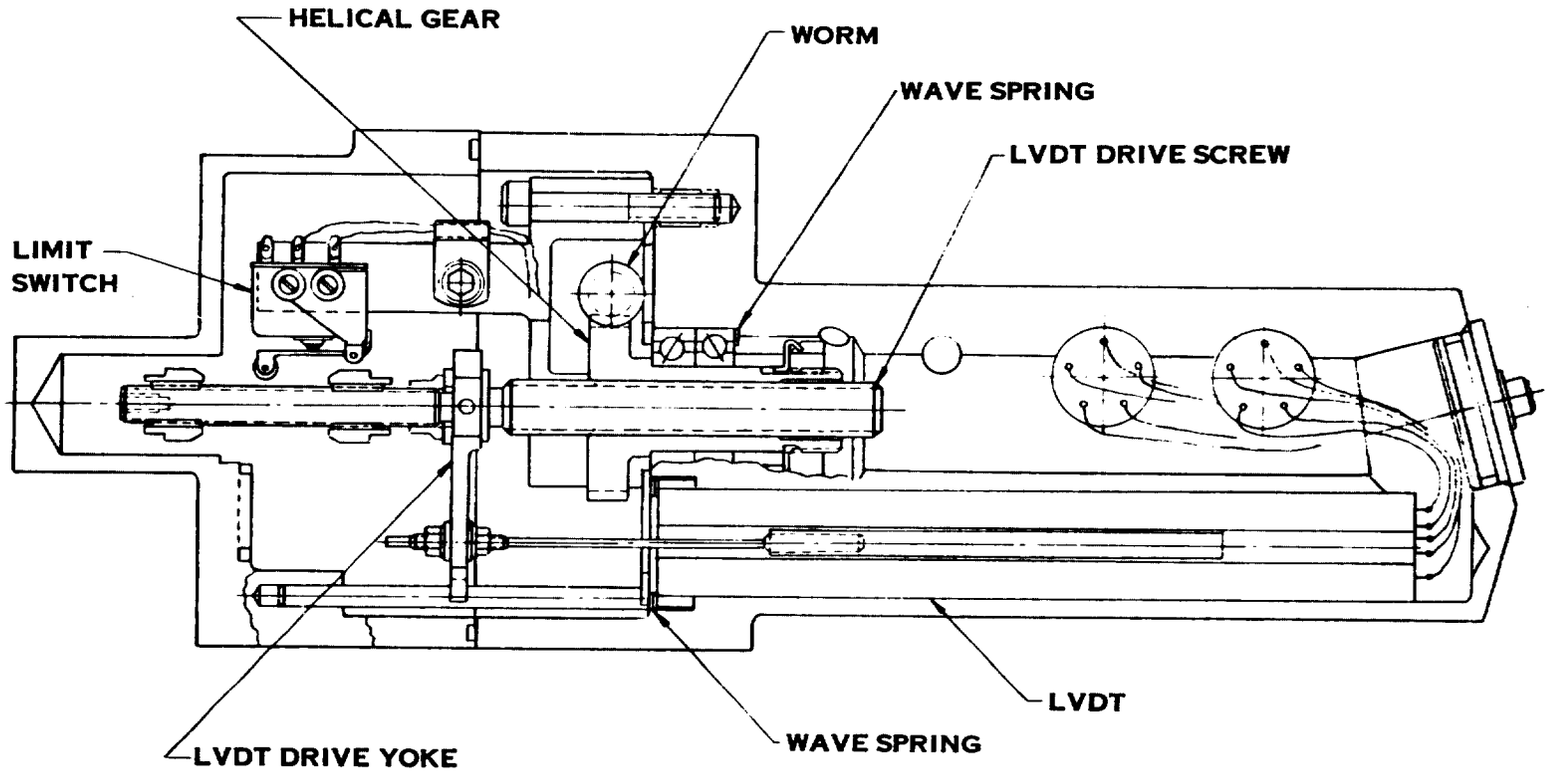

SECTION B-B (REF. FIGURE 25)

Figure 26. Beta regulator

trical signal to the EHV, returning it to the null position and terminating pitch change. Setting of the switch cams would normally be just outside of the normal operating range to prevent the mechanical stops from engaging at full rate from a hard-over input signal beyond the operating range.

The beta regulator has three electrical connectors: 2 for LVDT's and one for the limit switch; and three hydraulic connections: fluid pressure ports to open and closed pitch and a drain port. A vent hole connects the beta regulator housing cavity to the flexible shaft conduit which is vented to the engine reduction gear section.

Output torque of the beta regulator is 0 N-m (0 lb-in.) at 965N/cm^2 (1400 psi) pressure differential (ΔP) at no load, and 15.82 N-m (140 lb-in.) at 2069N/cm^2 (3000 psi) pressure differential at maximum load. Maximum output rpm (at no load) is 21,100.

The hydraulic motors are model number 43443-32 manufactured by the Ackley Manufacturing Company. Hydraulic motor speed/torque characteristics are shown in Figure 27 and speed/flow characteristics are shown in Figure 28. Maximum operating motor pressure differential is 2069 N/cm^2 (3000 psi) at maximum load and the minimum pressure differential is 965 N/cm^2 (14000 psi) at no load. Maximum flow to the motors is 2268 cm^3/s (36 gal/min) at 17,600 motor rpm and 935 N/cm^2 (1400 psi).

Materials selected for the more critical beta regulator parts are as follows:

Item	Material	Heat Treat	Surface Treatment
Bevel Gears	AMS 6265	90 R_{15N} Case 35-43 Rc Core	Dry film (Electrofilm)
Bearings	AISI 52100		
LVDT Drive	AMS 6415	32-38 Rc Screw 36-40 Rc Gear	Screw lapped Dry film (CF_x)

A summary of the Zerol bevel gear geometry and design characteristics is presented in Table XX. The LVDT characteristics and feedback loop accuracy are presented in Table XXI. Table XXII shows the maximum error between command and actual blade angle at +7° closed and 3347 fan rpm. This condition results in the maximum actuator operating torque and trunnion arm loading.

5.9 ELECTRO-HYDRAULIC SERVO VALVE

The electro-hydraulic servovalve (EHV) will be remotely located from the beta regulator in the engine pylon. The selected servovalve is a standard ABEX Corporation Model No. 425. Design characteristics of the servovalve are presented in Table XXIII and installation dimensions are shown in Figure 29.

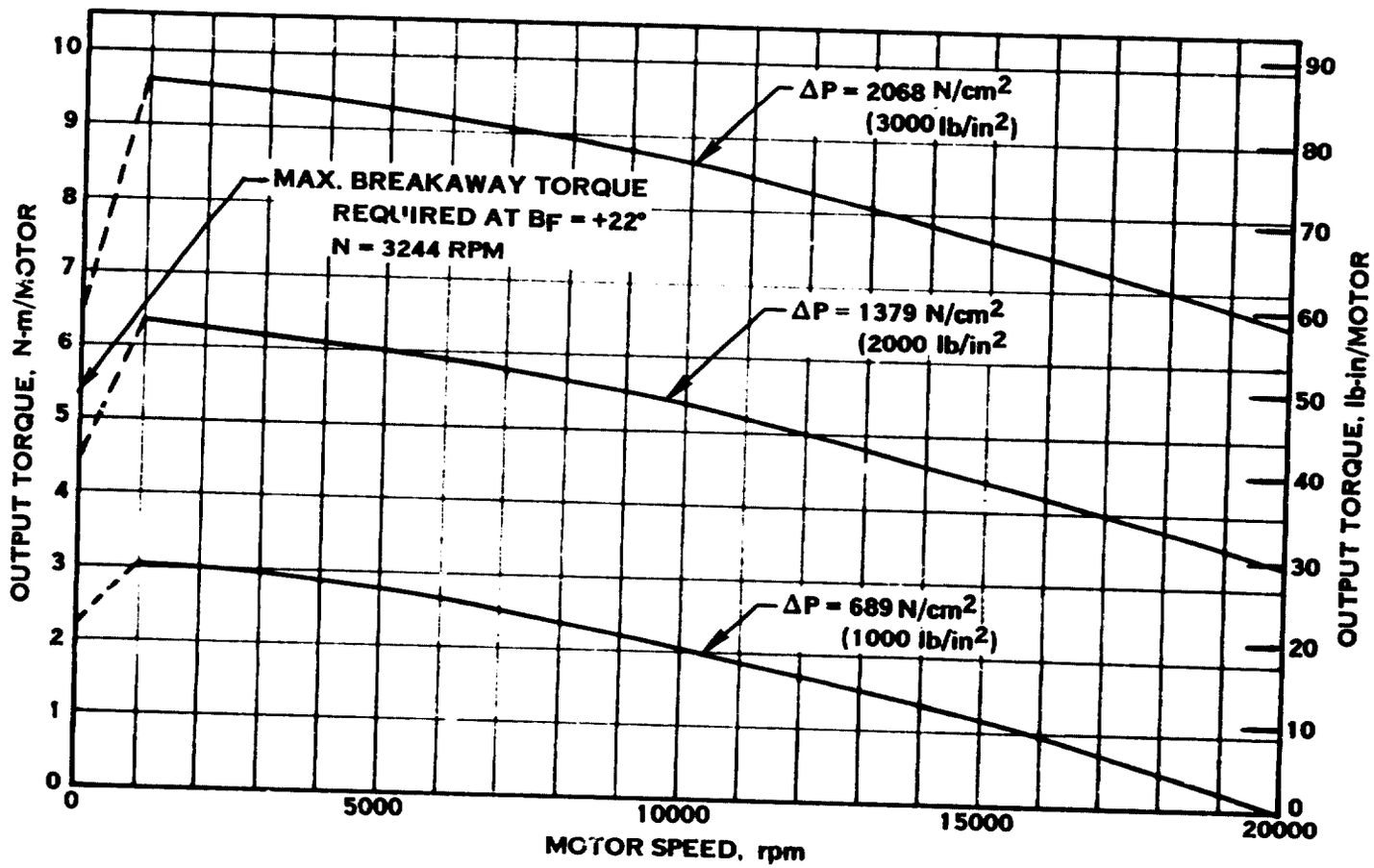

Figure 27. Hydraulic motor output torque vs rpm

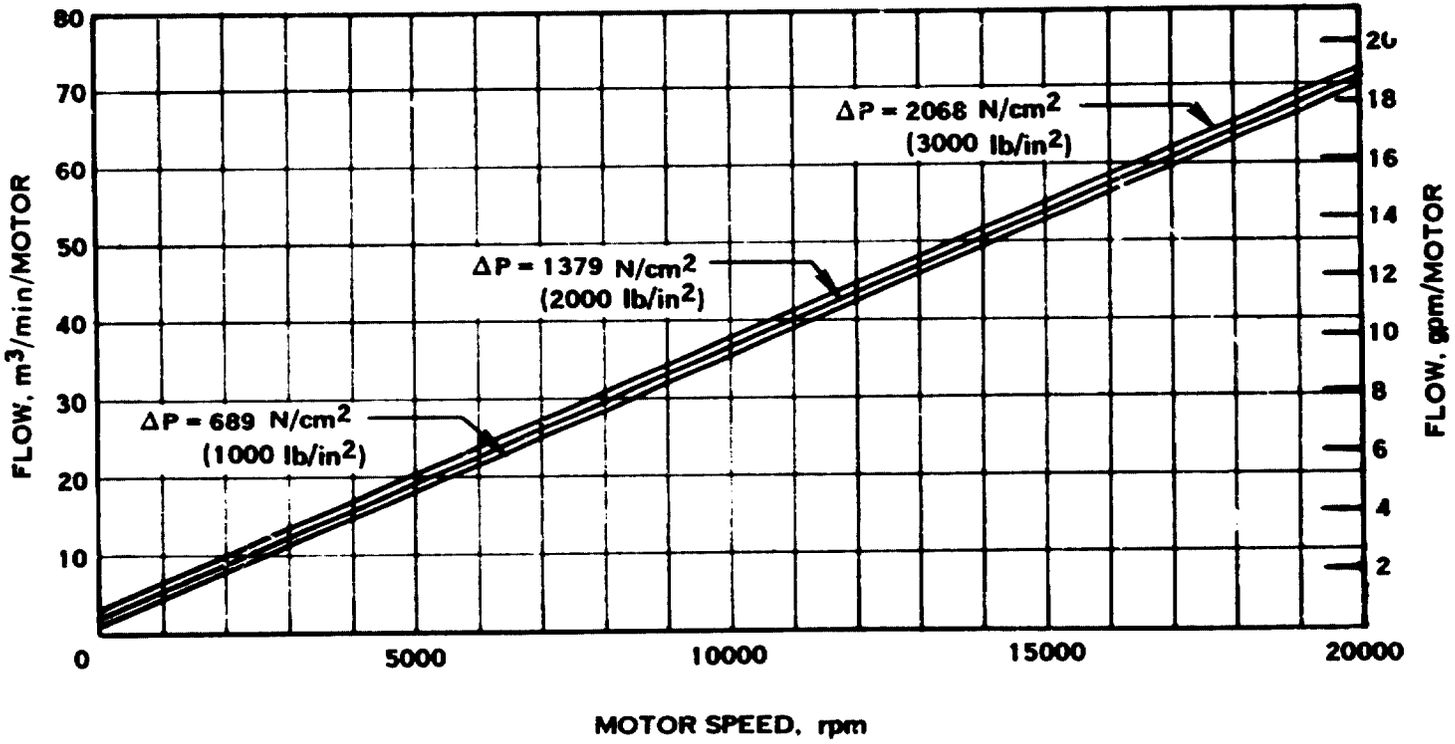

Figure 28. Hydraulic motor flow vs rpm

Table XX. Zerol Bevel Gear Data

(Gear Ratio = 1.2:1)

	Output Pinion		Input Gear
Number Teeth	20		24
Diametral Pitch	16		16
Pressure Angle	20°		20°
Spiral Angle	0°		0°
Shaft Angle	90°		90°
Torque/Mesh	9.6 N-m (85 lb-in.)		11.52 N-m (102 lb-in.)
Contact Stress		172,370 N/cm^2 (250,000 psi)	
Bending Stress		17,075 N/cm^2 (24,765 psi)	
Required Cycles		2×10^6	
Allowable Contact Stress		172,370 N/cm^2 (250,000 psi)	
Allowable Bending Stress		20,685 N/cm^2 (30,000 psi)	
Axial Thrust Load	320 N (72 lbs)		191 N (43 lbs)
Separating Component	383 N (86 lbs)		160 N (36 lbs)

Table XXI. LVDT Characteristics and Feedback Loop Accuracy

Characteristics:

Linearity:	± 0.10% over full range at room temperature
Thermal Coefficient:	± 0.27% over a temperature range of 244° to 394°K (-20° to 250°F)
Sensitivity:	0.74 mv RMS ± 1% per 0.00254 cm (0.001 in.) travel per volt RMS excitation and shall not vary more than ± 0.27% over a temperature range of 244° to 394°K (-20° to 250°F)
Stroke:	± 1.27 cm (± 0.5 in.) from null
Weight:	0.119 kg (0.262 lbs) maximum
MTBF:	695 operating hours, minimum
Input Voltage:	7.07 volts RMS with 10,000 ohms across the secondary.
Frequency:	3 kilocycles
Wave Form:	Sine Wave
Vendor:	Pickering; H.S. Part No. 763417

Loop Accuracy (Degrees Fan Blade Angle):

Item	Thermal 344° ± 50°K (160° ± 90°F)	Backlash(1)	Linearity(2)
Feedback Shaft (Axial)	± 0.002	± 0.008	
Feedback Shaft (Rotation)	0	± 0.001	
Screw	0	± 0.025	
LVDT Core Position	± 0.106	0	
LVDT Electrical		0	± 0.118 (full stroke)
	± 0.108	± 0.034	± 0.118

Combined Full Stroke Accuracy(3) = ± 0.260 for ± 50°K (± 90°F)

(1) Backlash can be eliminated by using a preload spring. The test regulator feedback loop is not preloaded.

(2) The linearity error can be reduced approximately 50% by programming compensation into the engine digital control and still maintain interchangeability of LVDT's. Complete compensation can be programmed for any single LVDT installation.

(3) Corrections from notes (1) and (2) reduce the error to ± 0.167.

Table XXII. Maximum Blade Angle Error at $\beta_F = +7^\circ$ and 3347 Fan rpm

Errors are based on modulating between increase and decrease pitch through the blade friction band of 192 N-m/blade (1700 lb-in./blade) at 3347 rpm and are given in degrees of fan blade angle.

Deflection Between No-Back and Blades: (1)

Harmonic Drive	0.146
Trunnion Arms	0.101
Sub-Total:	0.247

Backlash from Beta Regulator to No-Back:

2 Flex Shaft Splines	0.002
2 Sun Gear Splines	0.003
Differential Gearing	0.006
No-Back	0.151
Sub-Total:	0.162

Deflection from Beta Regulator to No-Back: (1)

Flex Shaft	0.071

Total Mechanical Blade Angle Error = $\underline{0.480^\circ}$ or $\underline{\pm 0.240^\circ}$

The hydraulic error due to control valve (EHV) motion required to overcome system leakage is dependent upon control loop gain and is additive to the above mechanical error. The feedback loop error of Table XXI is also added to obtain total system error.

(1) Deflection is directly proportional to twisting moment, 192 N-m/blade (1700 lb-in/blade) in this case.

Table XXIII. Electro-Hydraulic Servovalve Design Characteristics

Maximum Supply Pressure:	2758 N/cm^2 (4000 psi)
Rated Flow:	1575 cm^3/s (25 gpm) at 690 N/cm^2 (1000 psi) ΔP 2728 cm^3/s (43.3 gpm) at 2069 N/cm^2 (3000 psi) ΔP
O-Ring Seal Material:	Viton A
Fluid:	MIL-L-26399 or MIL-L-7808
Weight:	1.247 kg (2.75 lbs)
Electrical Resistance:	10 ohms/coil
Rated Current:	80.6 ma
Connector:	NAS 1683-H10-T5P8
Vendor:	ABEX Corporation
Model Number:	425
H.S. Part Number:	763416

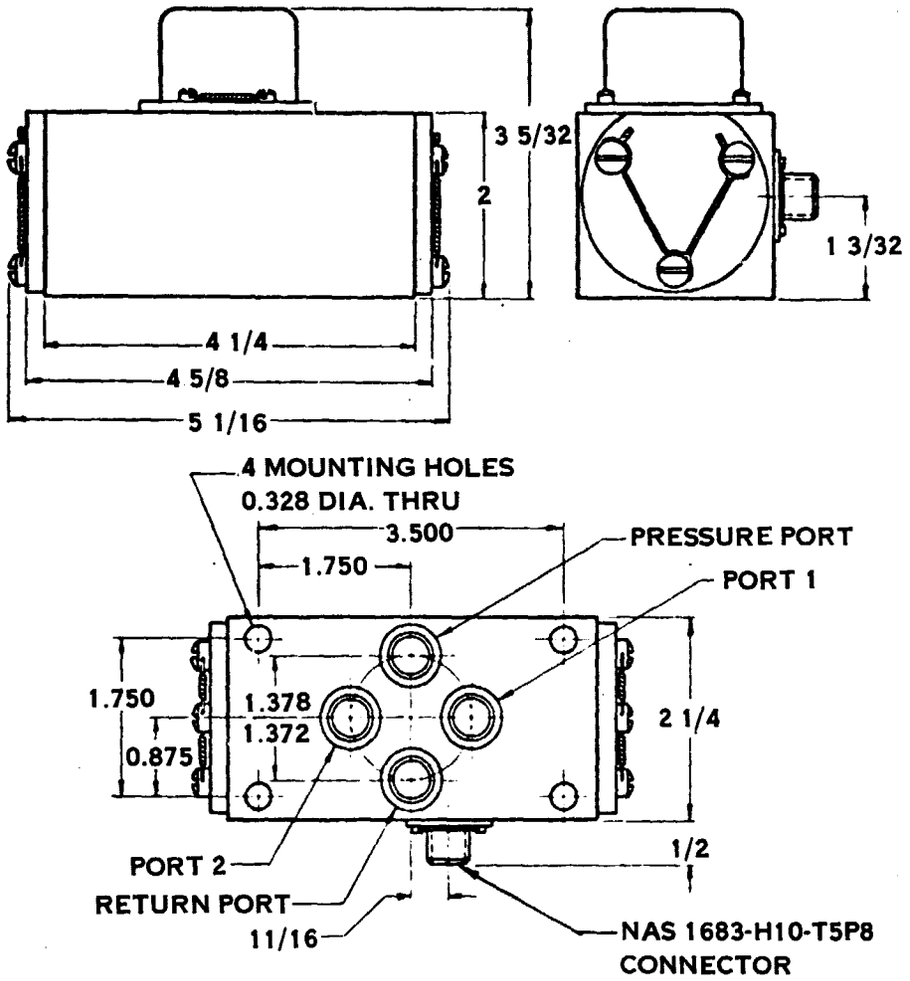

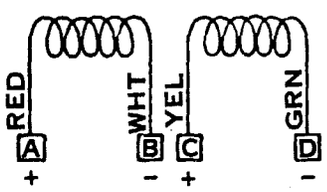

1. WITH ELECTRICAL POLARITY AS SHOWN, PRESSURE PORT IS CONNECTED TO PORT 1 AND RETURN PORT IS CONNECTED TO PORT 2.
2. ALL PORTS 0.505 DIA. MAX., COUNTERBORED FOR MS28775-113 HYDRAULIC "O" RINGS.
3. ALL DIMENSIONS IN INCHES

Figure 29. EHV installation data

5.10 SPLINES

All splines in the actuation system except the face spline, are standard involute splines designed to ANSI B92.1-1970 standards modified for the individual backlash requirements. Design summaries for all splines are presented in Table XXIV.

TABLE XXIV. SPLINE DATA

Item Number	Spline Location	Spline Type	Number of Teeth	Diametral Pitch	Pressure Angle	Pitch Diameter (in.)	Min. Tooth Engagement		Backlash (in.)	Torque (lb-in)	Contact Stress (psi)	Shear Stress (psi)	Bending Stress (psi)	Allowable Stresses		
							Axial (in.)	Radial (in.)						Contact Stress (psi)	Shear Stress (psi)	Bending Stress (psi)
1	No-Back Spring To Input Shaft	Major Dia Fit (Clamped)	37/41 (1)	32/64	30°	1.2813	0.12	0.0235	0.0015 0.0045	850	12,750	10,160	17,785	15,000	15,000	18,000
2	No-Back Spring To Output Shaft	Major Dia Fit (Clamped)	37/41 (1)	32/64	30°	1.2813	0.33	0.0235	0.0015 0.0045	2,400	12,560	10,325	15,990	15,000	15,000	18,000
3	No-Back Shaft Input to Shaft Output	Side Bearing	9/36 (2)	24/48	30°	1.5000	0.50	0.0226	No-Back Requirement Gap	850	11,145	4,060	3,980	12,000	15,000	18,000
4	No-Back Shaft Input to Spring	Side Bearing	9/36 (2)	20/40	30°	1.8000	0.25	0.0310	No-Back Requirement Gap	2,400	38,230	15,470	13,385	(4)	15,000	18,000
5	No-Back Output To Quill	Side Bearing	60	24/48	30	2.500	0.75	0.0226	0.002 0.005	2,400	5,760	4,265	—	6,000	15,000	18,000
6	Quill To Harmonic Input	Side Bearing	77	24/48	30°	3.2083	0.14	0.0227	0.0015 0.0045	2,400	6,195	4,620	—	6,000	12,000	15,000
7	No-Back Shaft Input To Aft Ring	Major Dia Fit	41	32/64	30°	1.2813	—	—	0.0035 0.0065	0	—	—	—	6,000	12,000	18,000
8	Flex. Shaft End Fitting To Drive Coupling	Side Bearing	11/13 (3)	32/64	30°	0.4063	0.70	0.0223	0.0005 0.0035	170	4,115	4,380	6,635	9,000	12,000	15,000
9	Input Sun Gear To Drive Coupling	Side Bearing	13	32/64	30°	0.4063	0.32	0.0223	0.003 0.006	170	9,000	9,580	14,510	9,000	12,000	15,000
10	Ground Sun Gear To Support	Side Bearing	16	24/48	30°	0.7500	0.20	0.0167	0.003 0.006	170	7,545	4,225	—	9,000	12,000	15,000
11	Drive Cone To Ring Gear	Side Bearing	75	16	22½° 30'	4.6875	0.04	0.059	0.002 0.005	850	2,050	2,795	—	5,000	12,000	15,000
12	Ring Gear To Housing	Side Bearing (Clamped)	154	24/48	30	6.4167	0.025	0.0167	0.003 0.006	1,450	7,072	3,955	—	12,000	12,000	15,000
13	Spline Plate To Housing	Side Bearing	154	24/48	30°	6.4167	0.025	0.0167	0.003 0.006	600	2,910	1,635	—	12,000	12,000	15,000
14	Brake Disk To Housing	Side Bearing	154	24/48	30°	6.4167	0.015	0.0167	0.003 0.006	1,200	9,695	5,455	—	12,000	12,000	15,000
15	No-Back Housing To Brake Disk	Side Bearing	184	32/64	30°	5.7500	0.015	0.0183	0.003 0.006	1,200	8,265	7,035	—	12,000	12,000	15,000
16	Harmonic Flex Shaft To Cam Support	Side Bearing	207	24	20°	8.6250	0.25	0.0435	0.003 0.006	45,000	4,655	6,820	—	5,000	12,000	15,000
17	Harmonic Circular Spline To Cam	Side Bearing (Clamped)	258	24/48	30°	10.7500	0.125	0.0227	0.003 0.006	45,000	11,480	8,835	—	15,000	15,000	15,000
18	Face Splines in Cam Support	Side Bearing (Clamped)	144	18.4615	15°	7.800 Gage Dia.	0.595	0.0563 (Mid-Face)	0.000	45,000 lb-in Torque Plus 45,000 lbs Clamp Force	21,535	16,710	—	25,000	20,000	20,000
19	GE Blade Trunnion To Arm	Side Bearing (Clamped)	39	24/48	45°	1.6250	0.25	0.0088	0.0005 0.0033	2,500	36,800	8,950	—	—	—	—
20	GE Lock Ring To Trunnion Arm	Side Bearing	81	32/64	30°	2.5313	—	—	0.002 0.005	—	—	—	—	—	—	—

(1) 4 missing teeth for lock cup tabs

(2) 27 missing teeth to permit relative rotational motion between no-back parts

(3) 2 missing teeth to provide flow path for lubrication fluid

(4) This spline does not rotate under torque load but is rotated to bearing stress applications. Similar splines have been run at 70,000 psi

SECTION 6.0

BEARINGS

Design summaries for the cam support duplex bearings, harmonic drive triplex bearings, differential gearing planet cage support duplex bearings and the differential planet gear roller bearings are presented in Table XXV.

Table XXV. Bearing Data

Bearing Item	Cam Support	Harmonic Drive	Planet Cage	Planets
Type	Duplex	Split Inner Race	Duplex	Roller
Bore	22.86 cm (9.00 in.)	1946 cm (7.66 in.)	5.080 cm (2.00 in.)	1.429 cm (0.5625 in.)
Number Balls	106	66	36	Torrington J-97 Bearing
Ball Diameter	0.4764 cm (0.1875 in.)	0.7144 cm (0.28125 in.)	0.3175 cm (0.125 in.)	
Contact Angle	30°	30°	30°	Radial
Dynamic Capacity	N/A	N/A	4181 N (940 lbs for 1×10^6 rev.)	3336 N (750 lbs for 1×10^6 rev.)
Load Share Factor	1.0	1.45	1.0	1.2
Cage Type, Material	One piece bronze silver plated	One piece steel silver plated	One piece bronze silver plated	Steel
Mean Load	32,470 N (7300 lbs)	N/A	200 N (45 lbs)	273.6 N (61.5 lbs)
Mean rpm	17.2	3450	1544	1164
B_{10} Life (Brg Hrs)	286	112	53,000	50,000
B_{10} Life (Aircraft Hours)	197,017	77,140	53,000	50,000
Required Life (Aircraft Hours)	36,000	36,000	36,000	36,000
MTBF (Aircraft Hours)	1,970,170	771,380	530,000	500,000

SECTION 7.0

ACTUATOR SYSTEM LUBRICATION

Because the actuator duty cycle is short and high flows are not required for cooling, lubrication flow requirements are low. Low flows provide sufficient lubrication of parts and reduce torque losses in the system due to windage. The lubrication schematic, Figure 30, shows the lubrication flow paths and pressures for the actuator system. A total flow of 15.77 cm^3/sec (1.00 quart/minute) is taken from the engine lube system by an orifice at the beta regulator output shaft cover. 3.15 cm^3/sec (0.20 quart/minute) each is directed through two orifices to lubricate the beta regulator output bearings and the bevel gears. The remaining 9.45cm^3/sec (0.60 qt/min) is directed through the flexible shaft casing to lubricate the shaft core and actuator parts.

After leaving the flexible shaft casing, fluid passes through the shaft spline and is metered under pressure from four orifices inside the sun gear drive coupling and shafts. The first three orifices distribute 1.58cm^3/sec (0.10 qt/min) each through the sun gear splines, no-back journal bearings, quill splines and spring.

The fourth orifice directs the remaining 4.73cm^3/sec (0.30 qt/min) flow inside the differential planet cage which distributes the fluid centrifugally to lubricate the cage bearings, planet bearings and planet gears. This fluid passes centrifugally outward through the brake disks to the forward end of the harmonic drive from which it passes through the lobed flex spline and passes aft through the cam support bearings to return to the gear reduction scavenge area through holes in the cam and cam support. Fluid from the forward end of the no-back lubricates the harmonic drive input spline and is then collected on the aft side of the wave generator behind an oil dam formed by the triplex bearing clamp ring. This fluid will be permitted to spill over the dam and pass to the rear on initial whirl tests. If it is determined by initial testing that the oil mist in the region of the triplex bearing provides insufficient lubrication for the bearing, positive lubrication will be provided by drilling holes in the wave generator connecting the oil dam to the inner race split lines. Oil from the aft end of the no-back is routed to the rear of the harmonic drive to prevent contamination of the triplex bearing with possible wear particles from the no-back. Fluid on the aft side of the harmonic drive is directed aft along the flex spline to lubricate the circular ground spline and exit through the duplex cam bearings. The dynamic cam seal is centrifugally vented by the exit holes to preclude a pressure head on the seal.

Beta regulator gears, feedback drive and bearings are lubricated by oil mist formed by fluid sprayed under pressure from the hydraulic motors against the bevel gear teeth.

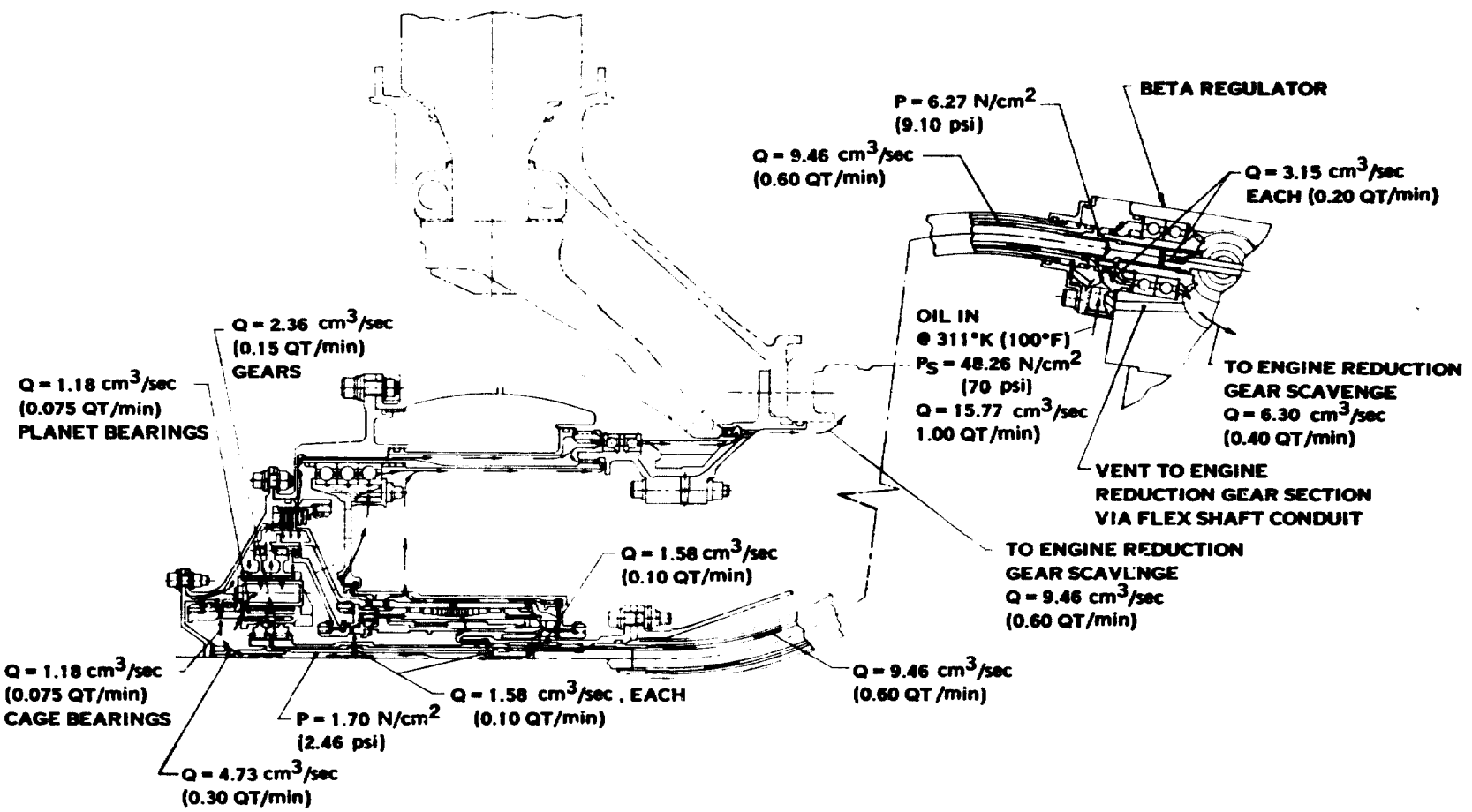

Figure 30. Lubrication schematic

SECTION 8.0

FAN BLADE PITCH ANGLE RANGE

The following summarizes the maximum blade pitch angle operating range capability based on the current actuation/rotor system design:

Reverse Through Stall

Mechanical Stops:	+37°30' closed to -105° open
Electrical Stops:	+31° closed to -98° open

Reverse Through Flat Pitch

Mechanical Stops:	-23° open to +98°30' closed
Electrical Stops:	-16° open to +91°30' closed

Since the trunnion arm is splined to the trunnion by a 39-tooth spline, the total blade angle operating range can be reindexed in increments of 360/39 = 9.23 degrees of blade angle in either direction.

SECTION 9.0

ACTUATION SYSTEM WEIGHT

Summarized in Table XXVI are the component and overall system weights for the flight engine system based on final design analysis. Also shown are weight adders to the experimental engine hardware to reduce development risk and cost. The 5.53 kg (12.2 lb) addition to the beta regulator and electrohydraulic servovalve is to take advantage of low cost existing components. The 4.54 kg (10 lb) adder to the overall system weight is based on changing the material of some parts from titanium to steel and eliminating specific final machining operations to reduce manufacturing costs. Titanium parts changed to steel were the rear cam support housing, cam support bearing nut, no-back and planet cage retaining nuts and the torque limiter brake housing. Milled lightening operations were eliminated on the cam and cam support housing flanges and wall thickness was increased on most of the no-back and differential cylindrical and conical parts in addition to the flexible shaft support cone. The weights of the flight weight and experimental engine actuation systems are 40.45 kg (89.2 lbs) and 52.79 kg (116.4 lbs), respectively.

Table XXVI. Actuation System Weight

Flight Weight Design

	kg	(lbs)
Arms & Rollers	7.66	16.9
Cam, Stops, Support	14.88	32.8
Harmonic Drive	7.57	16.7
No-Back	1.77	3.9
Differential Gear	2.54	5.6
Flexible Shaft & Housing	1.72	3.8
Beta Regulator	4.31	9.5
Total	40.45	89.2

Test System Weight Adders

Harmonic Risk Reduction	2.27	5.0
Beta Regulator	5.53	12.2
Weight Increase for Cost Reduction	4.54	10.0
Total Weight Adders	12.34	27.2
Final Weight of Experimental Engine Actuation System	52.79	116.4

SECTION 10.0

CONCLUSIONS

Design parameters for the detail design of the cam/harmonic drive variable pitch fan actuation system for the QCSEE engine have been presented in this report. The actuator system design satisfies the requirements of GE Specification M50TF1635-S1. In compliance with the Statement of Work, all actuation system components are designed for flight weight except for the beta regulator and the servo valve (EHV). The test beta regulator utilizes two commercial hydraulic gear motors coupled by bevel gears in a simple block-type housing. A flight weight beta regulator design would incorporate a single hydraulic gear motor, designed for the application, providing a direct output torque drive. A flight-weight servo valve and feedback assembly would be mounted with the motor in a light-weight forged housing.

SECTION 11.0

APPENDICES

Appendix A. Sample Design Calculations

Appendix B. Reliability

Appendix C. Failure Mode and Effects Analysis

Appendix D. Preliminary Design Study

Appendix E. Symbols

APPENDIX A. SAMPLE DESIGN CALCULATIONS

A.1 Trunnion Arm and Roller

A.2 Cam Assembly

A.3 Harmonic Drive

A.4 No-Back

A.5 Differential Gearing

A.1 TRUNNION ARM AND ROLLER (Figure 7, Section 5.1)

A.1.1 Stresses at Section B-B (Table IV)

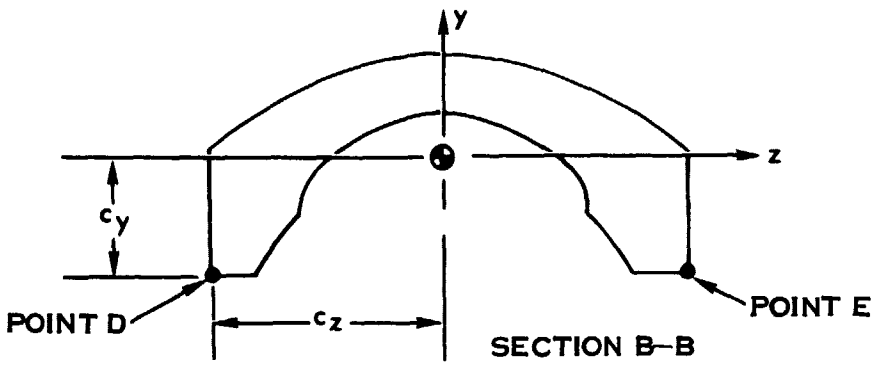

Bending Stress Due to Centrifugal Force on the Arm at 3347 Fan rpm:

$I_Z = 0.0717\ in^4$ $\qquad c_y = 0.525$ in

Moment, $M_X = 3400$ in-lbs (Figure 8, Section 5.1)

$$S = \frac{Mc}{I} = \frac{(3400)(0.525)}{0.0717} = 24{,}900 \text{ psi (tension)}$$

Bending Stress Due to the Axial Component, F_{R_A}, of Roller Force F_R:

$F_R = 700$ lbs $\qquad F_{R_A} = 402$ lbs

$M_X = -281$ in-lbs

$$S = \frac{Mc}{I} = \frac{(-281)(0.525)}{0.0717} = -2074 \text{ psi (compression)}$$

Bending stress due to the lateral component, F_{R_B}, of roller force, F_R:

F_{R_B} = 574 lbs $\qquad$ M_y = 2489 in.-lbs

I_y = 0.744 in^4 $\qquad$ c_z = 1.28 in.

$$S = \frac{Mc}{I} = \frac{(2489)(1.28)}{0.744} = 4623 \text{ psi (tension or compression)}$$

Bending stress due to torque on the section from force component, F_{R_B}:

The torque, equal to 444 lb-in., was assumed to be reacted by arm side beams as shown in the sketch. A conservative calculation of bending stress at the section was made by assuming fixity at the section and an inflection point in each side beam as shown.

$$T = 1.70V;\ V = \frac{444}{1.70} = 261 \text{ lbs}$$

$M_z = (261)(0.45) = 118$ lb-in.

t = 0.32 in.; h = 0.6 in.

$$S = \frac{6M}{th^2} = \frac{6(118)}{(0.32)(0.60)^2} = 6121 \text{ psi}$$

(tension or compression)

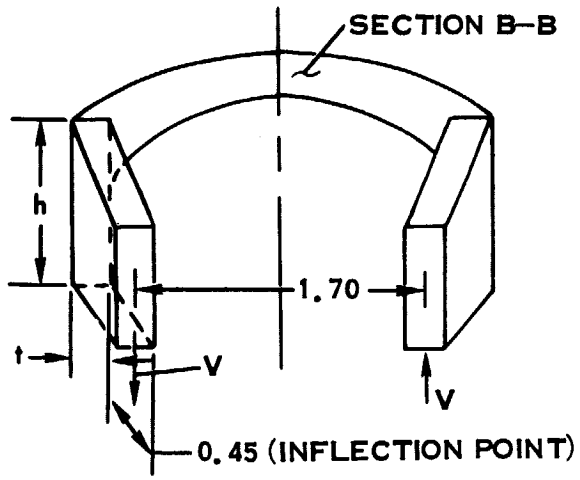

Summation of bending stresses at points D and E:

Mode of Loading	Bending Stress (psi) Point D	Point E
Centrifugal Force, F_c	+ 24,900	+ 24,900
F_{R_A}	- 2,074	- 2,074
F_{R_B} (lateral)	+ 4,623	- 4,623
F_{R_B} (torque)	+ 6,121	- 6,121
Total:	+ 33,570 (tension)	+ 12,080 (tension)

Maximum stress at point D: 0 to 33,570 psi or 16,785 ± 16,785 psi

Summation of bending stresses at points D and E for bird strike roller load, F_R equal to 4350 lbs:

	Point D	Point E
Centrifugal Force, F_C	+ 24,900	+ 24,900
Roller Load, F_R	+ 54,000	- 79,655
Total:	+ 78,900 (tension)	- 54,755 (compression)

A.1.2 Radial Arm Deflection at the Roller Centerline (Table V)

The trunnion arm was assumed to be a cantilever beam fixed at the mounting flange and loaded by the roller load on the end and centrifugal load over the length. The arm was divided into segments by the stations shown in Figure A-1 over length, L. Load on each segment was separated into vertical and horizontal components, F_1 and F_2, as shown. The bending moment, M, and the moment of inertia, I_Z, were calculated at each station from the arm loads. Deflection at the roller centerline was obtained by a double graphical integration of the equation:

$$\frac{d^2y}{dx^2} = \frac{M}{EI}$$

or

$$y = \frac{1}{E} \int_o^L \int_o^L \frac{M}{I} \, dx^2$$

A sample calculation of deflection from centrifugal load components, F_1, at 3347 fan rpm will be presented. A curve of M_1/I_Z was plotted versus x as shown in Figure A-2(a). The area under each segment of the curve was found numerically by multiplying the average M/I for the segment by the segment length, Δx. The accumulated area under the curve to the left of each station represents the slope of the beam at that station when divided by the value of E. This accumulative slope factor (neglecting E) was plotted versus x as shown in Figure A-2(b). The accumulated area under this curve to the left of each station represents the deflection of the arm at that station when divided by the value of E. Table A-I shows the values of M_1, I_Z, Δx and the areas under curves (a) and (b) in columns D and F, respectively.

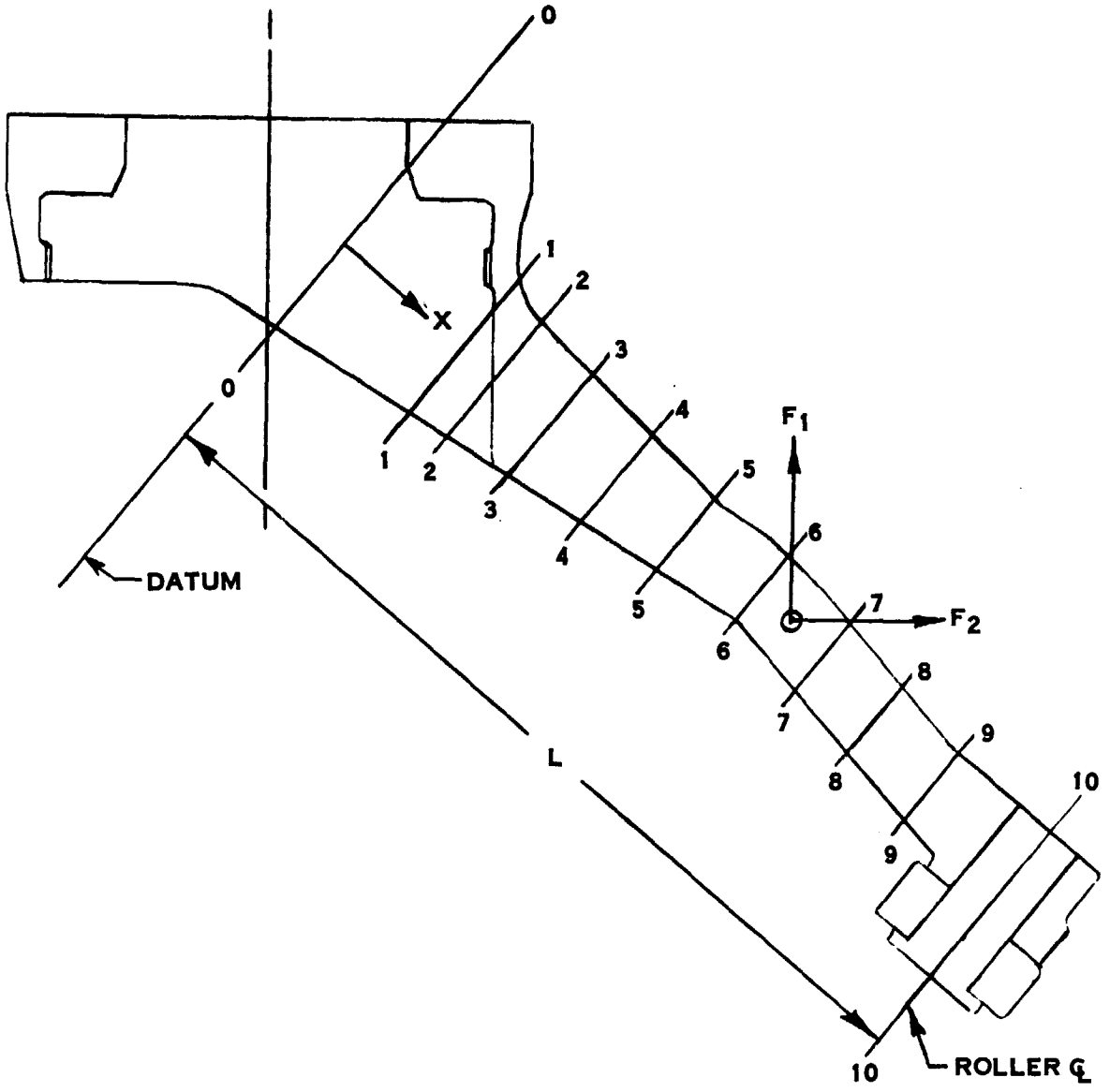

Figure A1. Arm deflection model

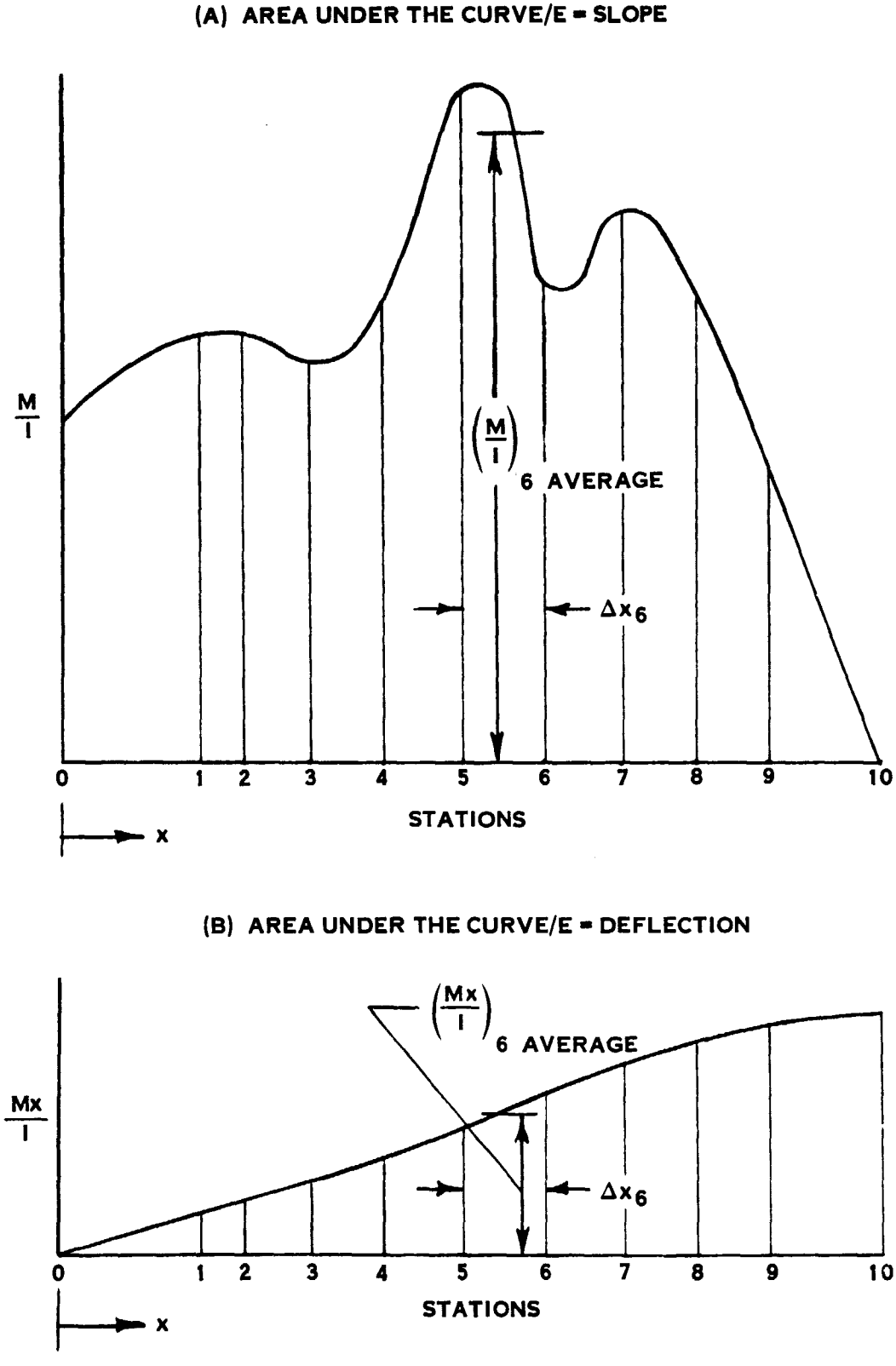

Figure A2. Graphical data used to calculate arm deflection

Table A-I. Graphical Integration Values of $\iint \frac{M}{I} dx^2$

Station	I_z (in^4)	M_1 (in-lbs)	(A) $\frac{M_1}{I_z}$ ($lbs/in^3 \times 10^{-3}$)	(B) ΔX (in)	(C) (A) ave. x (B) ($lbs/in^2 \times 10^{-3}$)	(D) Σ(C) ($lbs/in^2 \times 10^{-3}$)	(E) (D) ave. x (B) ($lbs/in \times 10^{-3}$)	(F) Σ(E) ($lbs/in \times 10^{-3}$)
0	0.130	3218	24.7	0	0	0	0	0
1	0.071	2148	30.3	0.87	24.4	24.4	10.6	10.60
2	0.0626	1875	30.0	0.26	7.8	32.2	7.4	17.95
3	0.0522	1487	28.5	0.42	12.2	44.4	16.1	34.05
4	0.0308	1078	35.0	0.48	14.4	58.8	24.8	58.85
5	0.0163	745	45.7	0.51	21.2	80.0	35.4	94.25
6	0.0140	467	33.4	0.51	21.0	101.0	46.2	140.45
7	0.0082	311	38.0	0.50	18.0	119.0	55.0	195.45
8	0.0061	200	32.8	0.48	17.0	136.0	61.0	256.45
9	0.0053	93	17.5	0.48	7.4	143.45	67.0	323.45
10	-	-	0	0.70	6.1	149.55	102.5	425.95

The radial arm deflection at the roller centerline (x = L) due to centrifugal force components, F_1, is:

$$y_1 = \frac{1}{E} \int_0^L \int_0^L \frac{M_1}{I_z} \, dx^2 \quad \text{where: } E = 15.8 \times 10^6 \text{ psi}$$

$$y_1 = \frac{(425.95)(10^3)}{15.8 \times 10^6} = 0.0269 \text{ in.}$$

By similar calculations, deflection due to centrifugal components, F_2, is:

$$y_2 = 0.0216 \text{ in.}$$

Total deflection at the roller centerline due to centrifugal force on the arm:

$$y = y_1 + y_2 = 0.0485 \text{ in.}$$

Deflections due to roller load were calculated in the same manner.

A.1.3 Roller Contact Stress (Table VI)

Roller contact stress was calculated for a spherically crowned cylinder loaded on a flat plate (Reference "Formulas for Stress and Strain" - R.J. Roark, Third Edition, Case 8, p. 289)

$R_2 = R_2' = \infty$ $\qquad$ $R_1 = 0.47$ in.; $R_1' = 19.5$ in.

$\mu_2 = 0.284$ $\qquad$ $\mu_1 = 0.30$

$E_2 = 30 \times 10^6$ psi $\qquad$ $E_1 = 27 \times 10^6$ psi

$$K = \frac{8}{3} \left[\frac{(27 \times 10^6)(30 \times 10^6)}{(30 \times 10^6)(1 - \overline{0.3^2}) + (27 \times 10^6)(1 - \overline{0.284^2})} \right]$$

$$K = 41.44 \times 10^6$$

$$\delta = \frac{4}{\frac{1}{\infty} + \frac{1}{\infty} + \frac{1}{0.47} + \frac{1}{19.5}} = 1.8357$$

$$\cos\theta = \frac{1.8357}{4}\sqrt{(0-0)^2 + \left[\frac{1}{0.47} - \frac{1}{19.5}\right]^2} + 0 = 0.9529$$

$\theta = 17.65^\circ$; $\infty = 4.12$; $\beta = 0.386$; P = 700 lbs

$$\sqrt[3]{\frac{P\delta}{K}} = \sqrt[3]{\frac{(700)\ (1.8357)}{41.44 \times 10^6}} = 0.0314$$

c = (4.12) (0.0314) = 0.130 in. ; d = (0.386) (0.0314) = 0.0121 in.

$$S_c = \frac{1.5\ P}{\pi\ c\ d} = \frac{1.5\ (700)}{\pi(0.13)\ (0.0121)} = \underline{212,000\ psi}\ \text{(maximum)}$$

A.1.4. Roller Bushing Stress (Table VI)

Pin diameter = 0.4375 in

Effective bushing length = 0.32 in

Projected bearing area, A = 0.14 in^2

Roller load, P = 700 lbs

Bushing compressive stress, $S_c = \frac{P}{A}$

$$S_c = \frac{700}{0.14} = \underline{5000\ psi}$$

A.1.5 Pin Bending Stress (Table VI)

I = 0.00177 $in.^4$; c = 0.218 in.

Roller load, P = 700 lbs

Maximum moment arm = 0.26 in.

Maximum moment, M = (700) (0.26) = 182 lb-in.

$$S = \frac{Mc}{I} = \frac{(182)\ (0.218)}{0.00177} = \underline{22,416\ psi}$$

A.1.6 Bearing Stress at the Pin Socket (Table VII)

The pin has a 0.002 - 0.003 inch diametral interference fit in the socket.

$$S_B = \frac{P}{A} + \frac{Mc}{I} = \frac{P}{(0.52)\ (0.44)} \pm \frac{6\ P\ (0.48)}{(0.44)\ (0.52)^2}$$

$S_B = 4.37\ P \pm 24.2\ P = 28.57\ P$ (maximum)

for P = 700 lbs, $S_B = 20,000$ psi

or, for P = 350 ± 350 lbs,

$S_B = \underline{10,000 \pm 10,000 \text{ psi}}$

(Reference sketch in Section A.1.7 for the above dimensions)

A.1.7 Arm Lug Stresses: (Table VIII)

The arm lug was divided into two separate lugs to react the roller pin loads for purposes of this analysis. The lug model sketch is shown below:

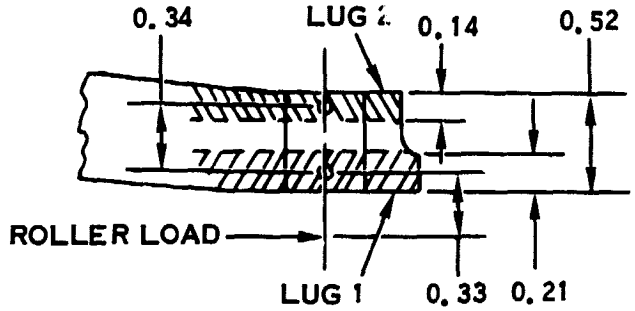

Pin load distribution in the lugs for operating loads is represented by the $\frac{P}{A} + \frac{Mc}{I}$ bearing stress relationship shown in diagram A below. The P/A relationship of diagram B is used for the bird strike load where local yielding is encountered.

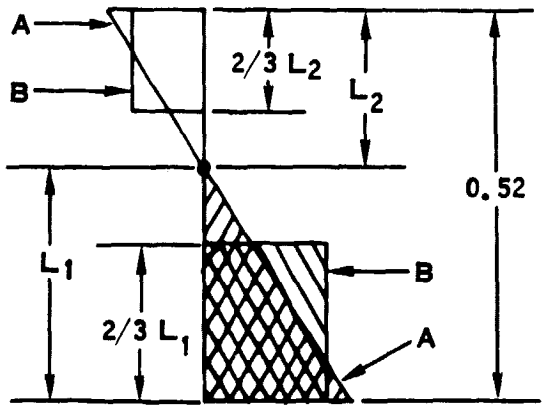

$2/3\ L_1 = 0.21$ in

$2/3\ L_2 = 0.14$ in

The lug reactions were calculated using the above load distribution and the stress analysis for lug 1 based on bird strike roller load equal to 4350 lbs is shown in Figure A3. The reference for this analysis is Section 5.3 of Sikorsky Aircraft Design Manual. The lug load was separated into longitudinal and transverse components and a separate analysis was conducted for each component, after which the results were combined.

The same analysis was used to obtain cyclic lug stresses due to operating loads (Table VIII) but these stresses were modified by a K-factor which reflected the peak stresses at the hole edge from Mc/I loading. Equation (g), P. 85, "Strength of Materials", Volume II, second edition by Timoshenko was used to obtain a stress modifier of 3.225 which is included in the cyclic stresses of Table VIII.

A.2 CAM ASSEMBLY (Figure 10, Section 5.2)

A.2.1 Cam Wall Bending Stresses (Table XI):

A NASTRAN (HS Deck H 729) computer program was used to obtain the bending stresses in the cam slot wall due to the concentrated roller load. NASTRAN is a large, flexible, general purpose computer program, which was developed and is supported by NASA. It uses a finite element structural or heat transfer model, wherein the distributed physical properties of a structure are represented by a finite number of elements. These are interconnected at a finite number of grid points, to which loads or heat sources are applied and for which displacements are calculated. The procedures for defining the loads are well documented in manuals. Mixed boundary value problems are easily accomplished as well as rotational or gravity load cases.

The range of analysis types in the program include: static response to concentrated and distributed loads to thermal expansion and enforced displacements; dynamic response to transient loads, to steady state sinusoidal loads and to random excitation; determination of real and complex eigen values for use in vibration analysis, dynamic stability, and elastic stability analysis. There is also limited capability for the solution of nonlinear problems.

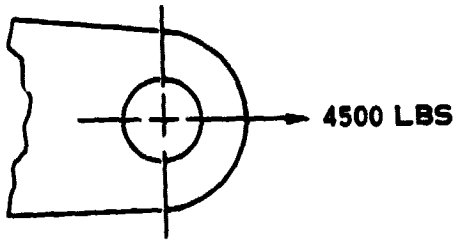

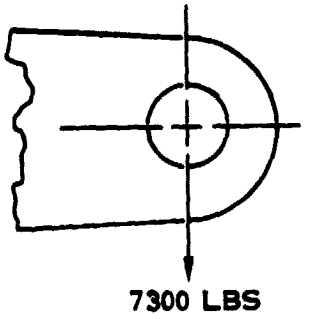

$A_T = (0.21)(1.04 - 0.44) = 0.126$ in.^{2}

$A_{Brg} = (0.44)(0.21) = 0.0925$ in.^{2}

$w/D = 1.04/0.44 = 2.37$

$a/D = 0.52/0.44 = 1.18$

$t/D = 0.21/0.44 = 0.48$

$K_t = 0.95$ (Ref. curve 1)

$K_{Bru} = 0.95$

$K_{Bry} = 1.10$

$A_1 = A_4 = (0.21)(0.365) = 0.077$ in.^{2}

$A_2 = A_3 = (0.21)(0.30) = 0.063$ in.^{2}

$$A_{av} = \frac{6}{4/0.077 + 2/0.063} = 0.0715 \text{ in.}^2$$

$A_{Brg} = 0.0925$ in.^{2}

$A_{av}/A_{Brg} = 0.715/0.0925 = 0.775$

$K_{try} = 0.90$

$K_{tru} = 1.06$

$S_{yield} = 107,000$ psi

$P_{ay} = (0.95)(0.126)(107,000) = 12,800$ lbs.

$P_{ay} = (1.10)(0.0925)(107,000) = 109,000$ lbs.

$P_{try} = (0.9)(0.0925)(107,000)$

$= 8920$ lbs

$$R_{ay} = \frac{4500}{10,900} = 0.413$$

$$P_{try} = \frac{7300}{8920} = 0.820$$

$$\text{M.S.} = \frac{1}{\left[(0.413)^{1.6} + (0.82)^{1.6}\right]^{0.625}} - 1$$

$$\text{M.S.} = \frac{1}{0.973} - 1 = 0.028$$

$$\text{Max. Lug Stress} = \frac{107,000}{1.028} = \underline{104,100 \text{ psi}}$$

Figure A-3. Stress Analysis of Lug 1

The bending stress at Point B was found to be 52,000 psi for the 700 lb. roller load. Based on 350 ± 350 lbs load and K_t equal to 3.4, the bending stress at B is 26,000 ± 35,000 psi. The bending moment at Point D was calculated by adding the moment at B and the moment about D due to shear at B; ($M_D = V_B a + M_B$). The moment at Point C was assumed to be 1/2 the total moment at D. Point C was found to have lower stresses than Point B.

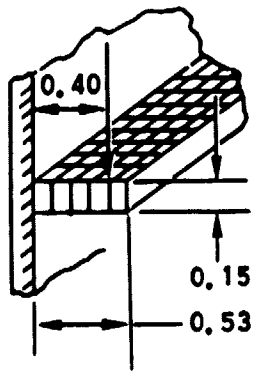

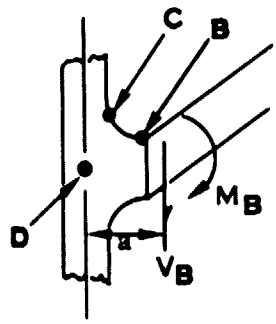

A.2.2 Cam Support Housing (Table XII)

Support housing stresses were obtained by using Hamilton Standard computer program H 561 which is the "Todd-Walker-Hein General Shell Program". This computer program is an IBM-370 program for performing linear, torsionless, static, dynamic, and buckling analysis of structures which can be modeled as collections of thin elastic shells of revolution which are joined and loaded in a general manner. The program calculates meridional, hoop, and in-plane shear stresses; axial, radial, and circumferential deflection, and meridional rotation. Machine plots can be obtained for input geometry, deflected shape, and stresses. H 561 has the capability of handling axially redundant branched shells with features such as pinned joints, sliding joints, axial and radial offsets, radial and axial interferences, and springs.

The program was used to determine housing stresses and deflections with applied cam thrust loads of 10,800 lbs forward and 7000 lbs aft. Critical stress points were found to be at D, E, F and G (Figure 10). Print-outs of the housing model, unloaded and loaded, are presented in Figure A-4.

Stresses at Point D:

The maximum meridional stress is 11,730 psi for an axial load of 10,800 lbs. Because the load is concentrated around the bolts, a distribution factor of 3.2 was used which increased the peak maximum stress to 34,760 psi.

S = 17,380 ± 17,380 psi

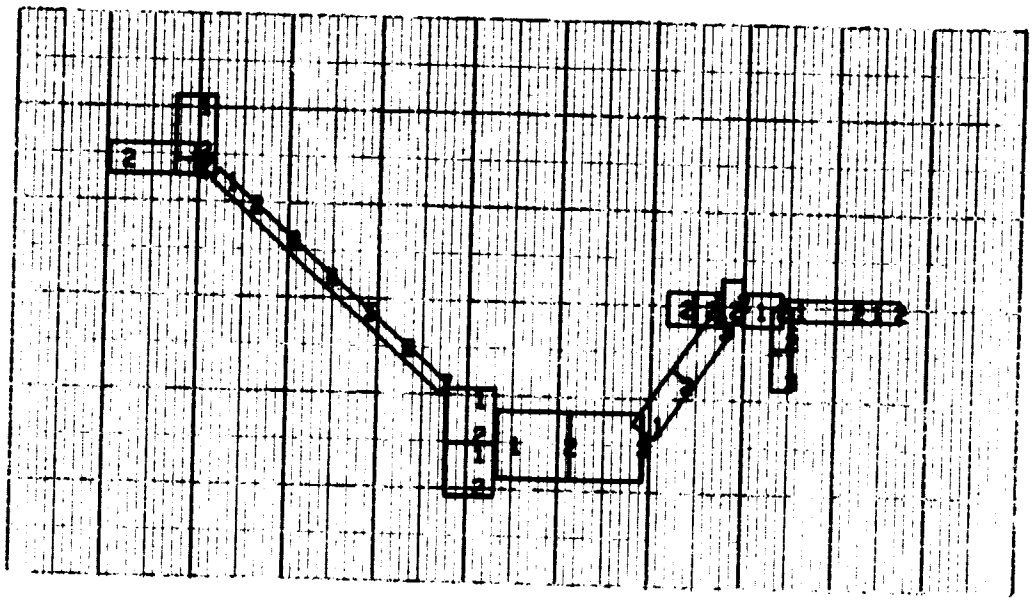

UNLOADED MODEL

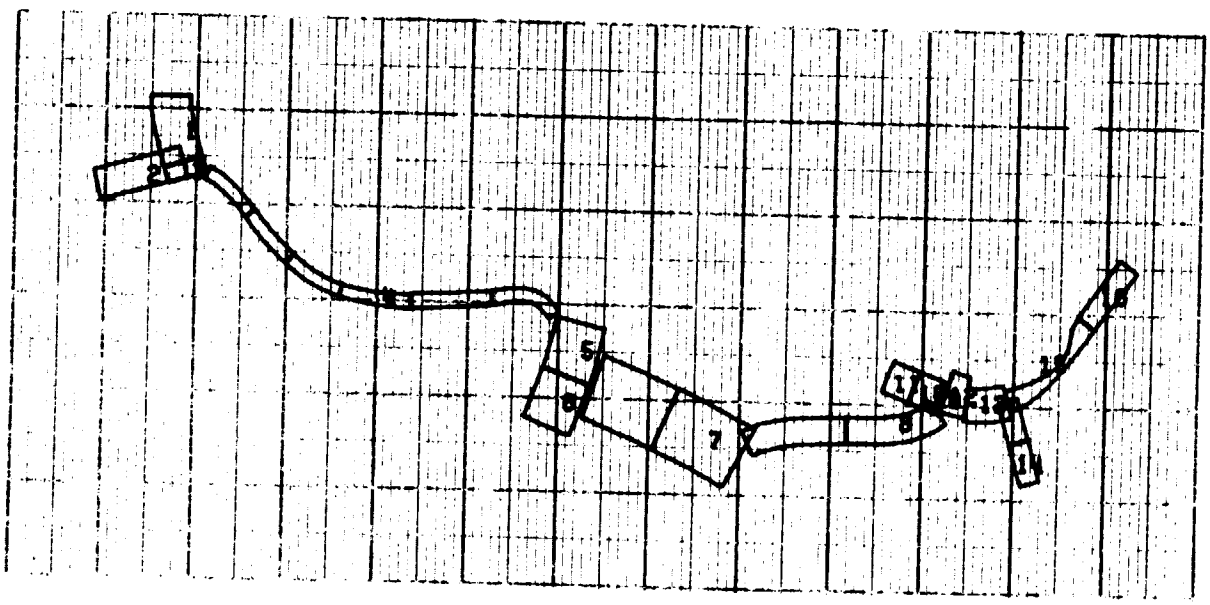

DEFLECTED MODEL UNDER LOAD

Figure A4. Support housing model

C-2

This stress is based on the forward thrust load only since the flange receives backing from the engine flange for aft loads.

Stresses at Point E:

The maximum meridional stress is 11,150 psi for the 10,800 lbs. forward load, and -7227 psi for the 7000 lbs. aft load.

The max. hoop stress is 3815 psi and -2473 psi, respectively, for the above loads.

The torsional stress is 3819 psi for a torque of 45,000 in-lbs acting on the housings.

Using Mohr's circle to combine the above stresses the working stress becomes -9200 to +13,400 psi for an axial load of -7000 to ±10800 lbs (based on a wall thickness of 0.075 in.).

$S = 2100 \pm 11300$ psi

Because the oil drain holes were located here, the wall thickness was increased to 0.12 in. Using a K_t equal to 3.0 and correcting the bending and membrane stresses for the revised thickness, the working stress was calculated to be $1000 \pm 18,600$ psi.

Stresses at points F and G were determined in a similar manner.

A.2.3 Bolted Flange Joint (Table XIII)

Spring Rate:

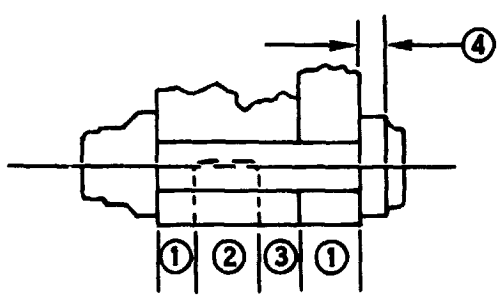

Spring Rate Equation: $K = \frac{AE}{L}$

Clamped Parts:

$$K_1 = \frac{(0.294)(30 \times 10^6)}{(0.40)} = 22.05 \times 10^6 \text{ lbs/in}$$

$$K_2 = \frac{(0.234)(30 \times 10^6)}{(0.40)} = 17.55 \times 10^6 \text{ lbs/in}$$

$$K_3 = \frac{(0.294)(15.8 \times 10^6)}{(0.50)} = 9.29 \times 10^6 \text{ lbs/in}$$

$$K_4 = \frac{(0.0615)(30 \times 10^6)}{(0.15)} = 12.3 \times 10^6 \text{ lbs/in}$$

K_H = combined spring rate of clamped parts

$$\frac{1}{K_H} = \frac{1}{K_1} + \frac{1}{K_2} + \frac{1}{K_3} + \frac{1}{K_4}$$

$$K_H = 3.433 \times 10^6 \text{ lbs/in}$$

Bolt Spring Rate:

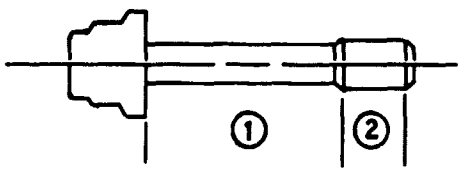

$$K_1 = \frac{(0.04227)(30 \times 10^6)}{1.0} = 1.268 \times 10^6 \text{ lbs/in}$$

$$K_2 = \frac{(0.049)(30 \times 10^6)}{0.40} = 3.675 \times 10^6 \text{ lbs/in}$$

K_B = combined bolt spring rate

$$\frac{1}{K_B} = \frac{1}{K_1} + \frac{1}{K_2}$$

$$K_B = 0.943 \times 10^6 \text{ lbs/in}$$

Bolt Load Equation: $P_B = P_P + \left(\frac{K_B}{K_B + K_H}\right) P_E$

Where:

P_B = Bolt load (lbs)

P_P = Bolt preload (lbs)

P_E = External (applied) load on the joint as a total body (lbs)

$P_B = P_P + 0.2155\, P_E$

Temperature Effect at 250°F:

C = coefficient of thermal expansion (in/in/°F)

L = Length (in.)

Titanium Housing: $C_1 = 4.8 \times 10^{-6}$; $L_1 = 0.5$

$\Delta L_1 = (4.8 \times 10^{-6})(0.5)(180) = 0.000432$ in

Steel Housing: $C_2 = 6.6 \times 10^{-6}$; $L_2 = 0.8$

$\Delta L_2 = (6.6 \times 10^{-6})(0.8)(180) = 0.000951$ in

Bolt: $C_3 = 6.9 \times 10^{-6}$; $L_3 = 1.3$

$\Delta L_3 = (6.9 \times 10^{-6})(1.3)(180) = 0.001614$ in

ΔL_T = total length change due to thermal expansion

$\Delta L_T = \Delta L_3 - (\Delta L_1 + \Delta L_2) = 0.000231$ in

ΔP = loss of preload due to thermal expansion

$$\frac{\Delta P}{3.433 \times 10^6} + \frac{\Delta P}{0.943 \times 10^6} = 0.000231$$

$\Delta P = 171$ lbs

Preload:

Bolt wrench torque = 90 to 100 lb-in

Coefficient of friction range = 0.15 to 0.10

Bolt preload = 1725 to 2900 lbs

Maximum bolt stress at maximum preload and torque is 100,560 psi (based on minimum section properties and combined shear and normal stress).

The moment acting on the bolted joint is 80.5 in-lbs/in from H561 computer program.

$$\text{Joint moment per bolt} = \frac{(80.5)(2\pi)(3.68)}{18} = 103 \text{ lb-in/bolt}$$

$$\text{External bolt load, } P_E = \frac{10,800}{18} = 600 \text{ lbs/bolt}$$

Determination of joint separation under load:

Minimum preload = 1725 - 171 - (1- 0.2155)(600) = 1083 lbs

Bearing area, A = tb

where: t = 0.60 in., the clamped surface height.

b = the effective circumferential width, in

$$\text{Preload bearing stress} = \frac{P}{A} = \frac{1083}{(0.60)b} = \frac{1805}{b} \text{ psi}$$

$$\text{Moment bearing stress} = \frac{6M}{t^2 b} = \frac{6\,(103)}{(0.60)^2 b} = \frac{1717}{b} \text{ psi}$$

Since the preload bearing stress is greater than the moment bearing stress, the joint will not separate. Also there is no flange levering effect on the bolt load since the joint does not separate. Angular deflection of the housing induces bending in the bolt.

Bolt stress due to angular deflection of the housing:

The difference in slope between the bolt head and nut is 0.00053 in/in from computer program H 561. Consider the bolt as a beam with end moments:

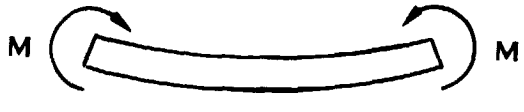

$$M = \frac{\theta EI}{L} = \frac{(0.00053)(30 \times 10^{6})(1.192 \times 10^{-4})}{1.30} = 1.46 \text{ lb-in}$$

Where I is the moment of inertia of the necked-down portion of the bolt.

Bolt bending stress:

$$S = \frac{Mc}{I} = \frac{(1.46)(0.1007)}{7.85 \times 10^{-5}} = 1859 \text{ psi}$$

Where I is the minimum moment of inertia of the bolt.

Bolt stress due to the applied tensile load as modified by the spring rate factor:

$$S = \frac{P}{A} = \frac{(0.2155)(600)}{0.0318} = 4066 \text{ psi}$$

Where A is the minimum bolt cross-sectional area.

Total maximum bolt stress at room temperature due to:

Preload	100,560
Axial load	4,066
Moment	1,859
	106,485 psi

Minimum bolt stress at 250°F and 0 applied load:

$$S = 100,560\left(\frac{2900 - 171}{2900}\right) = 94,630 \text{ psi}$$

Bolt stress range: 94,630 to 106,485 psi

$S = 100,560 \pm 5930$ psi

Allowable no. cycles: 10^{8}

A.3 HARMONIC DRIVE (Figure 13, Section 5.3)

A.3.1 Bearing Life:

Ball spring rates were calculated for the triplex bearing based on 0.0004 in radial mis-match of one of the three bearings. The results, presented in Figure A-5,

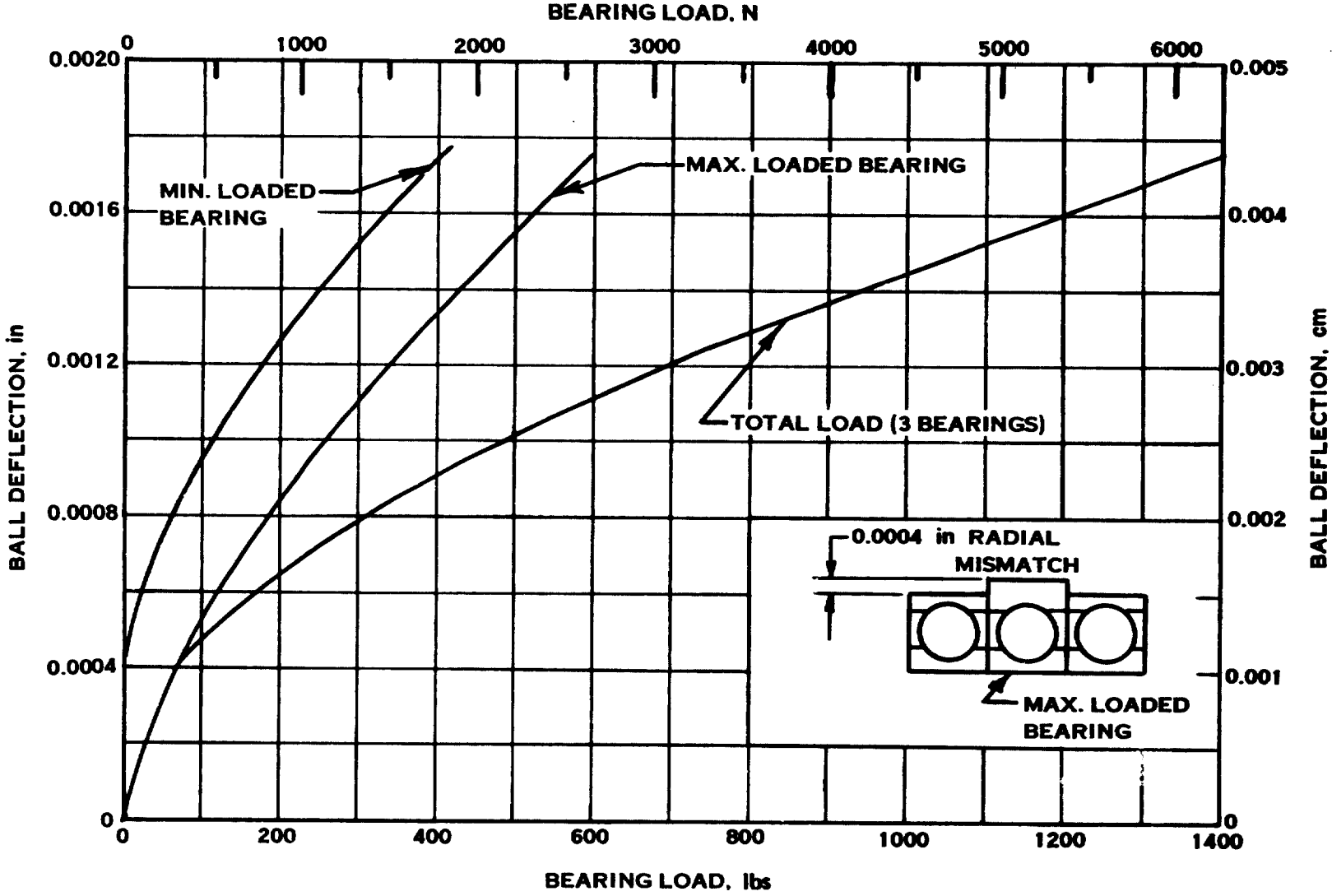

Figure A5. Harmonic bearing load share

represent a load share distribution between the three bearings. This distribution was used in the harmonic drive computer program to determine ball load vs. azimuth position at various output torques. These results are shown in Figure A-6.

A factor for increased life of the split inner race as compared with a one-piece race is derived in Figure A-7. The ball loads and life factors were used to obtain bearing life versus torque for the triplex set by using A. B. Jones' rolling element computer program. These bearing set life results are presented in Table A-II and Figure A-8.

The mission duty cycle (Figure 1) and blade twisting moment vs. blade angle curve (Figure 2) were converted to plots of harmonic output angle versus mission flight condition and output torque versus output angle as shown in Figures A-9 and A-10, respectively. Cubic mean output torques were calculated for each mission flight condition as summarized in Table A-III. Bearing life was obtained from A. B. Jones' computer program for each condition and was combined with percent of mission time to determine total bearing B_{10} life and MTBF as presented in Table A-IV.

A.3.2 Flex Spline Tooth Stresses at Point A (Figures 13 and 15):
(Reference: "Designing by Photoelasticity" - Heywood, Equation 6.36)

$$S_{Tooth} = K_t \left[\frac{1.5a}{e^2} + \sqrt{\frac{0.36}{b\,(e)}} \left(1 + \frac{1}{4}\ smr \right) \right] \ N/t$$

$$S_{Tooth} = K_t \left[\frac{1.5\ (0.0157)}{(0.0186)^2} + \sqrt{\frac{0.36}{0.0232\ (0.0186)}} \left(1 + \frac{1}{4}\ (0.059) \right) \right] \frac{N}{1.70}$$

$$S_{Tooth} = K_t \left[68.1 + 28.8\ (1.015) \right] \frac{N}{1.70} = K_t \left[68.1 + 29.3 \right] \frac{N}{1.70}$$

$$= K_t \left[97.4 \right] \frac{N}{1.70} = 57.3\ K_t\ N$$

$$K_t = 1 + 0.26 \left(\frac{e}{R} \right)^{0.7} = 1 + 0.26 \left(\frac{0.0186}{0.0060} \right)^{0.7} = 1.575$$

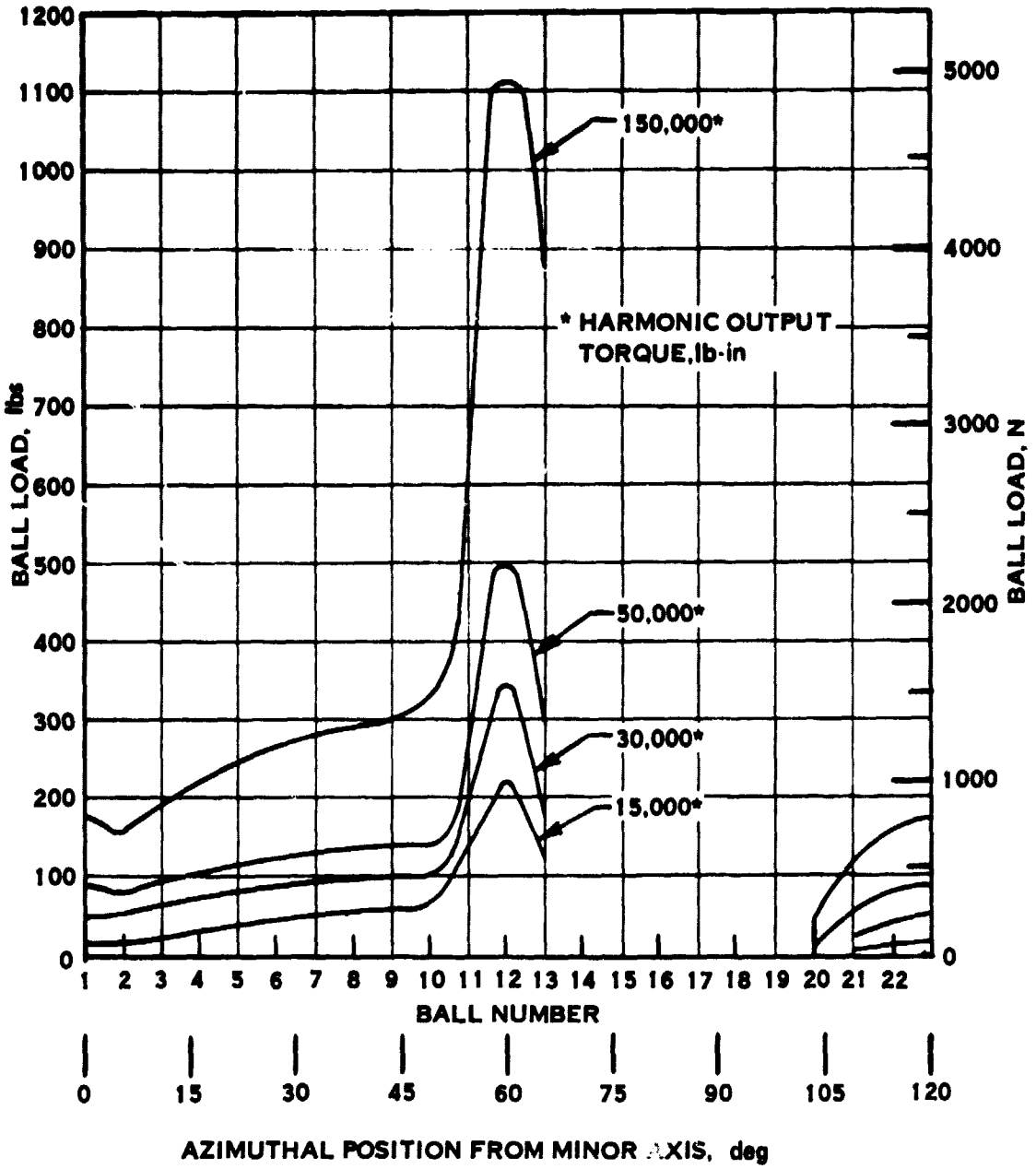

Figure A6. Harmonic bearing load distribution

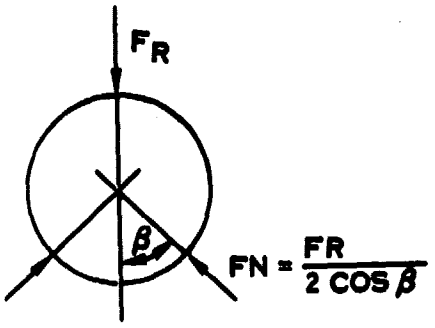

L_{is} = Standard inner race life

L_{i2} = Life of one half of the split inner race

L_i = Total life of two halves of the inner race

Life is increased because load is reduced for $\beta = 30°$:

$$\frac{F_N}{F_R} = 0.578$$

$$\frac{L_{i2}}{L_{is}} = \left(\frac{F_R}{F_N}\right)^3 = \left(\frac{1}{0.578}\right)^3 = 5.179$$

There are 2 split inner races per bearing

$$\therefore \frac{1}{L_i} = \left[\frac{1}{\left(L_{i2}\right)^{\frac{10}{9}}} + \frac{1}{\left(L_{i2}\right)^{\frac{10}{9}}}\right]^{0.9} = \frac{1.866}{L_{is}}$$

$$\frac{L_i}{L_{is}} = \left(\frac{5.179}{1.866}\right) = 2.777$$

Life reduction factor due to ball spin

$$= \left[1 - \frac{1}{3} \sin \beta\right]^3 = 0.578$$

Total life factor for split inner race:

$$C_s = 2.777\ (0.578) = 1.61$$

Figure A-7. Split Inner Race Life Factor

Table A-II. Harmonic Bearing Set Life vs. Torque

0.28125 Ball Dia, 51.6% Ball Conformity, 30° Initial Split Inner Race Contact Angle, 0.0004 Radial Mismatch

Output Torque (in.-lb)	Bearing Load Level	Program Outer Race Life (Hrs) L_o	Program Standard Inner Race Life (Hrs) L_{is}	Split* Inner Race Life (Hrs) L_i	Assembly Load Life Factor C_a	Bearing Set Life (Hrs) L
15000	Max Loaded	276	167	269	0.568	79.1
	Min Loaded	9040	5890	9480	0.472	
30000	Max Loaded	58.1	35.3	56.8	0.703	19.2
	Min Loaded	591	341	549	0.754	
45000	Max Loaded	22.7	13.6	21.9	0.771	7.57
	Min Loaded	138	78.4	126	0.844	
50000	Max Loaded	17.6	10.5	16.9	0.787	5.84
	Min Loaded	96.0	54.5	87.7	0.861	

$$\frac{1}{L} = \frac{1}{f_a}\left[\left(\frac{1}{L_{ox}}\right)^{10/9} + \left(\frac{1}{L_{ix}}\right)^{10/9} + \left(\frac{2}{L_{on}}\right)^{10/9} + \left(\frac{2}{L_{in}}\right)^{10/9}\right]^{0.9}$$

where: n denotes minimum loaded races
x denotes maximum loaded race
C_a = assembly load life factor = $\left(\frac{\text{Torque load}}{\text{Torque load + assembly loads}}\right)^3$

*Includes split inner race life factor, $C_s = 1.61$

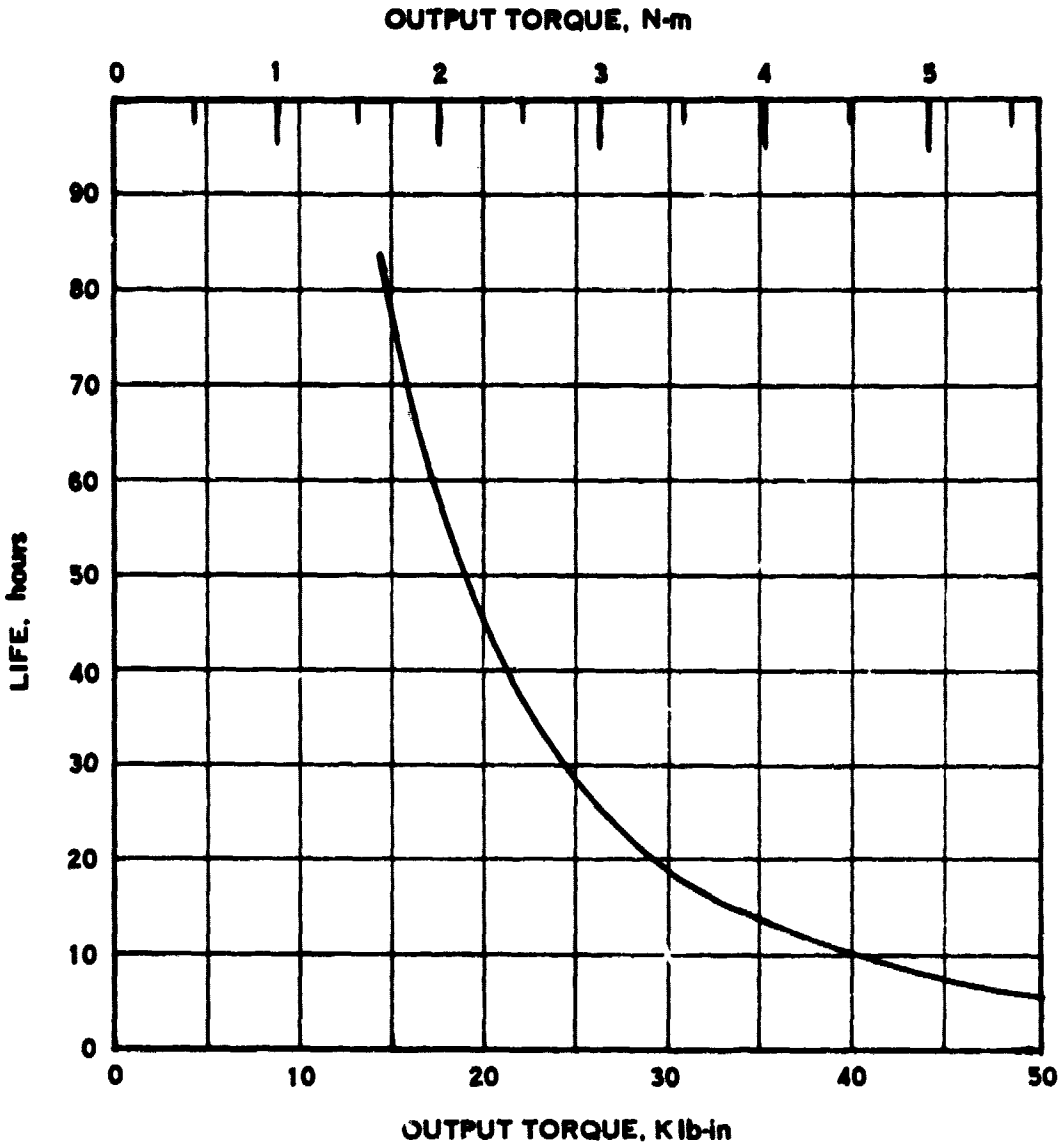

Figure A8. Harmonic bearing set life

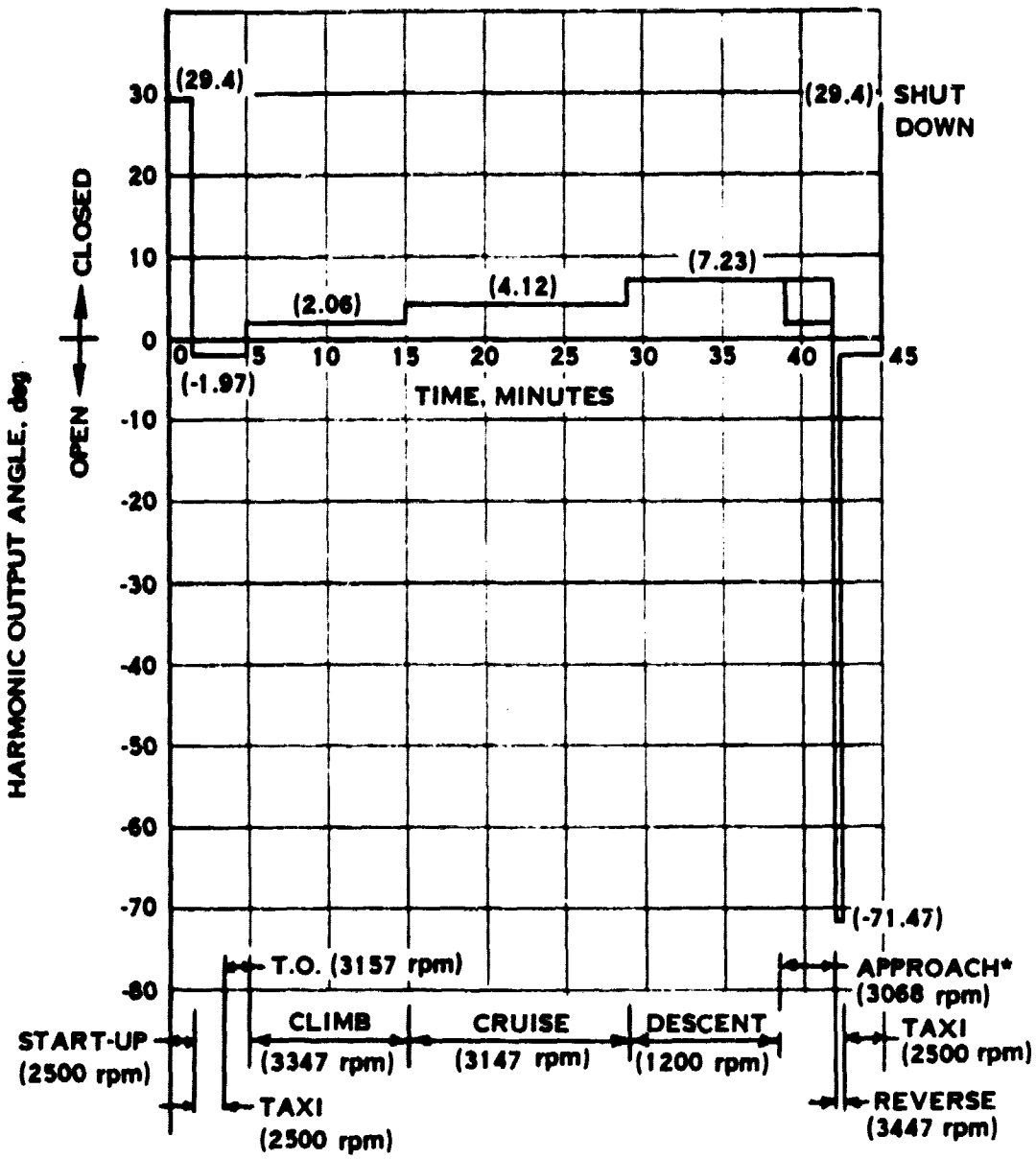

* ASSUME MODULATING OPERATION DURING APPROACH BETWEEN 2.06 AND 7.23 DEGREES HARMONIC OUTPUT ANGLE WITH TOTAL TRAVEL OF 186 DEGREES. INDICATED rpm REPRESENTS FAN SPEED.

Figure A9. Harmonic drive mission duty cycle

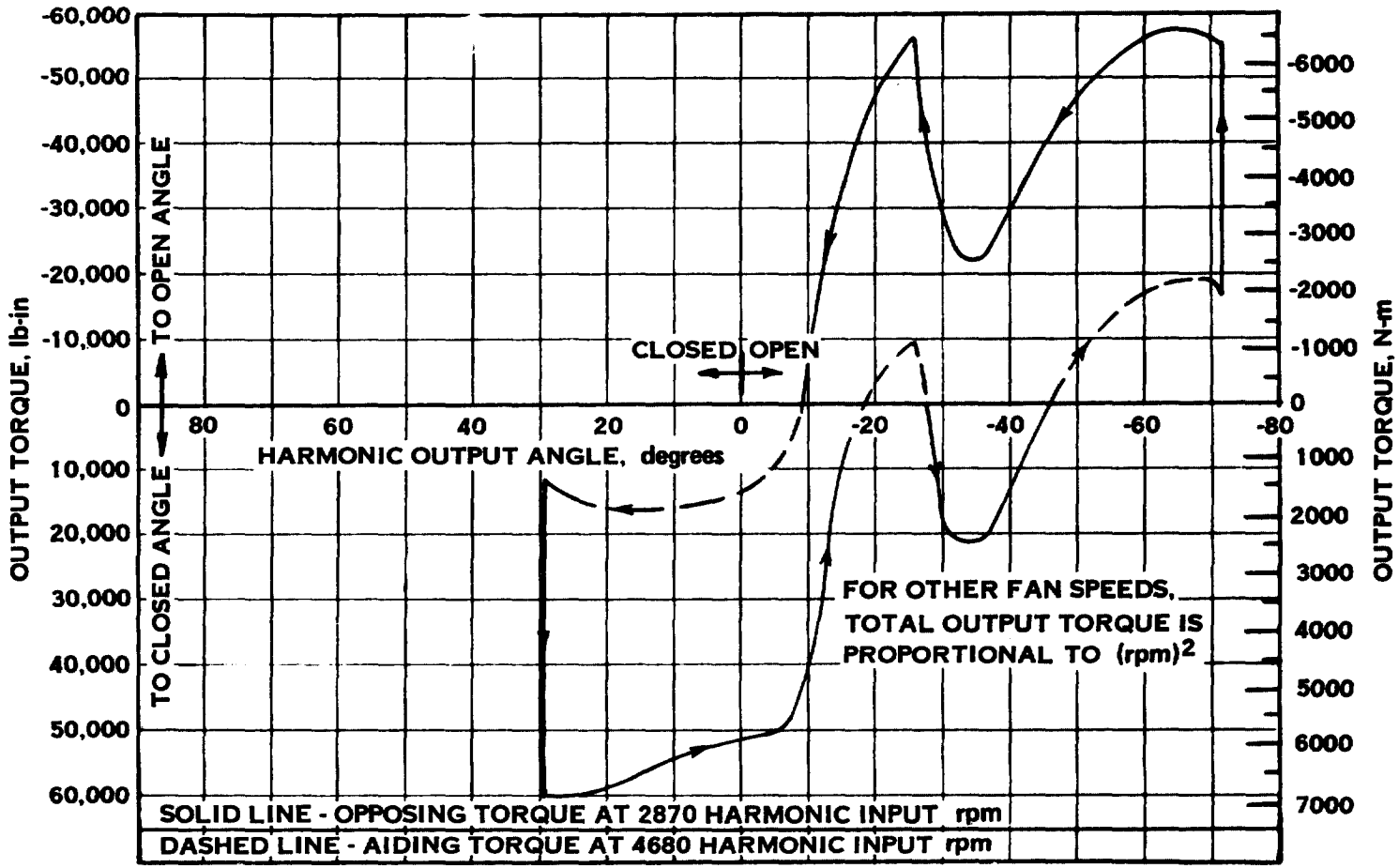

Figure A10. Harmonic drive total output torque at 3347 fan rpm - (reverse through stall)

Table A-III. Harmonic Loading for Mission Duty Cycle

Condition	Harmonic Output Range		Δ Harmonic Angle	Fraction of Mission	Cubic Mean Torque at 3347 rpm	Actual rpm	Cubic Mean Torque at Actual rpm
Start-up to Taxi	29.4	- 1.97	31.37	0.0772	56,480	2500	31,510
Take-off to Climb	- 1.97	2.06	4.03	0.0099	13,290	3157	11,820
Climb to Cruise	2.06	4.12	2.06	0.0051	14,250	3347	14,250
Cruise to Descent	4.12	7.23	3.11	0.0077	15,020	3147	13,280
Approach (Modulating)	7.23	2.06	186.00	0.4580	42,180	3068	35,440
Approach to Reverse	7.23	-71.47	78.70	0.1938	32,200	3068	27,060
Reverse to Shut Down	-71.47	29.4	100.87	0.2484	39,680	2500	22,140
			406.14	1.0001			30,860

Table A-IV. Harmonic Bearing Life

Condition	Cubic Mean Torque (lb-in.)	Fraction Of Time	Life @ 3447 rpm (Hrs)	Time / Life
Start Up to Taxi	31,510	0.0772	16.8	0.00458
Take-Off to Climb	11,820	0.0099	85.0	0.00011
Climb to Cruise	14,250	0.0051	82.5	0.00006
Cruise to Descent	13,280	0.0077	85.0	0.00009
Approach (Modulating)	35,440	0.4580	13.0	0.03521
Approach to Reverse	27,060	0.1938	25.8	0.00752
Reverse to Shut Down	22,140	0.2484	41.9	0.00592
				0.05352

$$\text{Life} = \frac{1}{0.05352} = 18.68 \text{ hours}$$

Life factor for CEVM material is 6.0

Life = (18.68)(6.0) = 112.1 hours

MTBF = 1121 hours

$$\frac{\text{hours}}{\text{mission}} = \left(\frac{\text{output degrees}}{\text{mission}}\right)\left(\frac{\text{input degrees}}{\text{output degrees}}\right)\left(\frac{\text{revolutions}}{\text{degree}}\right)\left(\frac{\text{minutes}}{\text{revolution}}\right)\left(\frac{\text{hours}}{\text{minute}}\right)$$

$$\frac{\text{hours}}{\text{mission}} = (406.14)(201)\left(\frac{1}{360}\right)\left(\frac{1}{3447}\right)\left(\frac{1}{60}\right) = 0.001096$$

MTBF = 1,022,400 missions

MTBF = 766,820 aircraft hours

Tangential load distribution of f $\frac{lb}{in.}$ on the flex spline teeth per lobe is approximately represented by a cosine shape over an arc, $2\gamma = 10$ degrees.

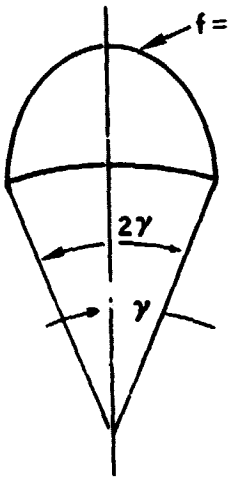

$$F_{Lobe} = 2\int_0^{\frac{\pi}{36}} frd\gamma = 2 f_{max} r \int_0^{\frac{\pi}{36}} \cos 18\gamma \, d\gamma$$

$$F_{Lobe} = \frac{2 f_{max}}{18} \int_0^{\frac{\pi}{36}} \sin 18\gamma = \frac{r f_{max}}{9}$$

$$f_{max} = F_{Lobe} \frac{(9)}{r}$$

Since there are 600 teeth;

$$F_{\substack{Tooth \\ max}} = f_{max} \frac{2\pi r}{600} = F_{Lobe} \left(\frac{9}{r}\right) \frac{2\pi r}{600} = 0.0944 F_{Lobe}$$

$$F_{Lobe} = \frac{T}{3R} = \frac{50,000}{3\,(4.35)} = 3,820 \text{ lb}$$

$$F_{\substack{Tooth \\ max}} = 360 \text{ lb}$$

$$N_{\substack{Tooth \\ max}} = F_{\substack{Tooth \\ max}} \left(\frac{1}{\cos \varphi_E}\right)$$

where: φ_E = effective pressure angle with friction effect

For $\mu_f = 0.06$, $\varphi = 20°$, $\varphi_E = 23.4°$

$$N_{\substack{Tooth \\ max}} = \frac{360}{0.919} = 392 \text{ lb}$$

$$S_{Tooth} = \left(\frac{392}{2}\right)\left(57.3\right) \pm \left(\frac{392}{2}\right)\left(57.3\right)\left(1.575\right)$$

$$= 11,200 \pm 17,700 \text{ psi}$$

Flex Spline Stress Concentration Factor (Reference: "Stress Concentration Factors" - R.E. Peterson, 1974, Figures 74 and 75)

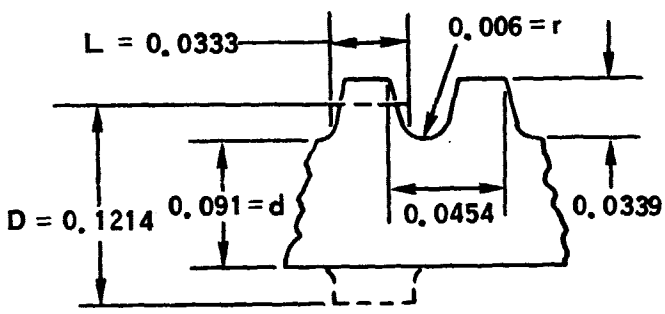

$$p/h = \frac{0.0454}{0.0339} = 1.34$$

$\gamma = 0.45$

$h_e = 0.45\ (0.0339) = 0.0152$

$D = 0.091 + 2\ (0.0152) = 0.1214$

$L/D = 0.274$

$r/d = 0.066$

$D/d = 1.335$

For D/d = 1.25 $K_t = 1.73$

For D/d = 2.00 $K_t = 1.87$

∴ For D/d = 1.335, $K_t = 1.75$

Flex Spline Member Stress:

Initial Fit-Up Stress:

$$S_{Fit\text{-}up} = \pm 14,800\ K_t \text{ (from shell computer program)}$$

Torque Loading Stress:

$$F = \frac{T}{3R} = \frac{50,000 \text{ in.-lb}}{3\ (4.35)} = 3,840 \text{ lb per lobe}$$

$A = 0.09\ (1.70) = 0.153\ \text{in.}^2$

$$S_{Torque} = \frac{F}{2A} = \frac{3480}{2(0.153)} = 12{,}500\ \text{psi (maximum)}$$

Stress varies between 0 and 12,500 psi

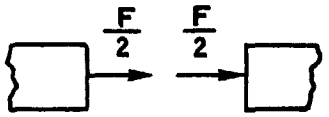

Therefore:

$$S_{Torque} = 6{,}250 \pm 6{,}250\ K_t$$

Total Member Stress:

$$S_{Member} = S_{Fit\text{-}up} + S_{Torque} = \pm 14{,}800\ K_t + 6{,}250 \pm 6{,}250\ K_t$$
$$= 6{,}250 + 21{,}050\ K_t$$

$$K_t = 1.75$$

$$S_{Member} = 6{,}250 \pm 21{,}050\ (1.75)$$
$$= 6{,}250 \pm 36{,}800\ \text{psi}$$

Combined Stress:

$$S_{Member} = 6{,}250 \pm 36{,}800\ \text{psi}$$
$$S_{Tooth} = 11{,}200 \pm 17{,}700\ \text{psi}$$

$$S_{Combined} = S_{Member} + A\,S_{Tooth}$$

$$A = \frac{1}{1 + C_o\left[\frac{S_{Member}}{S_{Tooth}}\right]}$$

$$C_o = .\left(\frac{60-\phi}{44}\right)^2$$

$$\phi = 20^\circ$$

$$C_o = \left(\frac{60-20}{44}\right)^2 = 0.827$$

$$A_{Steady} = \frac{1}{1 + 0.827\left(\frac{6,250}{11,200}\right)} = \frac{1}{1.461} = 0.685$$

$$A_{Cyclic} = \frac{1}{1 + 0.827\left(\frac{36,800}{17,700}\right)} = \frac{1}{2.72} = 0.368$$

$$S_{Combined} = \left[6,250 + 0.685\ (11,200)\right] \pm \left[36,800 + 0.368\ (17,700)\right]$$

$$= \left[6,250 + 7,690\right] \pm \left[36,800 + 6,500\right]$$

$$= \underline{13,940 \pm 43,300}\ \text{psi}$$

$$S_{Allowable} = 13,940 \pm 47,000\ \text{psi}$$

Flex Spline Tooth Bearing Stress:

Tooth engagement, h:

Tooth addendum = 0.0145 in.

Max engagement = 0.029 in.

Loss of engagement due to deflection = 0.0031 in.

Loss of engagement due to tolerances = 0.0040 in.

Loss of engagement due to break edges = 0.0020 in.

Minimum engagement = 0.0199 in.

Length of spline, L = 1.70 in.

$$S = \frac{P}{hL} = \frac{360}{0.0199\ (1.70)} = 11,000\ \text{psi}$$

A.3.3 Flex Spline Stresses:

A general multi-layer orthotropic shell of revolution computer program capable of analyzing shells subjected to axisymmetrical and unaxisymmetrical loads was used to analyze the flex spline. The HS deck number is HO88. Hoop and axial stresses and deflections were obtained from inputs of the forced harmonic deflections and shoulder friction forces at the forward end of the flex spline.

Flex spline wall geometry is shown in Figure A-11 and structural computer models are presented in Figures A-12 and A-13. Figure A-14 presents critical flex spline stresses including stresses at Point B, (Figure 13, Table XVI).

A.3.4 Flex Spline Torsional Stability: (Reference: "Formulas for Stress and Strain" - R.J. Roark, Third Edition, Case 27 Table XVI).

Maximum design torque = 150,000 lb-in.

Shaft shear stress, $S_s = \frac{Tc}{J} = \frac{T}{2\pi r^2 t}$

$$S_s = \frac{150,000}{2\pi (4.15)^2 (0.04)} = 34,655 \text{ psi}$$

$$L/r = \frac{4.25}{4.15} = 1.024$$

For $L/r < 5$, critical buckling stress:

$$S_s' = 0.10 \frac{Et}{r} + 5E \left(\frac{t}{L}\right)^2$$

$S_s' = \underline{42,200 \text{ psi}}$

Peak S_s = 34,655 psi

M.S. $= \frac{42,200}{34,655} - 1 = \underline{0.218}$

A.4 NO-BACK (Figure 20, Section 5.4)

A.4.1 Coil Stress at Point B (Section A-A):

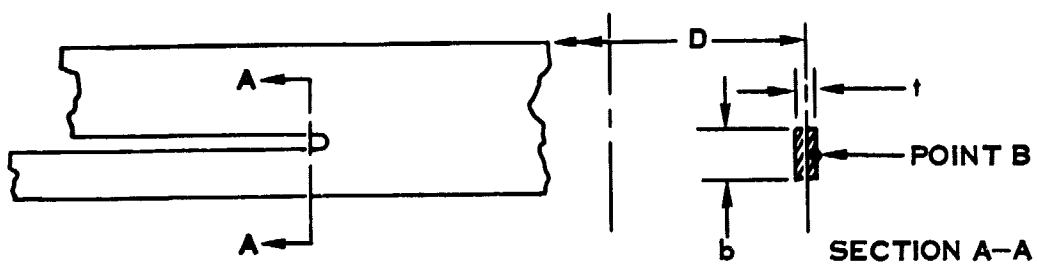

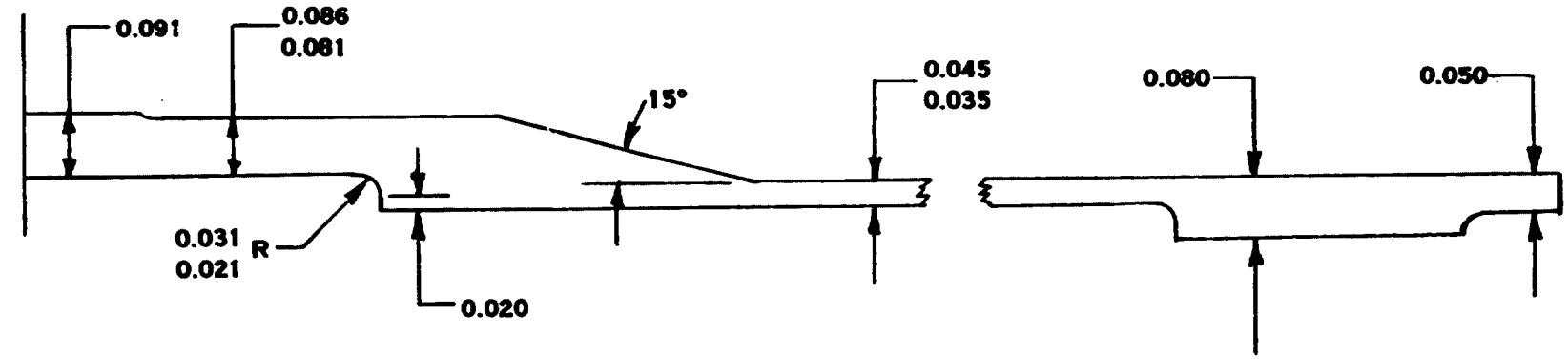

SCALE: 4/1
DIMENSIONS ARE IN INCHES

Figure A11. Flex spline wall thickness

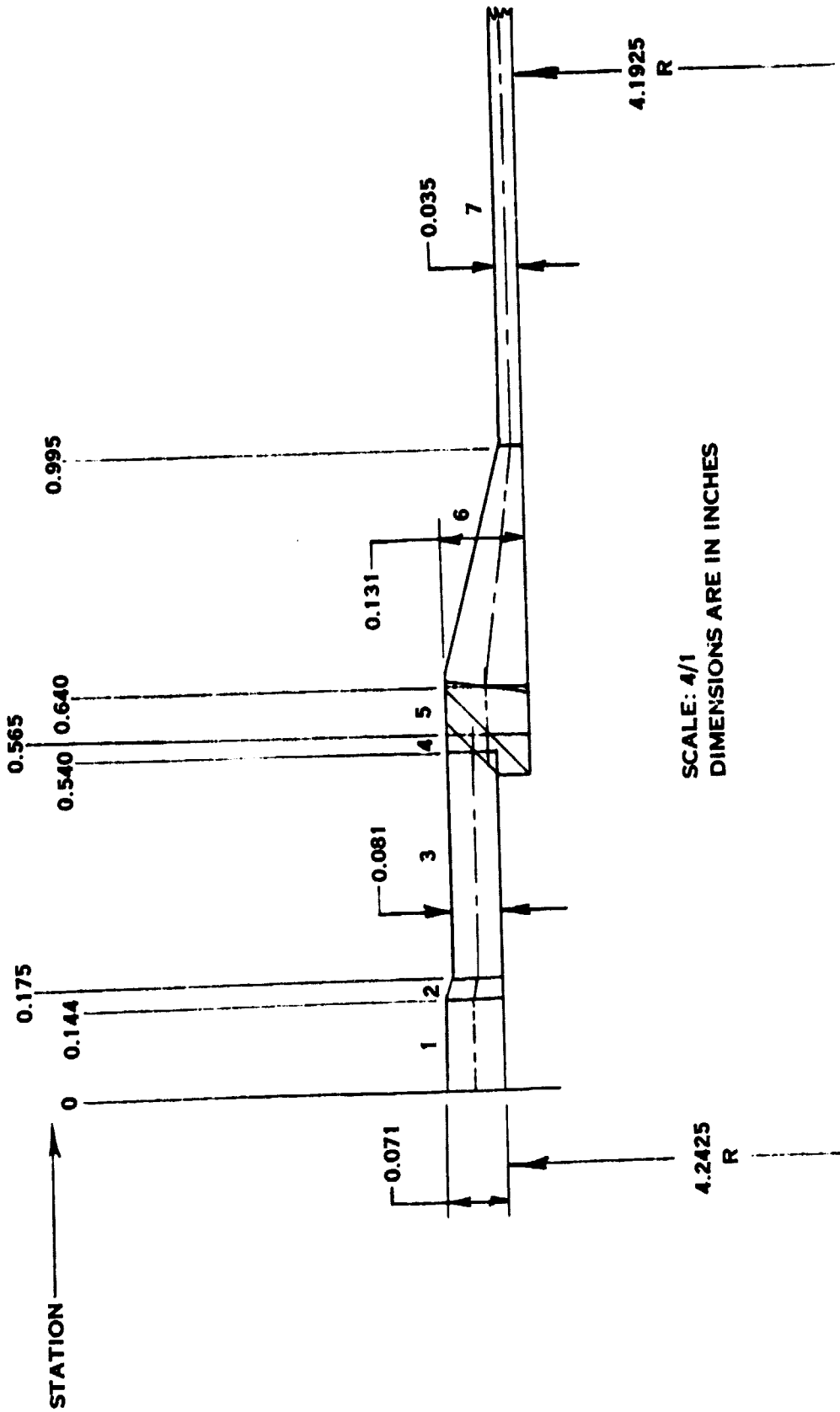

Figure A12. Flex spline model (forward end)

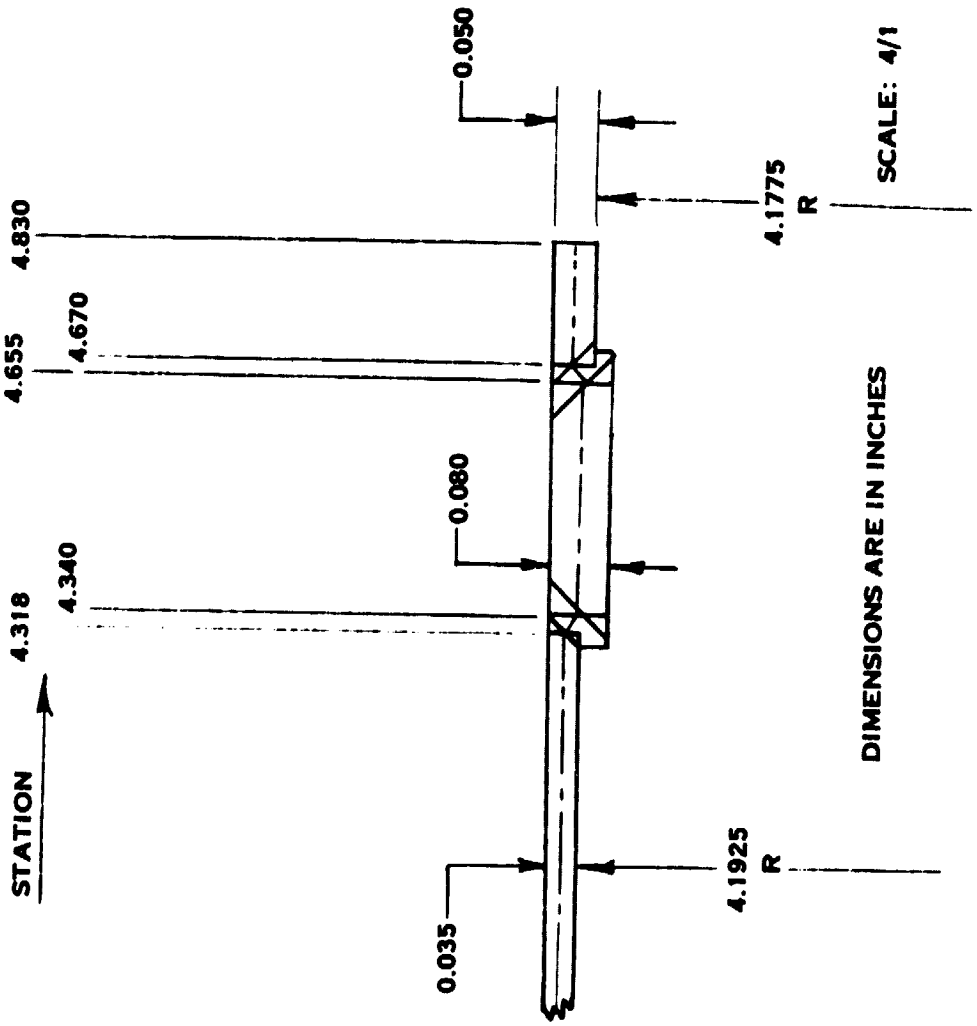

Figure A13. Flex spline model (aft end)

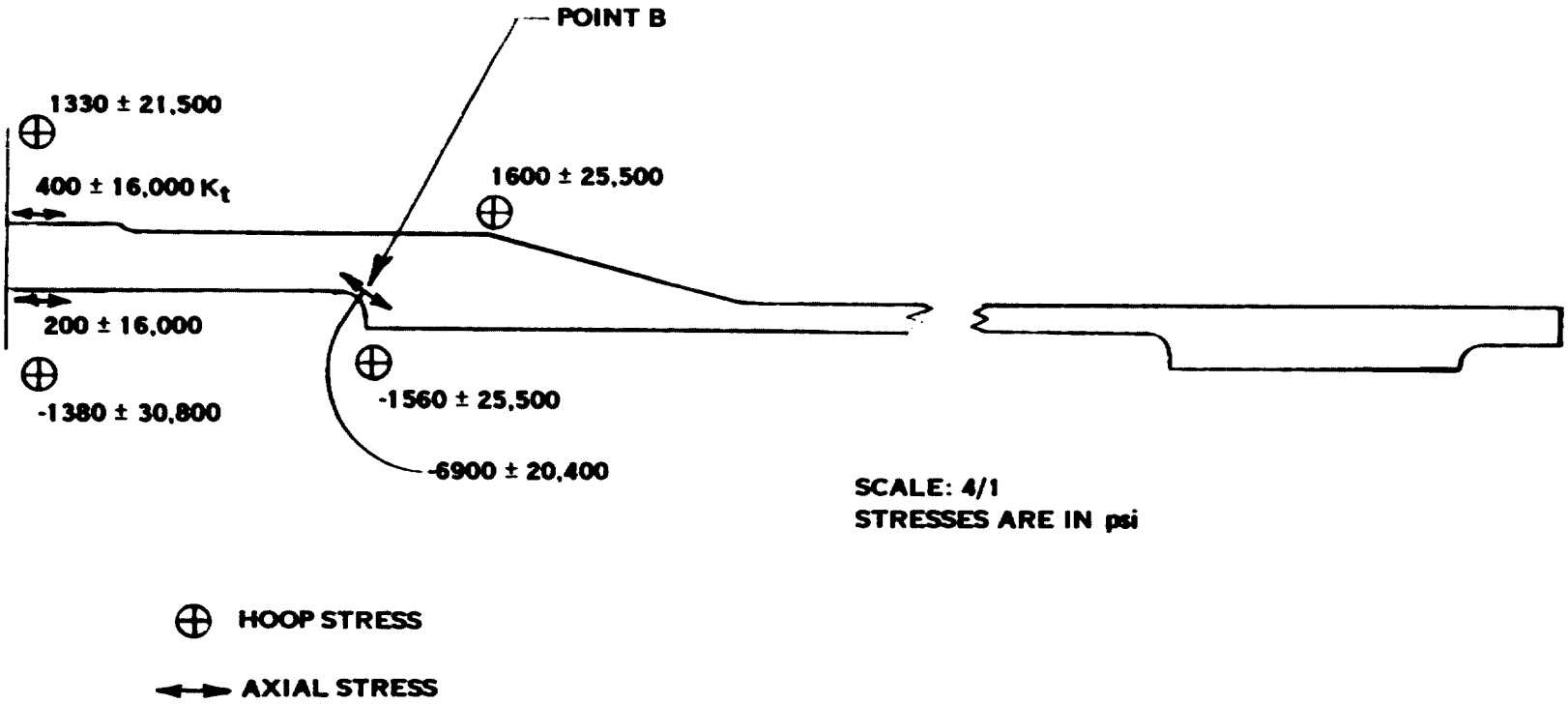

Figure A14. Flex spline stresses

Compressive stress due to maximum torque:

$$S_c = \frac{2T}{btD}$$

Where: T = 2400 lb-in.
b = 0.253 in.
t = 0.10 in.
D = 2.10 in.

$$S_c = \frac{2\,(2400)}{(0.253)(0.10)(2.10)}$$

$$S_c = 90,345 \text{ psi}$$

Bending stress due to diametral interference fit, δ_D:

$$S_b = \frac{KEt\delta}{D^2} = \frac{(1.0)(29 \times 10^6)(0.10)(0.0224)}{(2.10)^2}$$

K = 1.0
δ_D = 0.0224 in.
E = 29×10^6 psi

$$S_b = 14,730 \text{ psi}$$

Total coil stress = $S_c + S_b$ = 90,345 + 14,730
= 105, 075 psi (maximum)
= 14,730 psi (minimum)

$$S = 59,900 \pm 45,170 \text{ psi}$$

Allowable cycles: 10^8
Required cycles: 10^5

A.4.2 Maximum Pressure Between the Spring and Housing at Maximum Holding Torque:

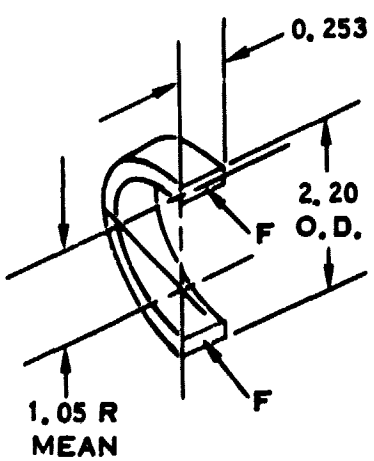

$$F = \frac{\text{Torque}}{\text{Radius}}$$

$$F = \frac{2400}{1.05} = 2286 \text{ lbs.}$$

Projected area, A = (2.2)(0.253)
= 0.5566 in^2

$$\text{Pressure} = \frac{2F}{A} = \frac{2\,(2286)}{0.5566}$$

= <u>8200 psi</u>

A.4.3 Input Quill Shaft Torsional Shear Stress (Figure 20, Section B-B)

Maximum input torque = 850 lb-in

$$J = 0.0678 \text{ in}^4$$

$$c = 0.6775 \text{ in}$$

$$S_s = \frac{Tc}{J} = \frac{(850)(0.6775)}{0.0678} = \pm 8500 \text{ psi for } K_t = 1.0$$

$K_t = 4.0$ at the lubrication holes

$S_s = \pm (4.0)(8500) = \pm 34,000$ psi

Allowable cycles: 10^8

Required cycles: 10^6

A.4.4 Output Shaft Stress at Point A (Figure 20, Section C-C):

Stress analysis of the slotted section of the output shaft under torque loading was made by assuming that the shaft is comprised of inner and outer circular rings connected by three equally spaced rigid spokes.

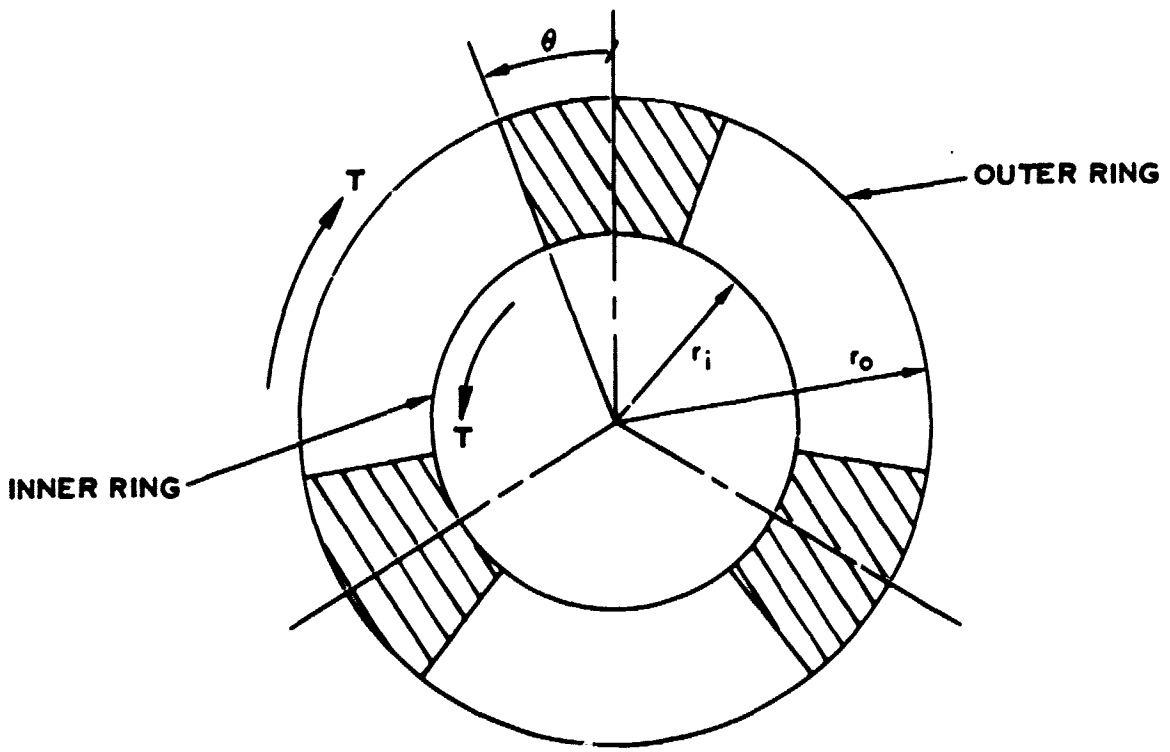

Shear and bending stresses in the spokes due to torque, T, are low but significant tangential and bending stresses are induced in the rings. Since the rings are ends of tubes, it is necessary to find the effective moment of inertia, I, and length, L, of the rings. This was accomplished by calculating the radial deflection of the tube ends loaded by three equally spaced concentrated 5-lb loads. The H088 computer shell program described in Section A.3.3 was used in conjunction with the tube models shown in Figure A-15 to obtain the radial deflections at the loads. These deflections were then substituted in the following ring deflection equation (Reference "Formulas for Stress and Strain" by R.J. Roark, Third Edition, Table VIII, Case 9) to solve for the effective I:

$$\delta = \frac{Fr^3}{2EI}\left[\frac{1}{s^2}\left(\frac{\theta'}{2}+\frac{sc}{2}\right)-\frac{1}{\theta'}\right]$$

Inner ring: $\delta_i = 0.9687 \times 10^{-5}$ in

$F = 5$ lbs

$r_i = 0.52$ in

$E = 30 \times 10^6$ psi

$\theta' = \pi/3$ radians (half angle between loads)

$s = \sin 60^\circ = 0.866025$

$c = \cos 60^\circ = 0.5000$

$$I_i = \frac{(5)(0.52)^3}{2(30 \times 10^6)(0.9687 \times 10^{-5})}\left[\frac{1}{0.75}\left(\frac{\pi}{6}+\frac{0.43301}{2}\right)-\frac{3}{\pi}\right]$$

$$I_i = 3.856 \times 10^{-5} \text{ in}^4$$

Solving for the effective ring length, L_i:

$$I_i = \frac{L_i t^3}{12} \qquad \text{where: } t = 0.085 \text{ in}$$

$$L_i = \frac{12\,(3.856 \times 10^{-5})}{(0.085)^3} = 0.7535 \text{ in}$$

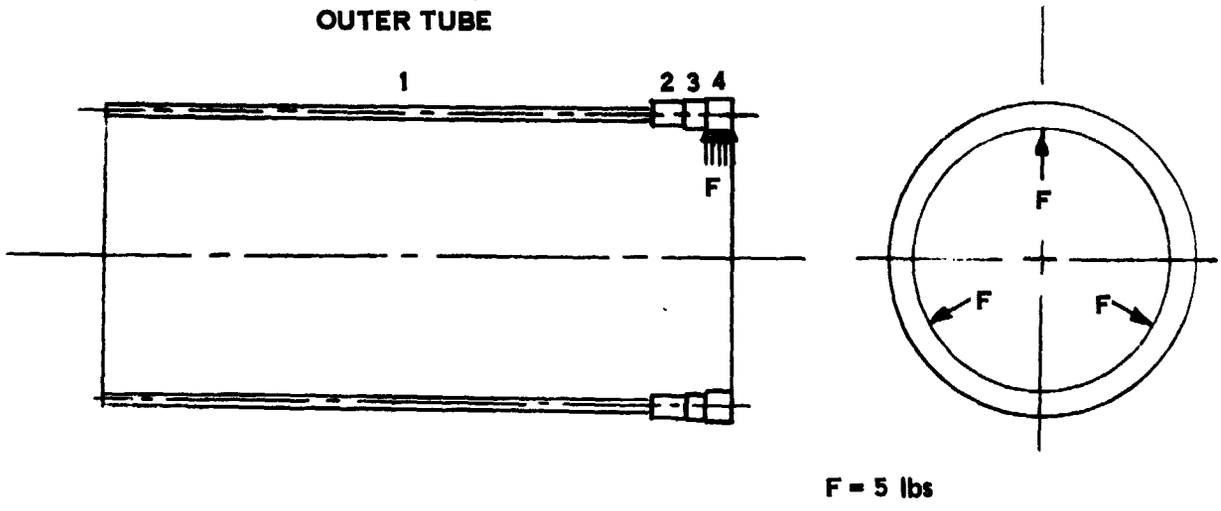

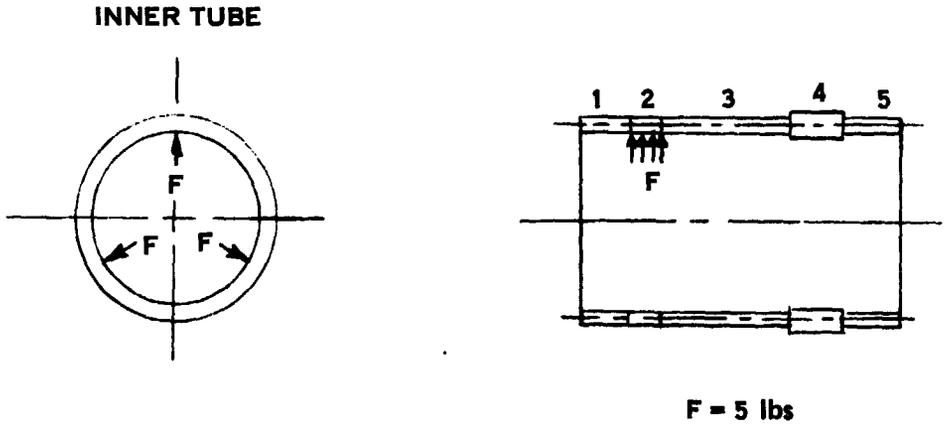

Figure A15. Computer models used to determine effective moment of inertia of the output shaft

Similarly for the outer ring:

$\delta_o = 1.451 \times 10^{-5}$ in

$r_o = 0.785$ in.

$I_o = 8.856 \times 10^{-5}$ in ^{4}

$t = 0.135$ in

$L_o = 0.4319$ in

Equations of equilibrium were written based on the free-body diagrams of the rings and spokes shown in Figure A-16.

Summation of torque on the inner ring:

$$T = 3 (H_{r_i} + 2 V_i r_i \sin\theta)$$

and for $\theta = 21°$: $T = 1.56 H + 1.118 V_i$

Summation of torque on the spoke:

$$0 = H (r_o - r_i) - 2 V_i r_i \sin\theta - 2 V_o r_o \sin\theta$$

and for $\theta = 21°$: $0 = 0.265H - 0.3727 V_i - 0.5626 V_o$

Matching the ring slopes assuming rigid spokes:

$$\frac{\delta_{Ao} - \delta_{Bo}}{2 r_o \sin\theta} = \frac{\delta_{Ai} - \delta_{Bi}}{2 r_i \sin\theta}$$

To get the slope equation in terms of the three unknown forces H, V_i and V_o, the radial deflections are written in terms of the forces multiplied by Wises' coefficients (Reference "Airplane Structures" by Niles and Newell, Vol. II, 3rd Edition, Section 17:7)

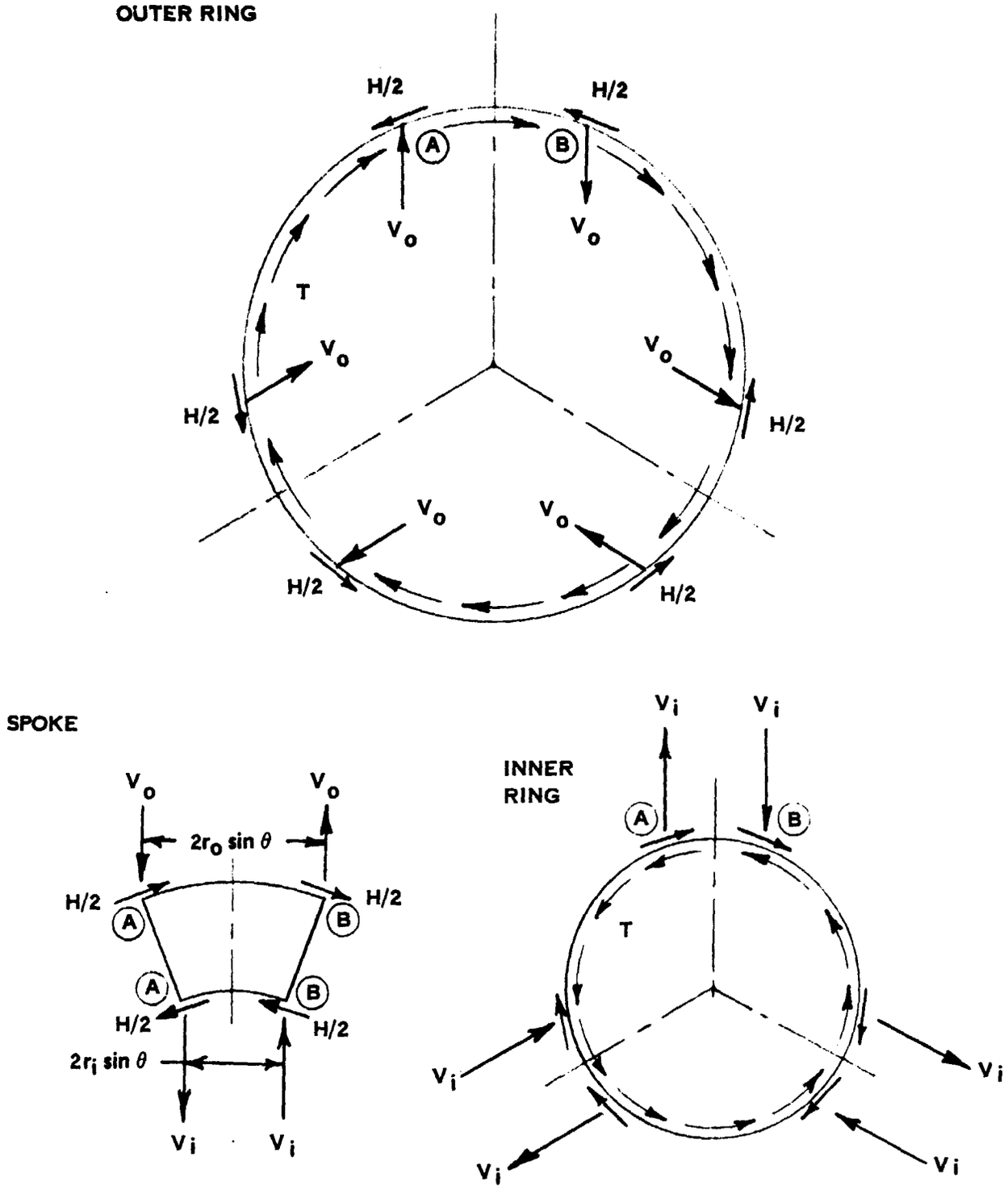

Figure A16. Free body diagrams of output shaft parts

$$\delta_{A_o} = \frac{r_o^3}{2\pi E I_o} \left\{ V_o \cos\theta \left[\overset{*}{cyy}(0) - cyy(2\theta) + cyy(120) \right.\right.$$

$$\left. - cyy(120 + 2\theta) + cyy(120) - cyy(120 - 2\theta) \right]$$

$$+ \left(V_o \sin\theta - \frac{H}{2} \right) \left[\overset{**}{cyx}(0) - cyx(2\theta) - cyx(120) \right.$$

$$\left.\left. - cyx(120 + 2\theta) + cyx(120) + cyx(120 - 2\theta) \right] \right\}$$

$$\delta_{BO} = \frac{r_o^3}{2\pi E I_o} \left\{ V_o \cos\theta \left[cyy(2\theta) - cyy(0) + cyy(120 - 2\theta) \right.\right.$$

$$\left. - cyy(120) + cyy(120 + 2\theta) - cyy(120) \right]$$

$$+ \left[V_o \sin\theta - \frac{H}{2} \right] \left[cyx(2\theta) + cyx(0) - cyx(120 - 2\theta) \right.$$

$$\left. - cyx(120 + 2\theta) + cyx(120) \right]$$

$$\left(\frac{\delta_{A_o} - \delta_{B_o}}{r_o} \right) 2\pi E = \frac{r_o^2}{I_o} \left\{ V_o \cos\theta \left[2\, cyy(0) \right.\right.$$

$$\left. - 2\, cyy(2\theta) - 2\, cyy(120 - 2\theta) + 4\, cyy(120) - 2\, cyy(120 + 2\theta) \right]$$

$$+ \left[V_o \sin\theta - \frac{H}{2} \right] \left[2\, cyx(0) - 2\, cyx(2\theta) + 2\, cyx(120 - 2\theta) \right.$$

$$\left.\left. - 2\, cyx(120 + 2\theta) \right] \right\}$$

*cyy (α) = Wise's coefficient for radial deflection due to a unit radial load at an angle α from the load.

**cyx (α) = Wise's coefficient for radial deflection due to a unit tangential load at an angle α from the load.

Similarly it can be shown:

$$\left(\frac{\delta_{A_i} - \delta_{B_i}}{r_i}\right) 2\pi E = \frac{r_i^2}{I_i} \left\{ V_i \cos\theta \left[2\,cyy\,(0) - 2\,cyy\,(2\theta) \right.\right.$$

$$\left. - 2\,cyy\,(120 - 2\theta) + 4\,cyy\,(120) - 2\,cyy\,(120 + 2\theta) \right]$$

$$+ \left[V_i \sin\theta + \frac{H}{2} \right] \left[2\,cyx\,(0) - 2\,cyx\,(2\theta) + 2\,cyx\,(120 - 2\theta) \right.$$

$$\left.\left. - 2\,cyx\,(120 + 2\theta) \right] \right\}$$

Substituting $\theta = 21°$, values for r, I and Wise's coefficients in the two slope equations and setting them equal to each other yields:

$$0 = 0.0^{\wedge}36H - 0.1935\,V_i + 0.1920\,V_o$$

Solving simultaneously with the two torque equations of equilibrium:

$$0 = 0.265H - 0.3727\,V_i - 0.5626\,V_o$$

$$T = 1.56\,H + 1.118\,V_i$$

Gives: $V_i = 0.194126\,T$

$H = 0.501903\,T$

$V_o = 0.107809\,T$

Due to symmetry, the moments, M and tangential forces, F in the rings are equal at Points A and B. They are also maximum at these points. The moment and tangential force at Point A for both inner and outer rings was found using Wise's coefficients and forces V and H.

Outer ring:

$$M_{A_o} = r_o \left\{ V_o \cos\theta \left[CMy\,(0) - CMy\,(2\theta) - CMy\,(120 - 2\theta) \right.\right.$$

$$\left. + 2\,CMy\,(120) - CMy\,(120 + 2\theta) \right]$$

$$+ \left[V_o \sin\theta - \frac{H}{2} \right] \left[CMx\,(0) - CMx\,(2\theta) + CMy\,(120 - 2\theta) \right.$$

$$- CMy(120 + 2\theta)\Big]\Big\}$$

$$F_{A_o} = r_o \Big\{V_o \cos\theta \Big[CFy(0) - CFy(2\theta) - CFy(120 - 2\theta) + 2\,CFy(120 - CFy(120 + 2\theta)\Big] + \Big[V_o \sin\theta - \frac{H}{2}\Big]\Big[CFx(0) - CFx(2\theta) + CFy(120 - 2\theta) - CFy(120 + 2\theta)\Big]\Big\}$$

Substituting values for r_o, V_o, H and Wise's coefficients gives the following maximum values:

$$M_{A_o} = - 0.02464T$$

$$F_{A_o} = 0.01675T$$

Similar analysis of the inner ring gives:

$$M_{A_i} = - 0.02006T$$

$$F_{A_i} = - 0.1750T$$

Combined bending and tangential stress at Point A:

Outer ring:

$$S = \frac{M_{A_o} c_o}{I_o} - \frac{F_{A_o}}{A_o}$$

where: $c_o = 0.0425$ in

$I_o = 8.856 \times 10^{-5}$ in^4

$A_o = 0.0585$ in^2

$$S = - 22.2T$$

Inner ring:

$$S = -\left(\frac{M_{A_i}\, c_i}{I_i} + \frac{F_{A_i}}{A_i}\right)$$

where: $c_i = 0.0675$

$I_i = 3.856 \times 10^{-5}$ in^4

$A_i = 0.064$ in^2

$S = 24.8T$

Determination of stress concentration factor, K_t (Reference "Stress Concentration Factors" - R.E. Peterson, 1974, Figure 76)

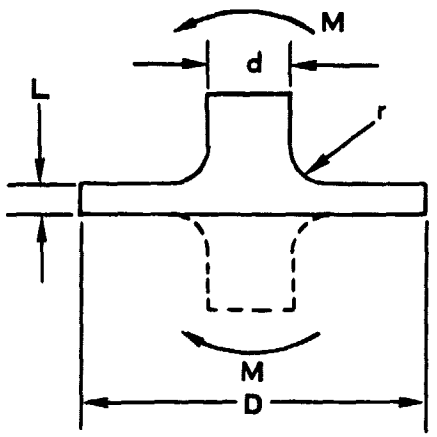

D/d = 3.0

Outer ring: $r/d = \frac{0.09}{0.45} = 0.20$

$L/D = \frac{0.135}{1.35} = 0.10$

$\Big\}$ $K_t = 1.40$

Inner ring: $r/d = \frac{0.09}{0.45} = 0.20$

$L/D = \frac{0.085}{1.35} = 0.063$

$\Big\}$ $K_t = 1.37$

The combined stress in the rings at Point A for the maximum torque of 2400 lb-in for each direction is:

Outer ring:

$$S = (22.2)(\pm 2400)(1.40) = \pm 74,600 \text{ psi}$$

Inner ring:

$$S = (24.8)(\pm 2400)(1.37) = \pm 82,550 \text{ psi}$$

Allowable number of cycles = 1.05×10^5

Required number of cycles = 0.96×10^5

A.5 DIFFERENTIAL GEARING (Figure 22, Section 5.6)

A.5.1 Input Sun Gear Torsional Shear Stress at Point A (Table XIX):

Maximum Dynamic Torque = ± 170 lb-in

$$J = 0.001154 \text{ in}^4$$

$$C = 0.1655$$

$$S_s = \frac{Tc}{J} = \frac{(170)(0.1655)}{0.001154} = 24,300 \text{ psi } (K_t = 1.0)$$

Determination of K_t: (Reference "Stress Concentration Factors" - R.E. Peterson, 1974, Figure 79)

$D/d = 0.24/0.165 = 1.45$ $\qquad$ $K_t = 1.26$

$r/d = 0.06/0.33 = 0.1818$

$$S_s = \pm (1.26)(24,300) = \pm \underline{30,620 \text{ psi}}$$

A.5.2 Planet Cage Stresses (Figure 23, Table XIX):

The planet cage due to symmetry, was separated into three elements with reaction loads as shown in Figure A-17.

Input sun gear torque equal to 170 in-lbs produces the following cage loads:

F = 93 lbs (tangential)

P' = 136 lbs (lateral)

Beam deflection from points C to D is calculated using the deflection equation for a cantilever beam as follows:

$$y = \frac{P' L^3}{3EI} = \frac{(136)(0.57)^3}{3(15.8 \times 10^6)(0.002286)} = 0.000232 \text{ in}$$

Where:

$I = 0.002286 \text{ in}^4$

$E = 15.8 \times 10^6 \text{ psi}$

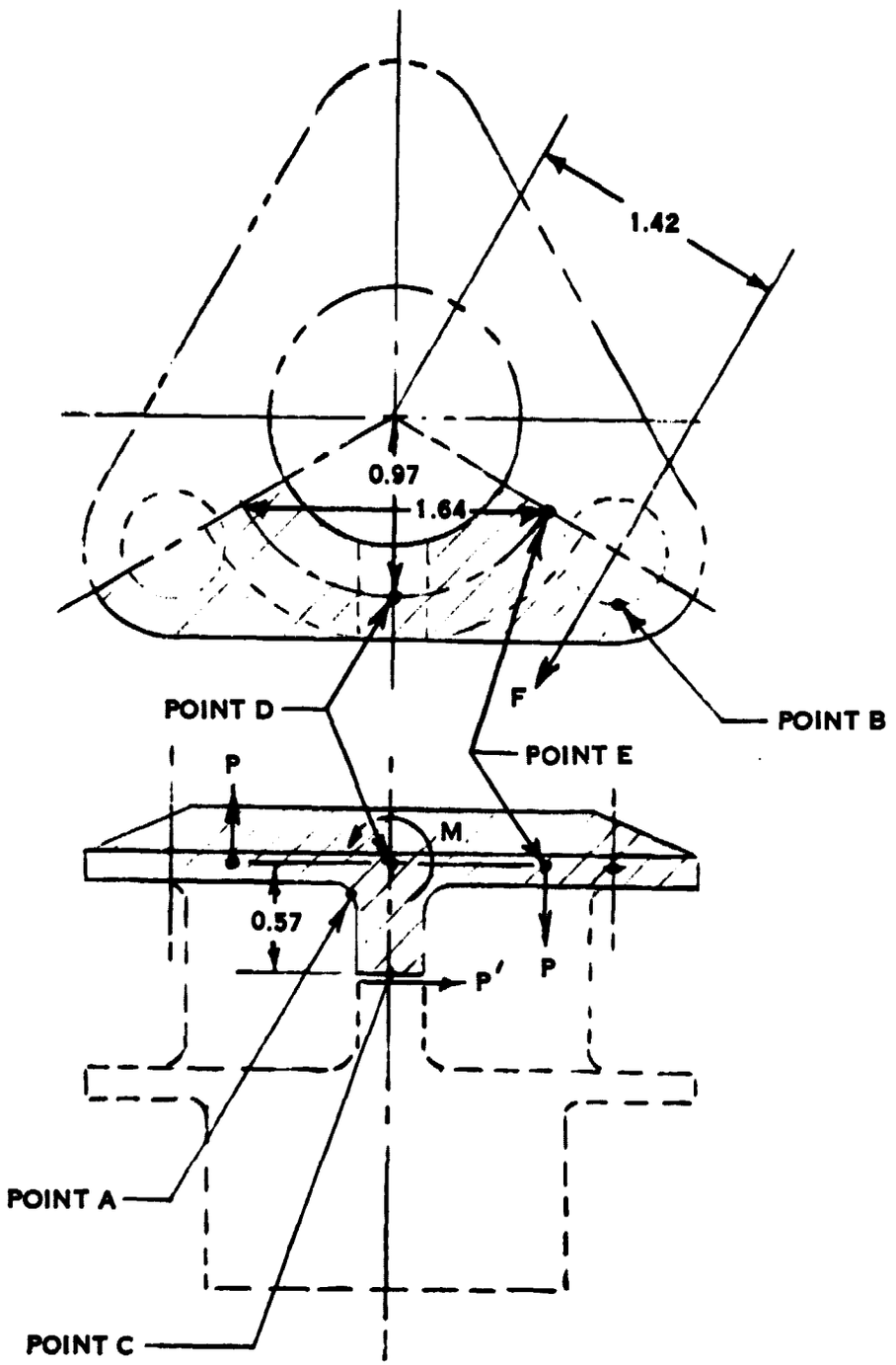

Figure A17. Planet cage elements

The cage was assumed to be an equivalent circular ring of 0.97 in. mean radius and an average moment of inertia, I equal to 0.002286 in^4 to calculate the deflection from points D to E. (Reference "Rings and arculate beams" by A. Blake, Figure 15, equation 88, Product Engineering, January 7, 1963)

$$M = P' L = (136)\,(0.57) = 77.52 \text{ in-lbs}$$

$$P = \frac{77.52}{1.64} = 47.27 \text{ lbs}$$

Using equation in Table of the Reference for a rectangle:

$$\lambda = \frac{EI}{GK} = 0.637 \qquad \text{Where: } K = 0.009$$

$$\phi = 60^\circ = 1.047 \text{ Radians}; \quad \psi = 0^\circ$$

$$B_1 = 2\,(1.047)\,(1) + 0 - 0.866 = 1.228$$

$$B_2 = 3\,(0) + 0.866 + 2\,(1.047 - 4 \sin 60^\circ - 4 \sin 60^\circ = 0.2198$$

$$y = \frac{Pr^3}{4EI} \left[B_1 + \lambda B_2\right]$$

$$y = \frac{(47.27)(0.97)^3}{4(15.8 \times 10^6)(0.002286)} \left[1.228 + (0.637)(0.2198)\right] = 0.000408 \text{ in}$$

At point A, $y = \frac{0.57}{0.82}\,(0.000408) = 0.000284$ in

Total deflection at point A:

$$Y_T = 0.000284 + 0.000232 = 0.000516 \text{ in}$$

Total deflection at point C:

$$y_T = \frac{1.42}{0.97}\,(0.000516) = 0.000755 \text{ in}$$

Slope of the gear shaft: $\Theta = \frac{0.000755}{0.57}$

$$\Theta = \underline{0.001325 \text{ in/in}}$$

Stress at point A:

$$S = \frac{Mc}{I} = \frac{(77.52)(0.19)}{0.002286} = 6445 \text{ psi } (K_t = 1.0)$$

$$K_t = 1.82$$

$$S = \pm (1.82)(6445) = 11,730 \text{ psi}$$

The stress at point B was calculated in the same manner as the trunnion arm lug using the lug analysis in Section 5.3 of Sikorsky Aircraft Design Manual.

Lug load due to centrifugal force on the planet gears at rpm equivalent to 3347 fan rpm is 255 lbs. Gear reaction load F is equal to 93 lbs.

t = 0.14 in; D = 0.56 in; W = 0.90 in; a = 0.45 in

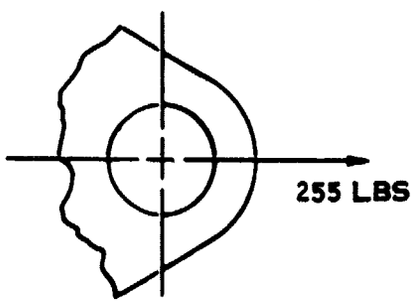

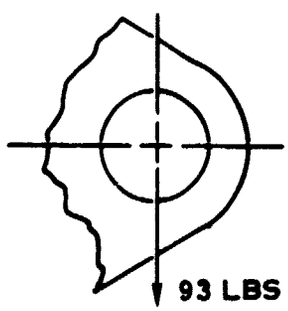

$A_T = (0.9-0.56)(0.14) = 0.0476 \text{ in}^2$

$A_{Brg} = (0.56)(0.14) = 0.0784 \text{ in}^2$

W/D = 1.61; D/t = 4.0

a/D = 0.80; t/D = 0.25

$K_t = 0.985$; $K_{Bru} = 0.55$

$K_{Bry} = 0.700$

Pay - (0.985)(0.0476)(101,000) = 4735

Correct for Peak Stresses at Edge

(Mc/I) with Factor of 4.0

$$Pay = \frac{4735}{4} = 1184 \text{ lbs}$$

$$Ray = \frac{255}{1184} = 0.215$$

$A_1 = A_4 = 0.0448 \text{ in}^2$

$A_2 = A_3 = 0.0238 \text{ in}^2$

$$A_{Av} = \frac{6}{\frac{4}{0.0448} + \frac{2}{0.0238}} = 0.0346 \text{ in}^2$$

$A_{Brg} = (0.56)(0.14) = 0.0784 \text{ in}^2$

$$\frac{A_{Av}}{A_{Brg}} = \frac{0.0346}{0.0784} = 0.441$$

$K_{try} = 0.56$

$P_{try} = (0.56)(0.0784)(101,000) = 4434 \text{ lbs}$

$P_{try} = 4434/4 = 1108 \text{ lbs}$

$$R_{try} = \frac{93}{1108} = 0.084$$

$$M.S. = \frac{1}{\left[(0.215)^{1.6} + (0.084)^{1.6} \right]^{0.625}} - 1$$

$$M.S. = \frac{1}{0.2437} - 1 = 3.10$$

$$S = \frac{101,000}{4.10} = 24,634 \text{ psi}$$

$$S = \underline{\pm 12,320 \text{ psi}}$$

APPENDIX B

Reliability

APPENDIX B

RELIABILITY

The pitch change actuator mechanism designed by Hamilton Standard for the G.E. QCSEE utilizes a simple mechanical cam operated mechanism. The actuator is energized from a hydro electro-mechanical control system which receives electrical signal from customer supplied equipment. An electrical feedback signal is generated at the control. A reliability prediction has been prepared for the pitch change actuator and control mechanism. The prediction is based on sources such as actual field experience accumulated by Hamilton Standard on equipment such as the 54H60 propeller on the P3 aircraft, Jet fuel control models 12, 25, & 60, and the Failure Data (FARADA) reliability reference manuals.

Duty cycle factors have been applied to some particular items to reflect the intermittent usage of the pitch change actuator.

The MTBF values presented are based on the best information currently available regarding the system configuration and piece part failure rates, but may be subject to change as the program develops and further information becomes available. Consequently, the figures presented are for information purposes and shall be considered objectives rather than guarantees.

Predicted failure rates and Mean Time Between Failure (MTBF) values are listed below:

Layout	Name	Failures Per Million Hours	MTBF
L-12886-4	Harmonic Drive	1.698	588,928
L-12886-5	Cam & Arm Assembly	7.424	134,698
L-12886-6	Differential & Flexible Drive Shaft	28.591	34,976
L-12886-8	Beta Regulator	28.851	34,660
	TOTAL	66.564	15,023

In addition to the above values, the following reliability predictions have been made for the system:

1. Mean Time Between In Flight Shutdown = 1,298,700
2. Mean Time Between In Flight Power Losses
   - A. Power changes require blade modulation = 40,000
   - B. Power changes do not require blade modulation = 1,298,700
3. Mean Time Between Premature Removals = 15,023
4. Mean Time Between Servicing Inspection = Condition Monitoring

The preceding values were determined from a preliminary study of the effects of certain failure modes on the hardware in regards to system performance degradation. Some of the basic considerations in this study are as follows:

A. In general, in-flight shutdowns would be caused by a failure which would result in any blade or blades to be out of synchronization with the others, or a failure which would cause the loss of blade control. The following failure modes are in this category:

1. Loss of blade control would occur if the no-back failed to hold. *
2. Failure of the harmonic drive output, input, spline teeth or bearings could cause the same kind of failure.
3. Failures which would cause a blade or blades to be out of synchronization include the fracture of a roller arm due to fatigue or the failure of a blade retention bearing which would cause an excessive load on an arm. Fracture of a cam track and disintegration of a roller would also result in blade synchronization failures.
4. Seizure of the no-back.

* Hydraulic pressure can be used to overcome the effects of these conditions.

B. In-flight power losses would result from any failure which would cause an in-flight shutdown.

In the event that power changes do not require modulation of the blades during flight, no failures other than those in A. above will affect in-flight power losses.

If blade modulation is required for the flight profile, failures which might prevent the ability to increase angle when necessary and called for would result from:

1. Seizure of the cam track roller
2. Seizure of the harmonic wave generator
3. Failure of the planetary gear train
4. Failure of the no-back assembly
5. Failure of the flexible rotary cable
6. Failure of the control assembly

The table on the previous page includes a value for each of the two cases described.

C. Mean Time Between Premature Removals appears to be synonymous with Mean Time Between Failures, as noted in the predictions for reliability for the entire assembly.

D. Mean Time Between Servicing/inspection is not applicable for the present hardware configuration. It may be desirable to provide a means of condition monitoring such as a vibration detecting device which would indicate possible degradation of the system. This type of warning to shut down an engine could reduce the possibility of costly and extensive damage.

APPENDIX C

Failure Mode and Effects Analysis

FAILURE MODE AND EFFECT ANALYSIS

Item	Part or Assembly Description	Mode of Failure	Effect of Failure on the System	Failure Classification Mil-Std-882 Class. Category	Remarks
1	Cam Follower Arm	Fracture	One blade moves to minimum twisting moment blade angle & may cause an increase in engine vibration	II	Shut engine down
2	Cam	Fracture of one cam slot wall	One blade tracks off-angle with the failed cam slot arm running against an adjacent arm or adjacent slot wall.	II	Shut engine down
3	Cam Support Brg.	Fracture	Possible jamming. Unable to change pitch.	II	Run fixed pitch
		Wear	Possible unbalance condition when bearing preload is lost.	I or II	Run fixed pitch or shut engine down
4	Harmonic Drive	Fracture of output, input or spline teeth	Loss of pitch change capability. Blades move to minimum twisting moment angle.	II	Shut engine down
		Bearing fracture	Possible jam. Unable to change pitch.	II	Run fixed pitch
		Bearing wear	Reduction in flex spline tooth engagement. Reduced non-ratcheting capacity.	I	Unlikely ratcheting at normal max. operating loads.

FAILURE MODE AND EFFECT ANALYSIS (CONT)

Item	Part or Assembly Description	Mode of Failure	Effect of Failure on the System	Failure Classification Mil-Std-882 Class. Category	Remarks
5	No-Back	Seizes	Unable to change pitch	II	Run fixed pitch or shut engine down
		Fractures Open	Blade pitch control is maintained by beta regulator and must be left on for static holding of beta.	I	Repair after flight
6	Differential	Fails open	Loss of pitch change. Blades hold on no-back at failure angle.	II	Run fixed pitch.
7	Flex Shaft, Drive Gearing or Motor	Fractures	Loss of pitch change. Blades hold on no-back at failure angle.	II	Run fixed pitch
		Jams	Unable to change pitch.	II	Run fixed pitch
8	LVDT or LVDT Drive	Fails	Loss of signal or erroneous signal from one unit.	II	Run fixed pitch
9	EH Valve	Fails hard over	Excessive error signal causes computer to shut down system.	II	Run fixed pitch
		Fails at null position	Blades will not change pitch	II	Run fixed pitch

APPENDIX D. PRELIMINARY DESIGN STUDY

In the second concept, blade pitch is controlled by a blade arm engaging a cam track which is positioned by the rotary output of a harmonic drive. Cam contouring reduces the torque requirement of the harmonic which minimizes the system weight.

The third concept is similar to the second except that two cam arms drive each blade. One cam is driven from each end of the harmonic, thus reducing the torque requirement of the harmonic by 50%. The disadvantage of this concept is that the effective gear ratio between the blades and the harmonic is geometric and cannot be contoured.

The fourth system utilizes a linear hydraulic actuator coupled to the blades by a link and torque arm. Position of the actuator is controlled by a hydraulic servo valve and feedback mechanism. Hydraulic power is transferred to the rotating fan through a sleeve type transfer bearing and an axial no-back is provided as part of the servo valve summing linkage.

The fifth concept has a ball screw and nut to provide pitch change. The nut is coupled to the blades by links and trunnions and has a sliding spline to the disc to prevent rotation of the nut. Thus rotation of the ball screw results in translation of the nut which causes rotation of the blade by virtue of the offset trunnions. This is a low ratio device and has a relatively long load path which results in a weight penalty.

The sixth arrangement is identical to the ball screw concept except that the ball screw is replaced by an Acme thread. This system is heavy because its low efficiency requires a large powering system.

The seventh concept is an arrangement of worm drives. Input rotation turns nine radially mounted drive shafts through a bevel gear arrangement. The drive shafts rotate countershafts and a worm drive mounted tangential to the blade spindle where a second worm drive provides blade pitch change. The two stages of worm drives result in a very low system efficiency and thus requires a heavy powering system. This system also has a large number of parts, which would degrade its reliability and increase its cost.

The power hinge arrangement has an input gear driving 15 pinions meshing with dual ring gears which in turn drive the blades through a dual bevel gear drive. Again, low system efficiencies result in high powering system weight. Also, additional structural weight is required to balance pinion moments and to react pinion centrifugal loads.

The vane motor concept is the same as the harmonic with bevel gears except that the harmonic is replaced with a vane motor. This concept requires relatively heavy cylinder walls in order to maintain seal extrusion gaps within acceptable values and large discs to transmit torque from the actuator to the bevel gears.

With the concept using individual blade actuators, each actuator is made up of two helical splines and a ball screw. Input motion rotates the ball screw and translation of the ball nut is converted to rotation at the blades by two helical splines. This system has moderately low efficiency because of the helical splines. Centrifugal load on the ball nut requires that the input torque be higher when the nut is being moved inboard. The principal disadvantage of this system is the large number of parts resulting in lower reliability and high cost.

A preliminary design of each concept was performed and a weight estimate of each was prepared. A summary of the weights is shown in Table D.2.1.

In addition to a weight comparison, trade studies were also made of reliability and production cost. These factors are listed in the pitch change system comparison, Table D.2.2. Also evaluated on a relative asis are development risk, development cost, maintainability, background and experimental verification and production cost estimates.

The independent actuator approach was eliminated because its complexity (298 parts) severely reduced its reliability and presented maintenance difficulties. The hydraulic actuator (although a proven, conventional concept) has a lower reliability due to the effect of dynamic piston seals and the addition of such hydraulic components as control valves, fluid transfer bearings, etc. In addition, the hydraulic system increases the risk of inadvertent oil leakage into the core engine air path with the attand effect or bleed air contamination and potential engine malfunction. This risk can, of course, be minimized by additional oil shielding but this will increase system weight and increase maintenance complexity.

Based on this, the choice was reduced to either the bevel gear harmonic or the cam drive harmonic, which are generically similar devices. As was true in the previous trade study, the cam drive harmonic is considerably more weight effective due to the ability to provide a more favorable gear ratio from the blade to the actuator, and the ability to contour the cam to minimize the total power requirements of the actuator.

Thus the cam drive harmonic actuator was selected because it has high reliability, was the lightest, had reasonable production costs and had good maintainability characteristics.

D.2.1.2 Selected Concepts

Four concepts were selected for further study on the basis of considering weight, and a qualitative assessment of reliability and maintainability. They were the following as shown by figures D.2.1 through D.2.4.

a. Harmonic with bevel gears.

b. Cam drive harmonic.

TABLE D.2.1
WEIGHT SUMMARY - PRELIMINARY TRADE-OF STUDY

Function	* Double Drive Bevel Gears	* Cam Drive Harmonic	Double Cam Drive	* Axial Hyd Piston	Ball Screw	Acme Screw	Worm Drive	Power Hinge (15 Pinion)	Single Vane Motor	* Indep. Blade Hel. Spline
Covers & Stops	10.34	10.50	12.66	11.1	13.62	13.62	9.5	10.34	10.34	9.94
Blade Mechanism	20.75	18.04	21.41	10.64	10.64	10.64	59.0 (worms)	20.75	20.75	41.54
Load Summing Mechanism	15.24	12.75	9.26	5.84	5.84	5.84	6.44 (bevel)	15.24	17.24	0.92
Inner Housing	8.90	3.56	4.0	7.75	8.0	10.0	31.13	8.90	8.90	9.0
Prime Mover	18.0	12.50	12.5	18.41	25.72	20.1	-	22.50	16.80	1.15
Safety Lock	1.22	1.0	1.0	12.10	3.68	-	-	1.22	10.30	0.5
Input Area	8.20	6.95	6.95	6.35	12.0	31.0	31.5	10.6	6.35	5.13
Transmission	-	-	-	3.47	2.94	7.0	-	-	3.47	-
Control	12.80	11.96	11.96	7.76	13.38	24.85	37.5	16.00	7.76	12.6
Total Dry Weight	95.45	77.26	79.74	83.42	95.82	123.05	175.07	105.55	101.91	80.78

* Selected systems

TABLE D.2.2
QCSEE PITCH CHANGE ACTUATOR COMPARISON

	Bevel Gear Harmonic	Cam Drive Harmonic	Hydraulic Piston	Independent Actuators
Reliability (MTBF)	77,000	67,000	29,000	5,400
Actuator Weight Δ	+41	0	+18	+6
Power System Weight Δ	0	0	-2	+7
Parts Count	60	114	158	298
Dev. Risk Rating	2	2	1	2
Dev. Cost Rating	2	2	1	3
Relative Prod. Cost Rating	1.1	1.0	0.75	2.2
Maintainability Rating	1	1	1	3
Background & Exp. Verification Rating	2	2	1	2

Relative Ratings: 1 - Good
2 - Fair
3 - Poor

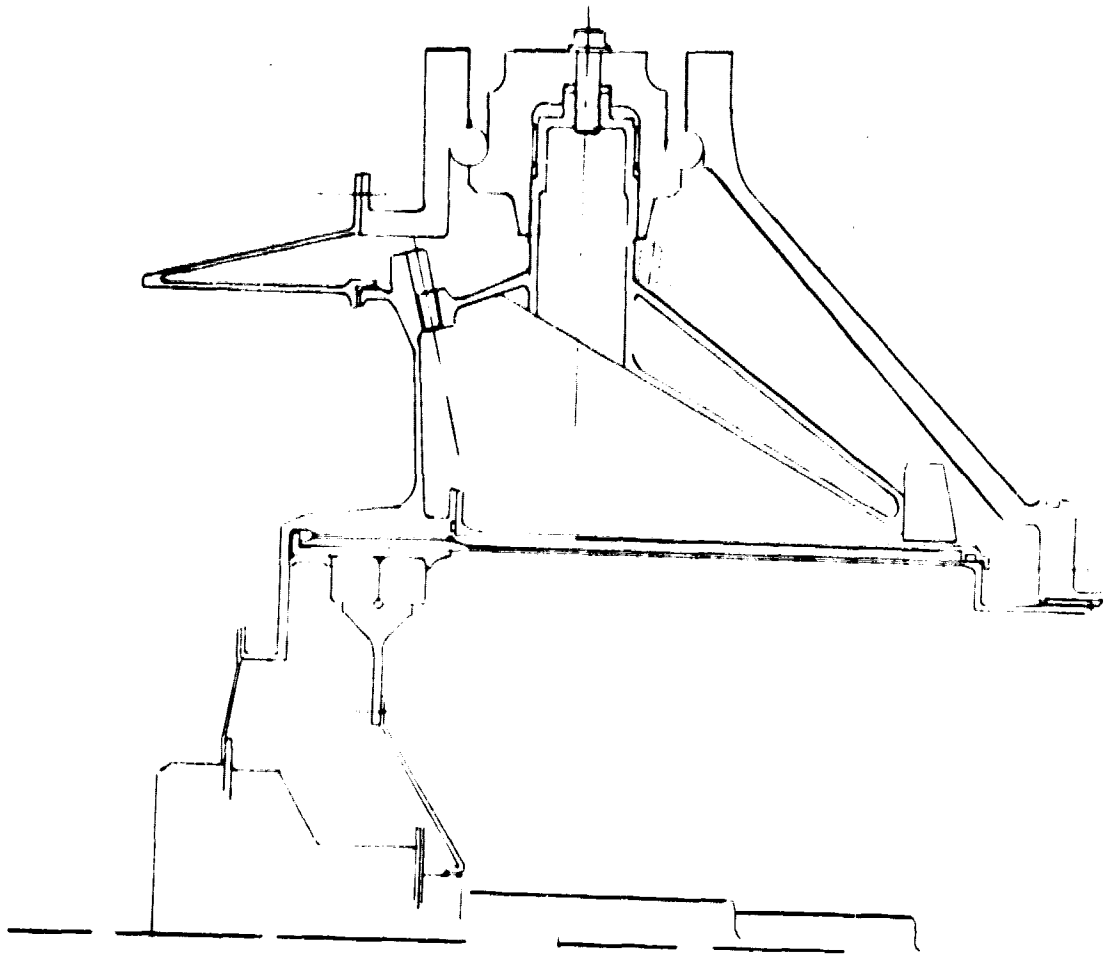

FIGURE D. 2. 1. HARMONIC WITH BEVEL GEARS

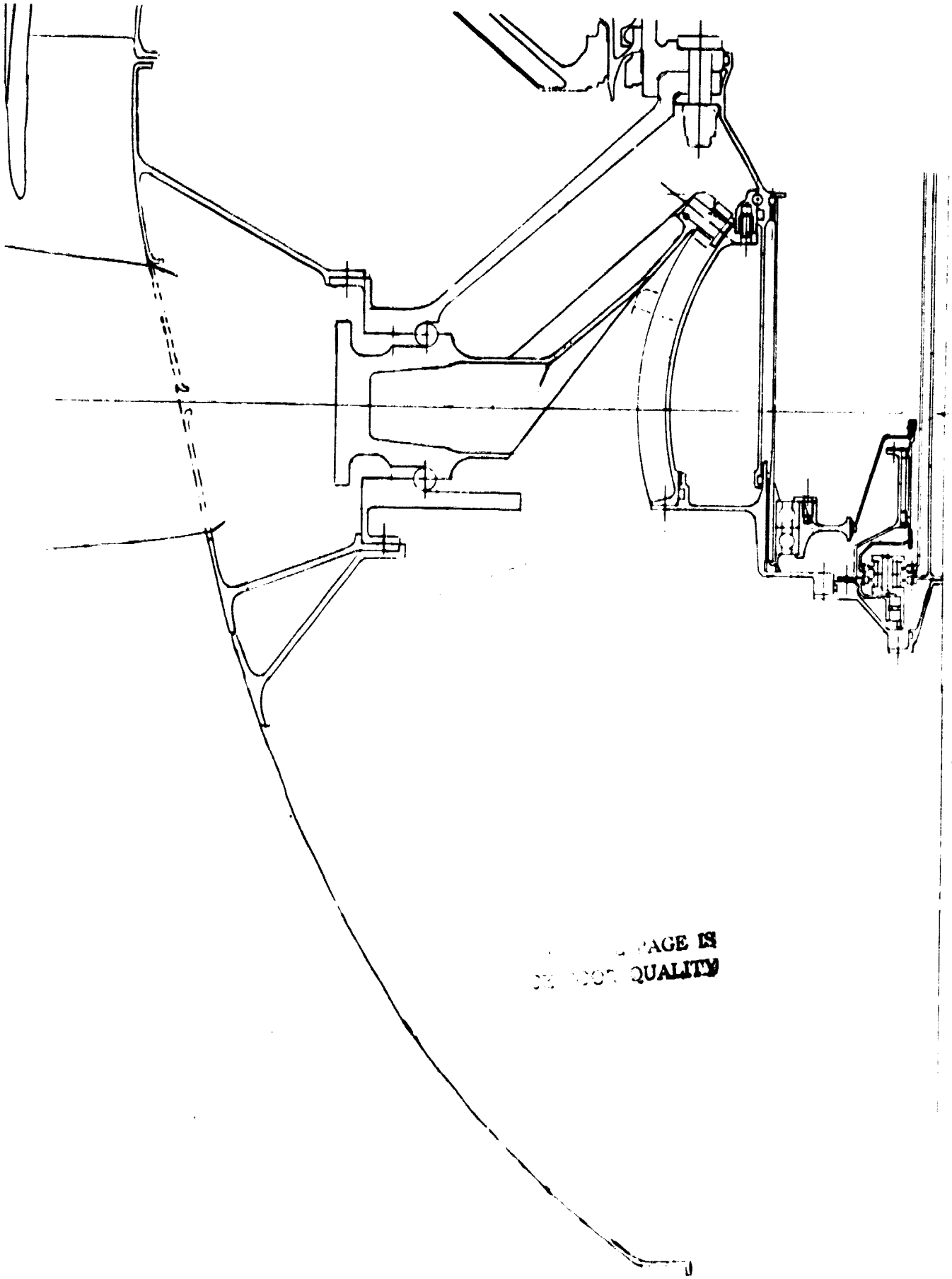

FIGURE D. 2. 2. CAM DRIVE HARMONIC

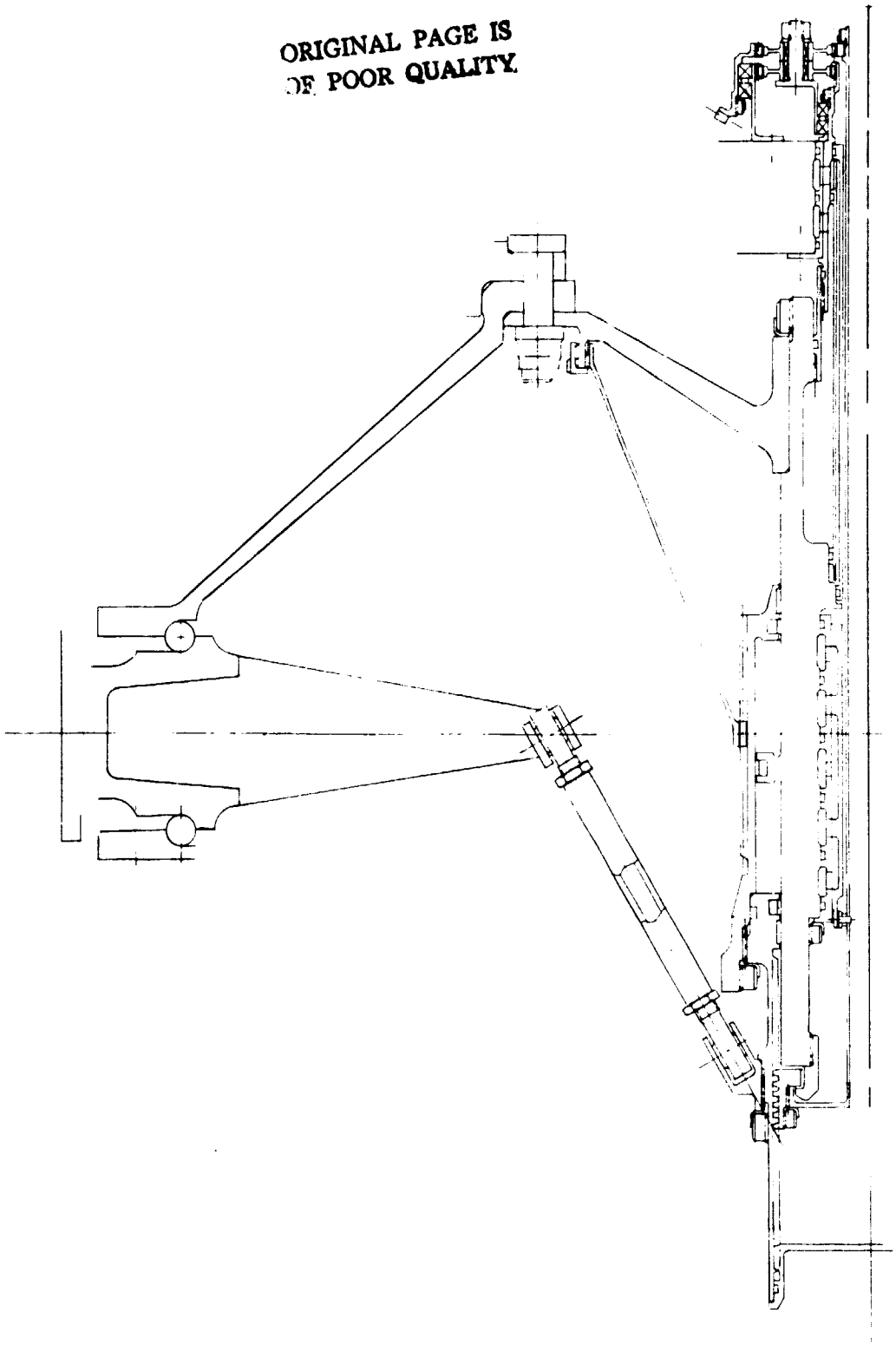

FIGURE D. 2. 3. HYDRAULIC PISTON

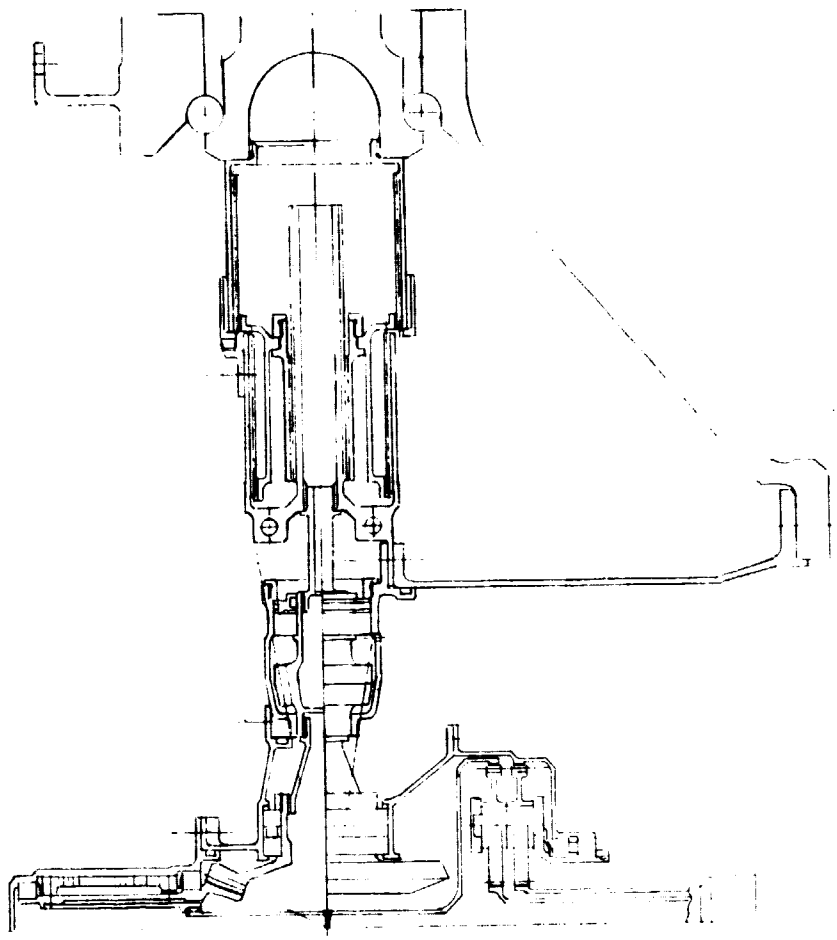

FIGURE D. 2. 4. INDEPENDENT BLADE HELICAL SPLINE ACTUATORS

c. Hydraulic piston.

d. Independent blade helical spline actuators.

The preliminary blade aero and mass twisting moments defined by G.E. were combined with the blade retention friction moments estimated by Hamilton Standard to determine the resultant blade torsional loading. In addition, the pitch change systems were designed for a bird strike load of 15,000 in-lbs/blade. Blade counterweighting was utilized where practicable to reduce the pitch change power requirement on all designs except the independent blade actuator concept, where envelope restrictions would not permit it.

D.2.2 PITCH CHANGE POWERING SYSTEM

Concept Arrangements

There are many ways of generating pitch change power from engine shaft power. However, a hydraulic system was considered for the trade study for the following reasons:

a. Ease of control

b. Ease of heat rejection

c. Adaptability to continuous modulation

All concepts use the same basic components, e.g., hydraulic motor, electro-hydraulic valve (EHV), linear variable differential transformer (LVDT), valve solenoid, and a pressure regulating valve. The difference between concepts lies in where the components are located and how they are interconnected.

The first arrangement has all of the powering system components mounted in the fan cowl with the interconnection between the hydraulic motor and the fan being either a gear and shaft arrangement or a rotary flexible cable. If the hydraulic motor is mounted internally and the remaining components are duct mounted, motor position feedback is provided by a flexible cable - either rotary or push-pull. With the LVDT mounted internally along with the hydraulic motor, the feedback signal is electrical. Another alternative is to locate all of the control elements on the fan forward of the pitch change system where the system can be maintained by removing the spinner.

Discussion

A comparison of the powering systems under consideration is shown in Table 2-3. Weight of the five systems was judged to be approximately equal and therefore was not a factor in the selection. Failure rates of systems 2, 3, and 4 were slightly higher than the feed forward system (System 1). System 1 was selected for the QCSEE application

TABLE D.2.3
GE QCSEE PITCH CHANGE POWER SYSTEM COMPARISON

	System 1 Feed Fwd. Drive Shaft & Gears	System 1 Feed Fwd. Rotary Flex Cable	System 2 Feedback Push-Pull Cable	System 3 Feedback Electrical EHV Cowl Mtd.	System 4 Feed Fwd. Electrical EHV Fan Mtd.
Reliability (MTBF)	41,500	37,000	27,800	27,800	27,800
Weight	19.16	19.16 (est)	19.16 (est.)	19.16 (est.)	19.16 (est.)
Dev. Risk	1	2	1	1	3
Dev. Cost	3	2	2	1	2
Prod. Cost	3	2	2	1	2
Parts Count	70	28	41	34	37
Maintainability	1	1	2	2	1
Fault Isolation	1	1	2	2	1
Background & Exp. Verification	1	3	2	1	1
Environment	1	1	2	2	2

Note: Highest Rating is (1)

because of superior fault isolation and maintainability obtained by locating all electro-hydraulic control components (Beta Regulator) as a quick change module in an accessible engine cowl location, and it eliminates high pressure hydraulics from the rotor group thus eliminating potential leakage into the core engine air path. The rotating flex shaft was selected over gears and rigid shaft drive based on basic simplicity and maintainability. Although the rigid shafting and gearing can be designed for removal in sections, the time to remove and replace the flexible shaft and casing will be much less. It is apparent, however from reliability data, that the flexible shaft will need to be engineering with full oil lubrication and carefully chosen wear materials to achieve the desired reliability.

APPENDIX E

Symbols

Symbol	Definition	Units S.I.	Units U.S.
A	Area	cm^2	in^2
C	Distance from the neutral axis to the extreme fiber of a cross-sectional area	cm	in
C	Coefficient or constant	-	-
d	Harmonic wave generator cam rise from minor to major axis	cm	in
D	Diameter	cm	in
E	Modulus of elasticity	N/cm^2	psi
f	Force per unit length	N/cm	lbs/in
F	Force	N	lb
g	Acceleration of gravity	m/sec^2	ft/sec^2
G	Modulus of rigidity	N/cm^2	psi
H	Force	N	lb
I	Moment of inertia of an area	cm^4	in^4
J	Polar moment of inertia of an area	cm^4	in^4
K	Harmonic drive torque constant	-	-
K	Spring rate	N/m	lbs/in
K_t	Stress concentration factor		
L	Length	cm	in
L	Bearing life based on 90% of a bearing group showing no evidence of fatigue	hours	hours
M	Moment	N-m	lb-in
n	Rotational speed	rpm	rpm
N	Force normal to a surface	N	lb

Symbol	Definition	Units S.I.	Units U.S.
P	Load	N	lb
P	Pressure	N/cm^2	psi
r	Radius	cm	in
R_C	Rockwell C hardness test number	-	-
R_{15N}	Rockwell 15N hardness test number	-	-
S	Stress	N/cm^2	psi
t	Thickness	cm	in
T	Twisting moment or torque	N-m	lb-in
V	Force	N	lb
x, y, z	Linear coordinates	cm	in
β_F	Fan blade angle	deg	deg
δ	Radial deflection or fit	cm	in
γ_D	Diametral deflection or fit	cm	in
θ	Slope of a member in bending	rad	rad
γ	Harmonic drive load distribution angle	deg	deg
μ	Poisson's ratio	-	-
μ_f	Coefficient of friction	-	-
ϕ	Pressure angle, gear and spline teeth	deg	deg